IS-T 1735

Thermal Depinning of a Single Superconducting vortex

by

Sok, Junghyun

PHD Thesis submitted to Iowa State University

Ames Laboratory, U.S. DOE
Iowa State University
Ames, Iowa 50011

Date Transmitted: June 19, 1995

PREPARED FOR THE U.S. DEPARTMENT OF ENERGY
UNDER CONTRACT NO. W-7405-Eng-82.

Thermal depinning of a single superconducting vortex

Junghyun Sok

Major Professor: Dr. Douglas K. Finnemore
Iowa State University

Thermal depinning has been studied for a single vortex trapped in a superconducting thin film in order to determine the value of the superconducting order parameter and the superfluid density when the vortex depins and starts to move around the film. For the Pb film in Pb/Al/Al_2O_3/PbBi junction having a gold line, the vortex depins from the artificial pinning site(Au line) and reproducibly moves through the same sequence of other pinning sites before it leaves the junction area of the Pb film. Values of the normalized order parameter Δ/Δ_o vary from $\Delta/\Delta_o=0.20$ at the first motion of the vortex to $\Delta/\Delta_o=0.16$ where the vortex finally leaves the junction. Equivalently, the value of the normalized superfluid density changes from 4% to 2.5% for this sample in this same temperature interval. For the Nb film in Nb/Al/Al_2O_3/Nb junction, thermal depinning occurs when the value of Δ/Δ_o is approximately 0.22 and the value of ρ_s/ρ_{so} is approximately 5%. These values are about 20% larger than those of a Pb sample having a gold line, but the values are really very close. For the Nb sample, grain boundaries are important pinning sites whereas, for the Pb

sample with a gold line, pinning may have been dominated by an array Pb_3Au precipitates. Because roughly the same answer was obtained for these rather different kinds of pinning site, there is a reasonable chance that this is a general value within factors of 2 for a wide range of materials.

TABLE OF CONTENTS

CHAPTER I. INTRODUCTION

With the development of methods to determine the location of a single vortex in a superconducting thin film and systematically move it from one pinning site to another, it has become possible to address many important problems relevant to the motion of an isolated vortex. First, measurements were made of the elementary pinning force on an isolated vortex, f_p and its temperature dependence in S-N-S(superconductor-normal metal-superconductor) junction[Hyun,1987]. Second, all of the basic physical phenomena of the S-N-S junctions were shown to apply to the higher impedance S-N-I-S(superconductor-normal metal-insulator-superconductor) junctions. Third, a method to push vortices in any desired direction was developed in S-N-I-S junction[Li, 1991]. Finally, a study of thermal depinning was made with the various kinds of pinning centers[Sanders et al., 1993]. All of these advances were made with Pb and PbBi as the superconductor and it is important to show that the same phenomena occur in Nb and materials useful for devices.

The basic idea is to place a cross-strip Josephson junction over the thin film and to use distortions in the Fraunhofer interference pattern to locate a single vortex in a Josephson junction. This method, first, was discovered by Miller et al.[Miller et al.,1985]. In these experiments, the central method is to create a single vortex in the thin film, determine its location, and then follow its trajectory under the influence of a known applied force. A particular vortex trapped in one film of the junction generates a unique field distribution in the barrier. Such a vortex field together with externally applied field produces a specified phase difference φ between electrons on opposite sides of the barrier. This, in turn, gives rise to

Josephson supercurrents and distortions of Fraunhofer patterns in a critical current vs. field(I_c vs. H) plot. There is a unique connection between the location of the vortex inside the junction and the shape of the distorted Fraunhofer pattern to make it possible to determine the location of the vortices. Hyun and Finnemore [Hyun et al., 1987; Hyun et al., 1989] investigated the motion of a single vortex in a cross strip S-N-S (PbBi/AgAl/PbBi) junctions. An accuracy in locating the vortex of about 2% of the junction width was achieved by their experiments. With the success of the precise determination of the vortex location, a transport current was used to apply a Lorentz force on the vortex and systematically move it back and forth across the film. By measuring the temperature dependence of the depinning currents, they showed that the elementary pinning force was of the form $f_p \sim (1-T/T_c)^{3/2}$. The magnitude of the force was also found to be on the order of 10^{-6} N/m at $T/T_c = 0.95$ and measurements of the difference in depinning current needed to push the vortex in the $+x$ and $-x$ directions revealed that the pinning potential is asymmetric.

For a vortex trapped in the PbBi film, Li and coworkers [Li et al., 1991; Li and Finnemore, 1991] showed that the same physical principles applied for a cross strip S-N-I-S (Pb/Al/Al_2O_3/PbBi) junctions. The main advantage of the S-N-I-S junction over the S-N-S junction was that the insulating layer increased the junction impedance, thus giving voltages in the microvolt range. This eliminated the need for the superconducting quantum interference device (SQUID) voltage detection and greatly simplified data acquisition. In addition, they showed that a transport current in the top PbBi film would induce currents that flow across the bottom Pb film and thus would move the vortex parallel to the long axis of the Pb film. Hence the vortex could be pushed in any desired direction by suitably altering currents in the two films. It was also found that the elementary pinning force per unit length in pure Pb was 2×10^{-7} *N/m*, a value that is about an order of magnitude smaller than the value found in PbBi [Hyun et al., 1987].

The central feature of this work, however, is not the response of a vortex to an applied force but rather the motion caused by thermal activation. Thermal activation of vortices in superconductors is important both as a problem in fundamental physics and because it has implications for practical devices. In superconducting microelectronics circuits, for example, the motion of a single vortex can be a major source of noise. In conductor materials used for large scale magnets, thermally activated motion of vortices can be a factor in dissipation and the relaxation of currents in the magnet. So it is useful to know how far the order parameter can collapse without the onset of vortex hopping and thermally activated flux flow. Sanders and coworkers [Sanders et al., 1993] investigated thermally activated hopping of a single Abrikosov vortex for a thin film Pb film. They started with a gold line 2 μm wide on the substrate constructed by standard photolithography techniques and then evaporated the 50 μm wide Pb strip to produce an artificial pinning structure(Au line). There is a good electrical contact between a Pb bottom superconducting layer (S) and a gold normal metal strip (N). Thus Cooper pairs can diffuse from S to N so that the normal metal will show some superconducting properties. In addition, normal electrons will diffuse from N to S so the presence of N tends to reduce the superconducting order parameter of S near the boundary. Because of this proximity effects, a gold strip in contact with the Pb film provides suitable pinning sites. It is important to recall that the spatial gradient in the order parameter (or free energy) determines the pinning force through the relation $f_p = \partial E/\partial x$ where E is the free energy. Hence large forces occur where

$\partial E/\partial x$ is large. As the temperature is gradually raised toward T_c, the vortex depins from the artificial pinning site and moves through a half dozen sites before it exits the film. In successive runs it was shown that the vortex reproducibly moves through the same sequence of other pinning sites on each run before it leaves the junction area of the Pb film. It was discovered that the trajectory of the vortex as it thermally depins is not random. The first thermal depinning occurs when the order parameter of the bulk superconductor is about 20% of the $T = 0$ value or when the superfluid density was about 4% of the $T = 0$ value.

For the choice of materials in the Josephson junction, we have selected Nb as superconducting electrodes because it is so widely used in circuitry and the fabrication method and properties of $Nb/Al/Al_2O_3/Nb$ junction have been investigated very well [Imamura et al., 1992; Imamura and Hasuo, 1992; Shiota et al., 1992; Huggins and Gurvitch, 1985; Morohashi et al., 1985; Morohashi and Hasuo, 1987]. Josephson junctions made of refractory materials, such as Nb and NbN, are common in high speed digital and analog circuits. In these applications, Josephson junctions must be stable to thermal cycling, have large gaps, high junction quality, and tolerate relatively high process temperature. One difficulty with Pb alloy junctions used previously is that they recrystallize at low temperature and hence are not stable. In addition, they form hillocks that punch pin-holes through the barrier. $Nb/Al/Al_2O_3/Nb$ junctions are superior because they are mechanically strong and have hard smooth surfaces. In addition, Nb has affinity for the Al layer to underlying Nb, and the thin Al_2O_3 layer is entirely grown on Al layer. Important electronic features include a small leakage current in the subgap voltage region, a sharply defined gap voltage, excellent mechanical stability both against long term storage and thermal cycles, and controllability of critical currents. Based on these reliable characteristics, Josephson integrated circuit technology including active superconducting devices such as superconductive quantum interference devices [Ketchen, 1991], quasiparticle mixers [Tucker and Feldman, 1985], and nonhysteretic logic gates[Likharev and Semenov, 1991] using Nb/Al/Al_2O_3/Nb junctions has developed steadily since their first application to Josephson circuits in 1985 [Kotani et al., 1985].

The purpose of this work is to use the Fraunhofer interference methods to study the thermal depinning of a single vortex from a wide variety of different pinning sites. In this experiment, we report the thermal depinning of a vortex from a variety of different pinning sites in Nb. The immediate goal is to determine the value of the superfluid density at which thermal depinning normally takes place. Earlier measurements in Pb and PbBi show that thermal depinning occurs whenever the reduced bulk order parameter is depressed below 0.2. By studying a wide variety of pinning sites in both Nb and Pb, an estimate can be made of the range of superfluid density needed to prevent thermally activated flux flow for an isolated vortex. Thus this becomes a measure of the point in the H-T plane where pinning mechanism disappears for the various pinning sites in the sample.

The long term goal of this work is to build new devices based on the systematic manipulation of vortices within a Josephson junction, which can be developed to an Abrikosov vortex memory device. A large part of the basic physics of locating the vortex and moving it around the junction has been established by Miller [Miller, 1984], Hyun [Hyun, 1987], and Li [Li,1991]. Miller found that the distortion of Fraunhofer pattern in the presence of trapped vortices inside the junction was related to vortex position and established the theoretical background to find the location of a vortex. Hyun completed the procedures of nucleation and systematic motion of a vortex in S-N-S junction and finally found out the magnitude and temperature dependence of the elementary pinning force. Li showed that S-N-I-S physics is the same as S-N-S physics and showed how to push vortices in any desired direction. Sanders made the first studies of thermal depinning[Sanders et al., 1993].

The work reported in this thesis includes the study of thermal activation of an Abrikosov vortex in the technologically important material, Nb. In chapter 2, we discuss the theory of locating the vortex inside junction. In chapter 3, we discuss the fabrication methods of samples and the details of measurement system. This chapter also includes the preliminary examinations of the basic properties of our Josephson junctions. In chapter 4, we present the main experimental results and discussions. A vortex is introduced by some other nucleation process, which allows a single vortex pinning to enter and move to a pinning site. Then the vortex pushed to a specified pinning site in the junction under the influence of the Lorentz force of a transport current. For each pinning the vortex will be located from the diffraction patterns using the theory. One can start warming the sample to determine the temperature where the vortex thermally depins and begins to move without the Lorentz force of a transport current. The results will be presented. Finally, applications and future work regarding the motion of a single vortex will be proposed.

CHAPTER II. THEORETICAL REVIEW

In this chapter, we review the background of Josephson effects which occur in superconductive weak links. Several Josephson equations are presented briefly. We describe the nature of the magnetic field dependence of the Josephson critical current, which is called the Fraunhofer pattern in the S-N-I-S Josephson junction. Then we discuss a model to explain how the trapped vortex inside the junction can affect the Josephson current and finally give the distorted Fraunhofer pattern.

The configuration of the trapped vortex has the unique relation with the distorted Fraunhofer pattern. The distribution of magnetic field parallel to the junction controls the phase difference for electrons on either side, so it is important to be able to describe these fields analytically. Let a parallel magnetic field line generated by the trapped vortex in one of the superconducting layers be confined into the normal metal region in Fig. 2.1a. This parallel field has spatial dependence associated with the position of the vortex. In addition, the external parallel field added to the vortex field creates a phase difference between top and bottom superconductors, so the Josephson current is changed. With the use of such a diffraction pattern to find the location of the trapped vortex, we can study the motion of an isolated vortex in S-N-I-S Josephson junction.

2.1 Josephson Equations

When two superconductors are brought close enough to one another with the fulfillment of certain other conditions primarily relating to its size, approximately 0.2 *nm*, then it may exhibit the remarkable macroscopic quantum tunneling of many

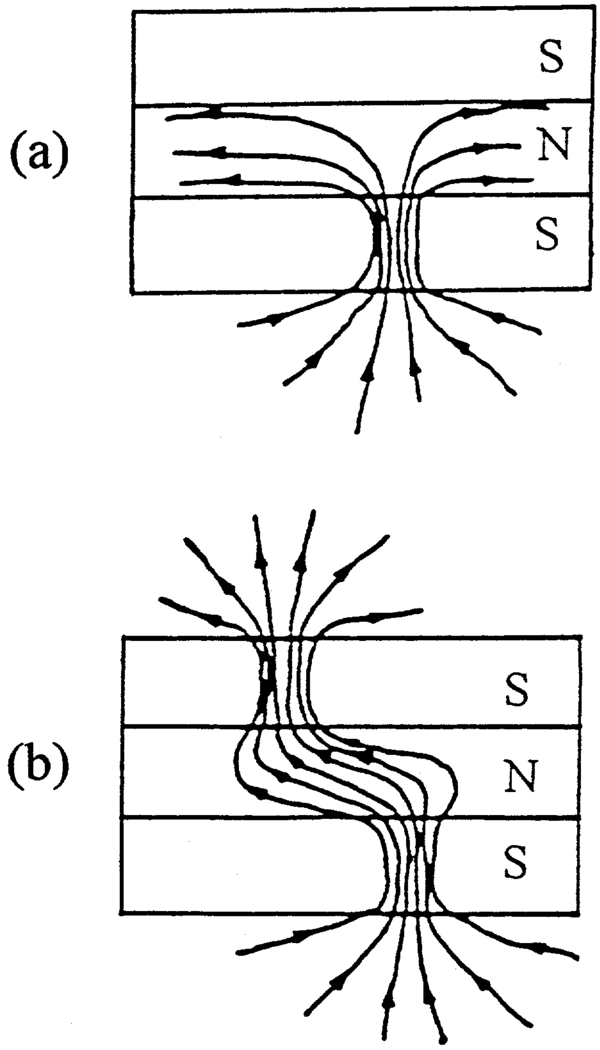

Fig. 2.1. Illustrations of a vortex trapped in a junction. The trapped vortex in only one superconducting layer is shown in (a). A misaligned vortex penetrating both the top and bottom superconducting layers is shown in (b).

condensed pairs known as the Josephson effect. The equations describing this effect were derived by B. D. Josephson in 1962 [Josephson, 1962].

There are two basic Josephson equations, one which relates the local Cooper pair tunneling current density (Josephson current) at any point in the junction to the phase difference across the junction at that point,and a second which relates the voltage across the junction to the time derivative of the phase difference. These are,

$$J_z(r) = J_o(r)\sin\varphi(r) \tag{2.1}$$

where φ is the phase difference across the junction at the polar coordinate $r = (x, y)$ and J_o is a temperature dependent amplitude which characterizes the Josephson tunneling, and

$$\frac{\partial\varphi}{\partial t} = \frac{2eV}{\hbar} \tag{2.2}$$

where V is an applied voltage across the junction.

There are various approaches one may take in deriving Josephson's equations, including the phenomenological [Feynman, 1965] and microscopic [Josephson, 1965; Josephson, 1969] approach. In the case of zero applied voltage ,a dc supercurrent through the barrier can exist, which depends sinusoidally on φ. (the so-called dc Josephson effect) If a constant nonzero voltage is applied across the junction, the phase difference φ is modulated in time, producing an alternating supercurrent through the barrier with a frequency which is dependent on the value of the applied voltage. (the ac Josephson effect) When combined with the first Josephson equation, we obtain

$$J_z = J_o \sin\left(\varphi + \frac{2e}{\hbar} Vt\right) \tag{2.3}$$

Thus, defining a Josephson oscillation frequency $w_J \equiv 2\pi f_J \equiv 2eV/\hbar$, we can write the relation as

$$f_J = \frac{V}{\Phi_o} \tag{2.4}$$

where Φ_o is the magnetic flux quantum and is equal to $hc/2e = 2.07 \times 10^{-7}\ G \cdot cm^2$ in CGS units. The value of oscillation frequency given by the ratio

$$\frac{f_J}{V} = \Phi_o^{-1} = 483.6\ MHz/\mu V \tag{2.5}$$

is so high that we can use this sensitive characteristic of the Josephson junction to develop the standard voltage. The dc Josephson effect was first observed by Anderson and Rowell [Anderson and Rowell, 1963], while the ac Josephson effect was discovered shortly thereafter by Shapiro [Shapiro, 1963].

2.2 Magnetic Field Dependence of the Josephson Current

We briefly discuss the effects of an externally applied magnetic field on the Josephson current flowing through the junction. First, we consider the spatial dependence of the phase difference $\varphi(x, y)$ in the presence of a magnetic field. This result is used to obtain the oscillating Josephson currents according to the function of parallel magnetic field, which has the form of a Fraunhofer-like diffraction pattern. This argument is then extended to deal with the case of perpendicular applied fields and trapped vortices.

2.2.1 Magnetic Field Response

Suppose two superconductors are separated by a weak region, such as a normal metal layer with thickness d_n, and a magnetic field is applied in the x(or y)-direction as shown in Fig. 2.2. The magnetic field leaks into the superconducting layer, the distance of the London penetration depth λ, finally giving an effective thickness of $d_n + 2\lambda$. The superconducting layers will generate screening currents in order to keep the penetrating magnetic field within a distance λ from the edges as shown in the figure. To describe the density of these screening currents, we introduce the order parameter Ψ as a wavefunction for the superconducting electrons, given by

$$\Psi = \left|\Psi(r,t)\right| e^{i\theta(r,t)} = n_s^{1/2} e^{i\theta(r,t)} \tag{2.6}$$

where $\left|\Psi(r,t)\right|^2 = n_s$, is defined as the superfluid density. The superconducting order parameter Ψ of this macroscopic quantum state has been shown by Gor'kov [Gor'kov, 1959] to be proportional to the local value of the energy gap Δ given by BCS theory [Bardeen et al., 1957; Fetter and Hohenberg, 1969]. Quantum

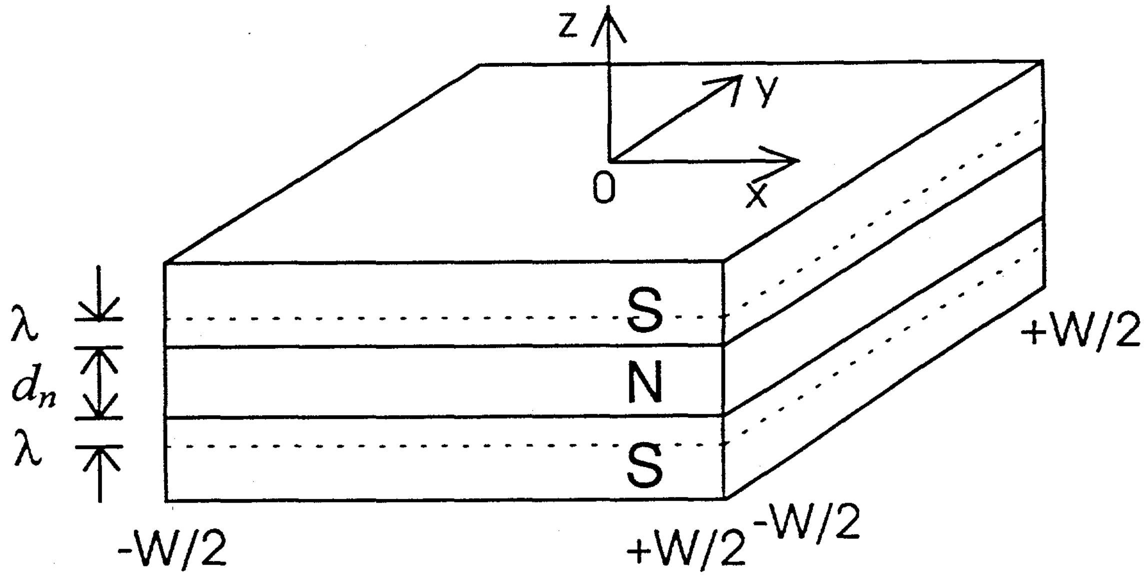

Fig. 2.2. Junction geometry showing directions, size, and field penetration depth λ.

mechanically, the current density in the external magnetic field $\mathbf{H}(=\vec{\nabla}\times\mathbf{A})$ is given by

$$\mathbf{J}=\frac{-i\hbar}{2M}q\left(\Psi^{*}\vec{\nabla}\Psi-\Psi\vec{\nabla}\Psi^{*}\right)-\frac{q^{2}}{Mc}\mathbf{A}|\Psi|^{2} \tag{2.7}$$

Since superconducting electrons move as Cooper pairs, the mass M and charge q should be replaced by $2m$ and $2e$ where e and m are the charge and mass of an electron respectively. By substituting (2.6) into (2.7), this becomes

$$\vec{\nabla}\theta=\frac{M}{\hbar q n_{s}}\mathbf{J}+\frac{2\pi}{\Phi_{o}}\mathbf{A} \tag{2.8}$$

Next, we integrate this equation around the contour which encloses the barrier between superconductors [Barone and Paterno, 1982]. The screening current densities J drop out of the integration by appropriate choice of the contour, and we neglect the integral contribution of the barrier thickness d_n. The result is

$$\frac{\partial\varphi}{\partial y}=\frac{-2\pi}{\Phi_{o}}d_{eff}H_{x} \tag{2.9}$$

where $d_{eff}=d_{n}+\lambda_{1}+\lambda_{2}$, λ_{1} and λ_{2} are field penetration depths in each superconducting layers.

Similarly,

$$\frac{\partial\varphi}{\partial x}=\frac{2\pi}{\Phi_{o}}d_{eff}H_{y} \tag{2.10}$$

In the presence of magnetic field **H** inside the junction, the general expression for the phase difference φ is

$$\vec{\nabla}\varphi = \frac{2\pi}{\Phi_o} d_{eff} \mathbf{H} \times \hat{z} \tag{2.11}$$

where $\hat{z}$ is a unit vector normal to the plane of the junction. Note that this equation relates the spatial dependence of the phase difference across the junction, and thus the Josephson current, to the spatial dependence of the magnetic field in the junction.

By integrating (2.11), the phase is

$$\varphi(r) = \varphi_o + \Theta(r) \tag{2.12}$$

where φ_o is a field independent constant and the magnetic field dependent phase angle Θ is given by

$$\Theta(r) = \frac{2\pi}{\Phi_o} \Phi(r) \tag{2.13}$$

and

$$\Phi(r) = d_{eff} \iint \mathbf{H} \cdot (\hat{z} \times d\vec{r}) \tag{2.14}$$

where $\Phi(r)$, given in equation (2.14), is the flux enclosed between the z-axis and the radial coordinate r in the barrier plus the penetration layers. Note that the phase difference φ at position $\vec{r}$ in the magnetic field **H** is defined as the ratio of the total flux normally threading the area of $d_{eff}\hat{z}\times\vec{r}$ to the flux quantum Φ_o.

The total Josephson current I is obtained after inserting (2.12) into (2.1) and integrating over the junction area.

$$\begin{aligned} I &= \iint dxdy J_o \sin(\varphi_o + \Theta(x,y)) \\ &= I_1 \sin\varphi_o + I_2 \cos\varphi_o \end{aligned} \qquad (2.15)$$

where $I_1$and I_2 are the *cos* and *sin* integrations over the junction area respectively. Maximization of equation (2.15) with respect to φ_o gives the maximum Josephson current I_c

$$\frac{I_c}{I_o} = \left\{ \langle \sin\Theta(x,y)\rangle^2 + \langle \cos\Theta(x,y)\rangle^2 \right\}^{1/2} \qquad (2.16)$$

where I_o is the maximum zero field Josephson current, $I_o = \iint J_o dxdy$ and the brackets $\langle\cdots\rangle$ denote spatial average over the junction area.

Now, in order to find the appropriate expression of $\Theta(x,y)$, consider a square junction of width W and thickness d_n sandwiched between two crossed superconducting strips. The junction lies in the x-y plane and is centered at the origin, such that the junction extends from - $W/2$ to + $W/2$ in both x- and y-directions and from - $d_{eff}/2$ to + $d_{eff}/2$ in the z- direction. Frequently the reduced coordinate will be used in which the junction extends from -1 to +1 in x- and y-

directions. Also it is assumed that the small junction limit applies, $\lambda_J \geq W$, where λ_J is the Josephson penetration depth.

2.2.1.1 Uniform Field Parallel to the Junction

As shown in Fig. 2.2, a constant field H_y is applied along the y- direction. Then the phase can be obtained from eq.(2.13) as

$$\Theta(x) = \frac{2\pi}{\Phi_o} d_{eff} H_y x \tag{2.17}$$

By inserting (2.17) into (2.16), we get

$$\frac{I_c}{I_o} = \left| \frac{\sin(\pi\Phi / \Phi_o)}{(\pi\Phi / \Phi_o)} \right| \tag{2.18}$$

where $\Phi = W d_{eff} H_y$ is the total flux threading junction barrier parallel to the flat surface. This is a periodic function of the critical current (maximum Josephson current) with respect to the external magnetic field. This function is plotted in Fig. 2.3a which has the form of the Fraunhofer pattern. This characteristic was first observed by John Rowell [Rowell, 1963] as, in fact, was Josephson tunneling [Anderson and Rowell, 1963].

Another expression for the critical current in terms of the parallel field needed for one flux quantum threading junction barrier H_o is given as

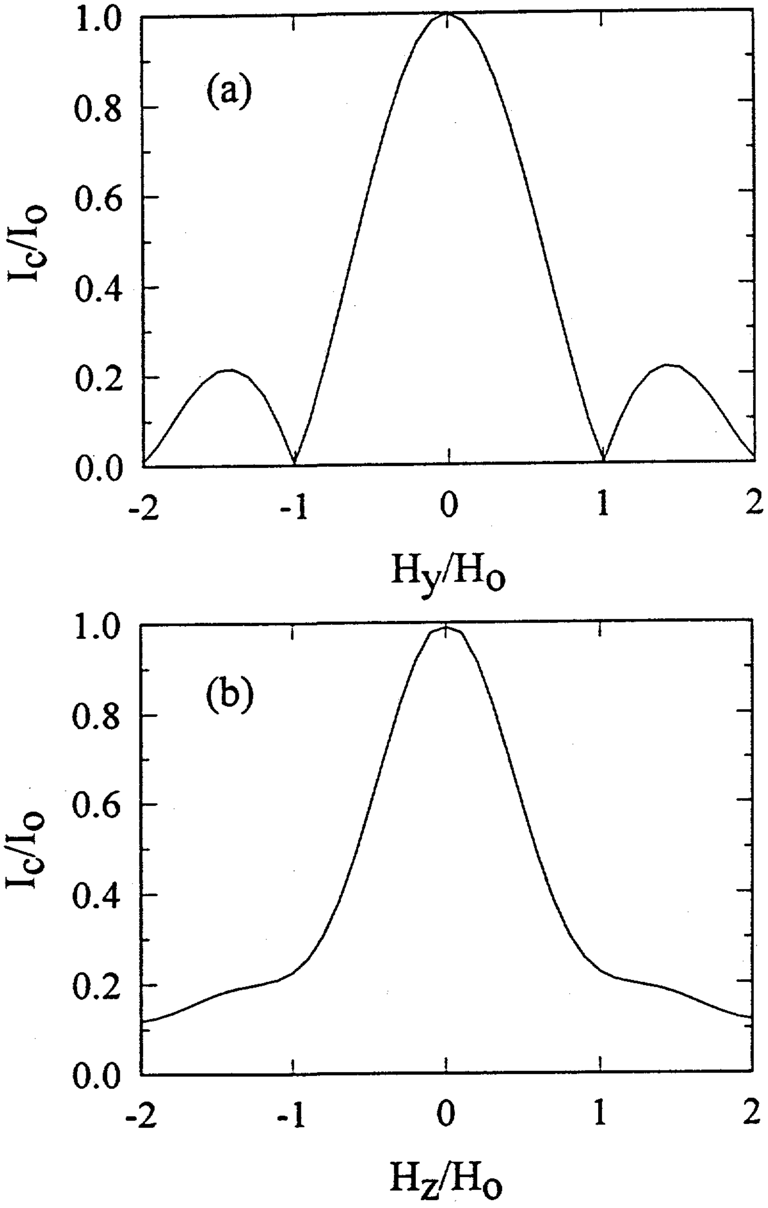

Fig. 2.3. Theoretical critical currents as a function of the external magnetic fields, H_y and H_z respectively.

$$\frac{I_c}{I_o} = \left| \frac{\sin(\pi H_y / H_o)}{(\pi H_y / H_o)} \right| \tag{2.19}$$

where $H_o = \dfrac{\Phi_o}{d_{eff} \cdot W}$ at which the first minimum of the critical current occur. H_o taken from the Fraunhofer measurement gives an idea of the effective thickness, d_{eff}, that is related to the London penetration depth λ of superconducting layers.

2.2.1.2 Uniform Field Perpendicular to the Junction

When a uniform field is applied perpendicular to a plane of a junction, the induced screening currents at the surface of the superconducting films generate local magnetic field parallel to the plane of the junction as shown in Fig. 2.4. This field changes the phase difference $\varphi(x,y)$ across the junction and then alters the Josephson current density.

Miller et al.[Miller et al., 1985] worked out the appropriate expressions for the interior magnetic field and corresponding phase across the junction for a cross type S-N-S Josephson junction. In the first approximation, $\Theta(x,y)$ is given by

$$\Theta(x,y) = -8\pi \cdot \left(\frac{H_z}{H_o}\right) \cdot \left(\frac{xy}{W^2}\right) \tag{2.20}$$

The critical current is now calculated by inserting (2.20) into (2.16). The result is

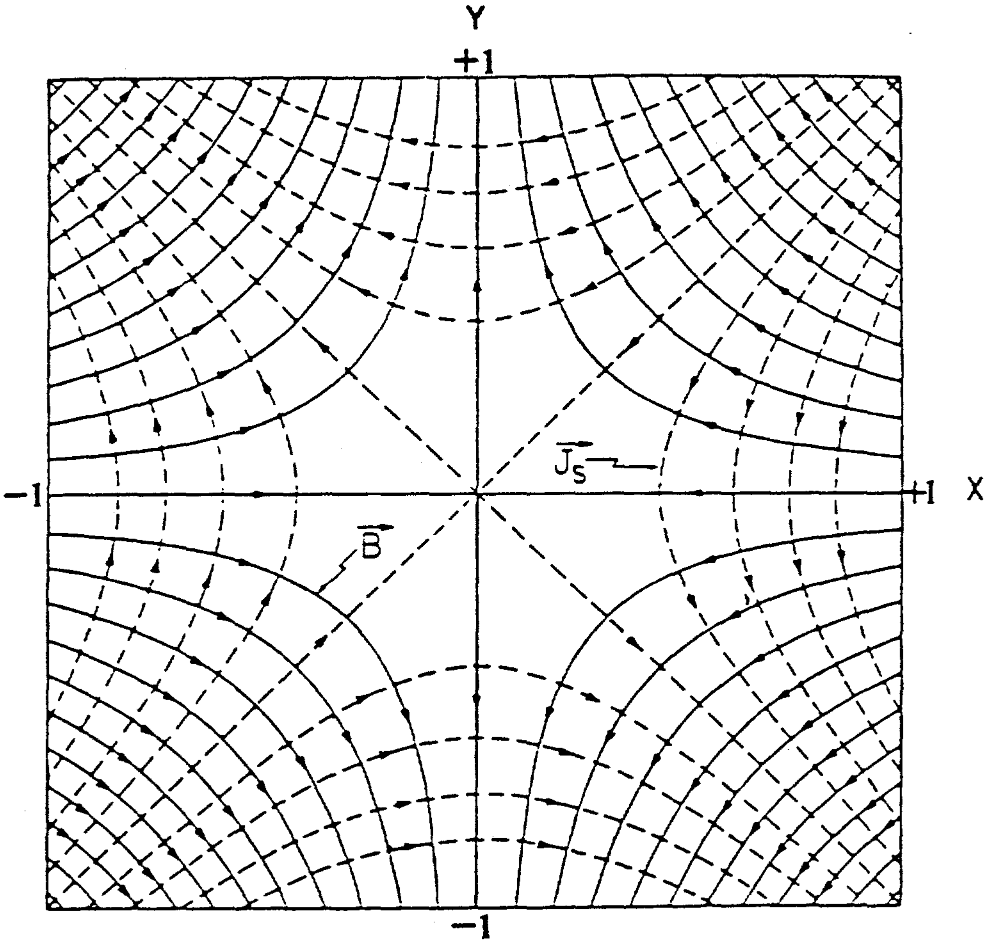

Fig. 2.4. Field lines inside the junction and induced current in the top surface(inner surface) of the bottom superconductor due to the perpendicular field along the + *z* axis. The *x* and *y* coordinates are in units of *W*/2.

$$\frac{I_c}{I_o} = \left|\frac{Si(\alpha)}{\alpha}\right| \tag{2.21}$$

where $Si(\alpha) = \int_0^\alpha \frac{\sin x}{x} dx$, the sin integral, and $\alpha = 2\pi \cdot \frac{H_z}{H_o}$. This function is plotted in Fig. 2.3b. I_c decreases quadratically as H_z increases at low field ($\alpha << 1$), and as $\frac{1}{H_z}$ at large field ($\alpha >> 1$). A good fit to this behavior was done by Miller et al.[Miller et al., 1985] using their S-N-S Josephson junctions.

2.2.2 Electrodynamics of the Josephson Junction

As we discussed above, external electric and magnetic fields can change the phase difference φ in time and space. We can combine these spatial and temporal dependence to describe the phenomenology of a Josephson tunnel junction. Assuming nonzero magnetic field in both *x*- and *y*- directions, we obtain same as (2.9) and (2.10).

$$\begin{aligned} \frac{\partial\varphi}{\partial x} &= \frac{2\pi}{\Phi_o} d_{eff} H_y \\ \frac{\partial\varphi}{\partial y} &= -\frac{2\pi}{\Phi_o} d_{eff} H_x \end{aligned} \tag{2.22}$$

These relations together with the Josephson current-phase relation (2.1) can be combined with the Maxwell equation,

$$\vec{\nabla}\times\mathbf{H}=\frac{4\pi}{c}\mathbf{J}+\frac{1}{c}\frac{\partial\mathbf{D}}{\partial t} \tag{2.23}$$

which in our case reduces to

$$\frac{\partial H_y}{\partial x}-\frac{\partial H_x}{\partial y}=\frac{4\pi}{c}J_z+\frac{1}{c}\frac{\partial D_z}{\partial t} \tag{2.24}$$

With $D_z=4\pi\sigma=4\pi CV$, $C=\varepsilon/(4\pi d_n)$ is the junction capacitance per unit area and ε is the dielectric constant associated with the barrier of thickness d_n. Finally we obtain,

$$\frac{\partial^2\varphi}{\partial x^2}+\frac{\partial^2\varphi}{\partial y^2}-\frac{1}{v^2}\frac{\partial^2\varphi}{\partial t^2}=\frac{1}{\lambda_J^2}\sin\varphi \tag{2.25}$$

where $\lambda_J=\left(\frac{\hbar c^2}{8\pi e d_{eff}J_o}\right)^{1/2}\left\{=\left(\frac{\hbar}{2e\mu_o d_{eff}J_o}\right)^{1/2}(\text{in MKS unit})\right\}$ (2.26)

is called the Josephson penetration depth, and

$$v=c\left(\frac{1}{4\pi C d_{eff}}\right)^{1/2}=c\left(\frac{d_n}{\varepsilon\cdot d_{eff}}\right)^{1/2} \tag{2.27}$$

is the propagation velocity of the electromagnetic field in the barrier.

Equation (2.25) wholly governs the electrodynamics of the Josephson junction for nonzero V. The character of the parameter λ_J is easily found by considering the time-independent case in the limit of small φ ($\sin\varphi \approx \varphi$). Then one dimensional solution $\varphi \approx \exp(-x/\lambda_J)$ is obtained. Thus λ_J has the meaning of a penetration depth, in analogy with the London penetration depth λ_L. λ_J relates to the dc Josephson supercurrents flowing in the junction. The idea is that the Josephson currents will generate magnetic fields (the self-fields) which are allowed to penetrate the superconductor to within a distance λ_J from the edge. These fields are screened from the interior of the superconductor by the generation of screening currents which flow in a direction opposite to the Josephson current. This effect forces the Josephson currents to be confined to the edges of the junction. Note that the typical values of the London penetration depths λ_L are of the order of tens of nanometers whereas λ_J is of the order of hundreds of micrometers.

The small and large junctions are defined in comparison with the λ_J. In small junction λ_J is larger than the size of the junction(*W*) and the Josephson current density through the junction area is essentially uniform. In large junction where $\lambda_J < W$, on the other hand, the self-field is not negligible and the Josephson currents are confined to the edges of the junction. In our experiments, we focus on the small junction limit, where J_o is spatially uniform.

2.3 Distortion of the Fraunhofer Pattern

Vortices of magnetic flux trapped in a Josephson junction can have a profound effect on the critical current of the junction [Hebard and Eick, 1978]. There are two types of vortex structures for a trapped vortex, one that channels through both superconducting films and a second that goes through just one film. as shown in Fig. 2.1. In the case of Fig. 2.1b, the locations where the vortex penetrates the top and bottom superconducting layers will in general not be exactly lined up because the pinning sites are randomly located. If a vortex perfectly lines up, it will not significantly affect the Josephson current because there is no net field parallel to the layer. In the case of Fig. 2.1a, the flux lines are confined in the barrier, and leak out of the edge of the junction because the top superconducting layers expels the flux from the vortex. In both cases, the resulting parallel component of the flux lines in the junction will affect the Josephson current in that region because the phase difference φ is altered by the field.

When a vortex is trapped inside the junction as shown in Fig. 2.1a, one pole of the vortex is inside the junction and the other pole is outside the junction. The inner pole acts like a source (or sink) of magnetic flux with total flux equal to Φ_o, while the outer pole is completely shielded by the superconductor so that it does not have any influence on the current characteristics of the junction. Therefore such a single vortex may be regarded as a magnetic monopole as long as we are concerned about the Josephson current only. It is assumed here that the core size of the vortex is much smaller than the size of a junction.

Generally, many vortices may be trapped within the junction, that is, many positive or negative vortices according to the direction of the trapped field lines. They can be in one layer or in both layers magnetically coupled each other.

Now we will introduce the basic assumptions used in our experiments. First, the magnetic coupled vortex (or dipole) is assumed to be a linear superposition of the fields from two single vortices as shown in Fig. 2.5c. Second, the single vortex can be approximated by a magnetic monopole charge in Fig. 2.5d. Third, individual

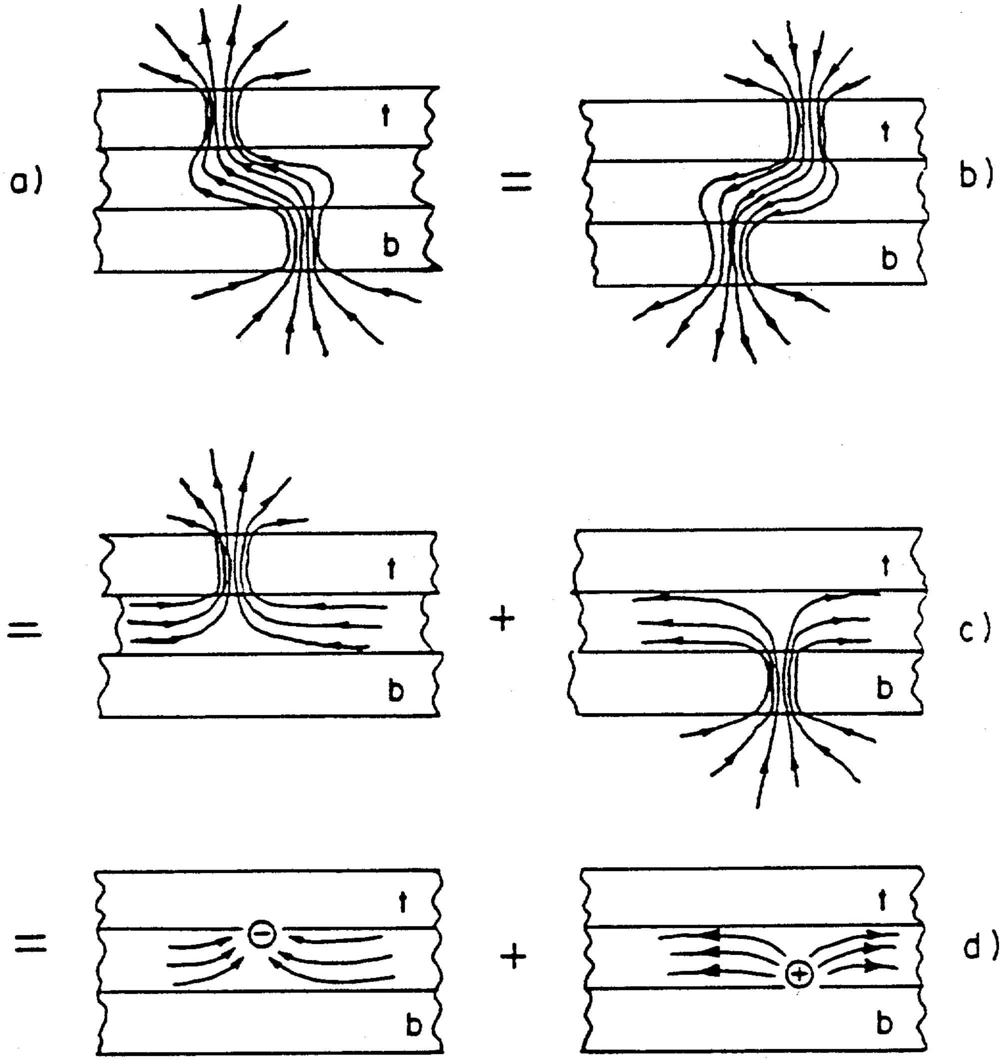

Fig. 2.5. Theoretical treatment of a vortex.

(a) A misaligned dipole vortex in a junction. *t* and *b* denote the top and the bottom superconductor respectively.

(b) Theoretically equivalent dipole to (a). The theory treats the flux lines inside the junction only.

(c) Linear superposition.

(d) Magnetic monopole charge approximation.

single vortices are independent from each other, so that the total field arising from the vortices inside the junction is the linear superposition of the fields contributed by all individuals. Thus, the total phase difference across the junction is to be the linear superposition of phase contributed by all individual vortices plus the external field.

2.3.1 Field and Phase Produced by a Single Vortex

Let's consider the field and phase produced by a single vortex at $\mathbf{r}_\pm$. The magnetic field intensity due to the vortex, $\mathbf{H}_{vortex}$, has spatial dependence on the position of the vortex at $\mathbf{r}_\pm$, and given by [Miller et al., 1985]

$$\mathbf{H}_{vortex} = \pm \frac{\Phi_o}{2\pi|\mathbf{r}-\mathbf{r}_\pm|\cdot d_{eff}} \cdot \frac{\mathbf{r}-\mathbf{r}_\pm}{|\mathbf{r}-\mathbf{r}_\pm|} \tag{2.28}$$

where $\mathbf{r}_\pm$ is the vector from the origin to the vortex and the "+" or "-" signs are associated with a positive or negative vortex respectively. Magnetic field lines due to a positive vortex are shown in Fig. 2.6a.

The phase produced by this vortex can be obtained by considering the magnetic flux enclosed in the area between the z- axis and $\mathbf{r}$. The magnetic flux enclosed in the area between the z- axis and $\mathbf{r}$ is $\pm\frac{\Phi_o}{2\pi}\Theta_\pm(\mathbf{r})$, where $\Theta_\pm$ is the angle between $-\mathbf{r}_\pm$ and $\mathbf{r}-\mathbf{r}_\pm$ as shown in Fig. 2.6b. We know that $\Theta_\pm$ exactly represents the relative phase at point $\mathbf{r}$ caused by the vortex at $\mathbf{r}_\pm$ as shown by equation (2.13). After a simple calculation and proper choice of the constant phase φ_o, we find that the phase at $\mathbf{r}$ produced by a vortex at $\mathbf{r}_\pm$ can be obtained as

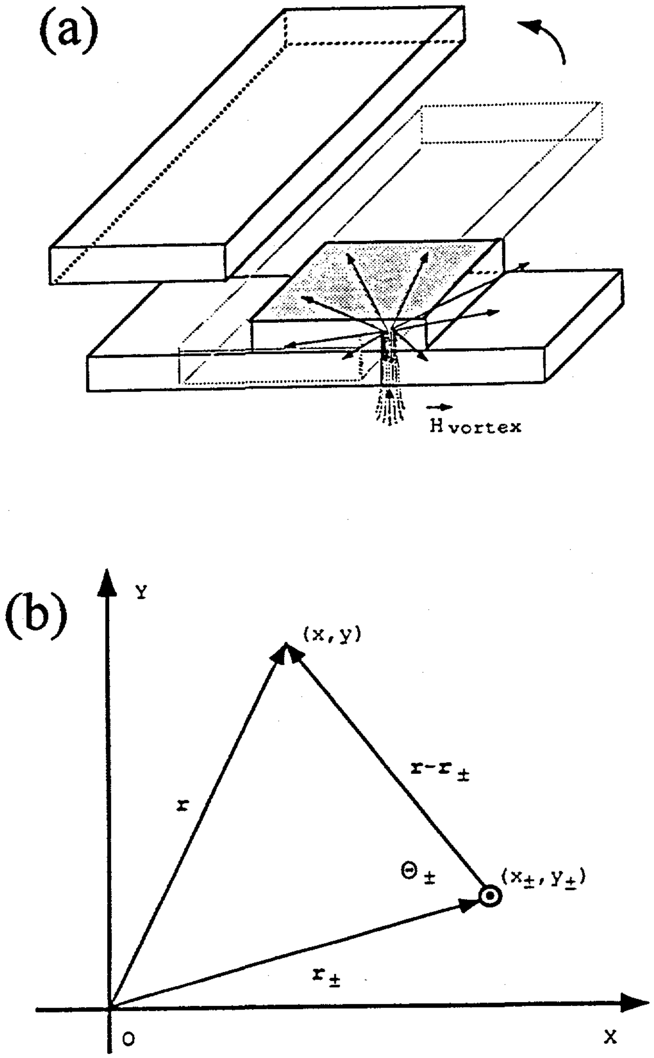

Fig. 2.6. The magnetic flux lines generated by a vortex trapped in the bottom superconducting layer as shown in (a). The top superconducting layer has been lifted up to show the flux lines in the barrier which are parallel to the junction. The phase at $\mathbf{r}$ due to the vortex at $\mathbf{r}_\pm$ is calculated by the coordinate system of (b). The angle $\Theta_\pm$ is just the relative phase at $\mathbf{r}$.

$$\Theta_{\pm}(x,y) = -\tan^{-1}\left(\frac{y-y_{\pm}}{x-x_{\pm}}\right) \tag{2.29}$$

The total phase difference across the junction contributed from all individual vortices is

$$\Theta_{v}(\mathbf{r}) = \sum\nolimits_{+}\Theta_{+}(\mathbf{r}) - \sum\nolimits_{-}\Theta_{-}(\mathbf{r}) \tag{2.30}$$

In this linear superposition of the phase, we neglect core effects because their influences on I_c scales with the ratio of the core area to the junction area, which is negligibly small in our experiments. Any boundary conditions of vortex-generated flux line leaking out of junction area are not considered in equation (2.29), that is, infinite extent of the junction area is assumed. As a result, the accuracy of equation (2.30) is questionable when an individual vortex is near an edge.

When a single vortex is trapped inside a junction, the screening currents are generated to exclude flux lines from the superconducting layers, so resultant direction of the vortex field near the core is radial in the x-y plane of the junction inside. The screening currents are circular near the vortex, while at the boundary of the junction, they should be parallel to the edge. Therefore, the field lines are perpendicular to the edge. This configuration of the flux lines can be achieved by introducing image vortices outside the junction area.

By assuming the single vortex to be a magnetic monopole charge, the problem becomes mathematically same as the 2-D electrostatic problem, where an electric charge is in a grounded rectangular box. The charge generates infinite number of image charges outside the box. In the single vortex situation, the images are produced all over the x-y plane to form the image vortex lattice [Hyun, 1987]. The estimation of the phase arising due to a single vortex will be actually the sum of that from the real vortex plus an infinite number of image vortices.

$$\Theta(\text{vortex}) = \Theta(\text{real vortex}) + \sum_{\text{all}} \Theta(\text{images}) \tag{2.31}$$

As the number of images grows, more exact solution can be obtained. According to equation (2.29), those images further away from the junction contribute less to the phase change. The exact solution of estimating the phase from all images was obtained by J. R. Clem [Clem, unpublished]. Practically 24 images came out to be good approximation in the previous work [Hyun, 1987].

The phase term contributed by image vortices is not negligible, especially when the vortex is near the edge of the junction. The magnetic field line generated by a single vortex near the edge is strongly bent toward the edge and perpendicular to it in order to satisfy the boundary conditions. The phase induced by such a kind of field greatly differs from that of the single vortex in the infinitely large plane. Thus the image correction is rather important. For the critical current calculations, hereafter, the correction by including all the images has been considered for the phase and field produced by the vortex.

2.3.2 Josephson Current Density Dependent on a Single Vortex

In the above discussion, we know that a vortex trapped inside the junction produces the phase difference across the barrier and then the Josephson current density changes according to the equation (2.1). In addition, we expect the Josephson current density follows the magnetic field distribution pattern. Fig. 2.7 shows the distribution of the normalized Josephson current density $J(\mathbf{r}) / J_o$ for a positive vortex at $\mathbf{r}_\pm = (0.01,\ 0.01)$ in reduced coordinate, near the center of the square junction. We know that according to equation (2.29), the phase due to the vortex changes from $-\pi$ to π as the observing point crosses the diagonal line of the first quadrant and also the phase is zero on the diagonal line of the third quadrant. If we set the constant term in phase, φ_o, to be $\pi/2$, the current distribution has the lowest value $(-J_o)$ on the diagonal line in the first quadrant and the highest value $(+J_o)$ on the diagonal line in the third quadrant. The solid contour lines in Fig. 2.7 represent $+J$ while the broken lines represent $-J$. If the vortex is located at the center of the junction, the current distribution is perfectly symmetric with respect to the diagonal line through the 2nd and 4th quadrant along which the current density is zero. So the total critical current, I_{co}, becomes zero. The positive (negative) contribution to the Josephson current increases as the vortex moves out of the center of the junction as shown in Fig. 2.8 for a positive vortex at $(0.5,\ 0.0)$. The positive contribution corresponding to the solid contour lines occupies the most of the junction area, so the resultant positive total current I_{co} increases. Similarly, if the position of the vortex is $(-0.5,\ 0.0)$, the resultant negative total current I_{co} increases. Here one must note that only the magnitude of the total current has physical meaning because the current characteristics are to be same in both + and - z- directions. Thus the current distribution as a function of the vortex position has four fold symmetry in a square Josephson junction as the junction geometry does. With two vortices involved, the distributions of Josephson current density have

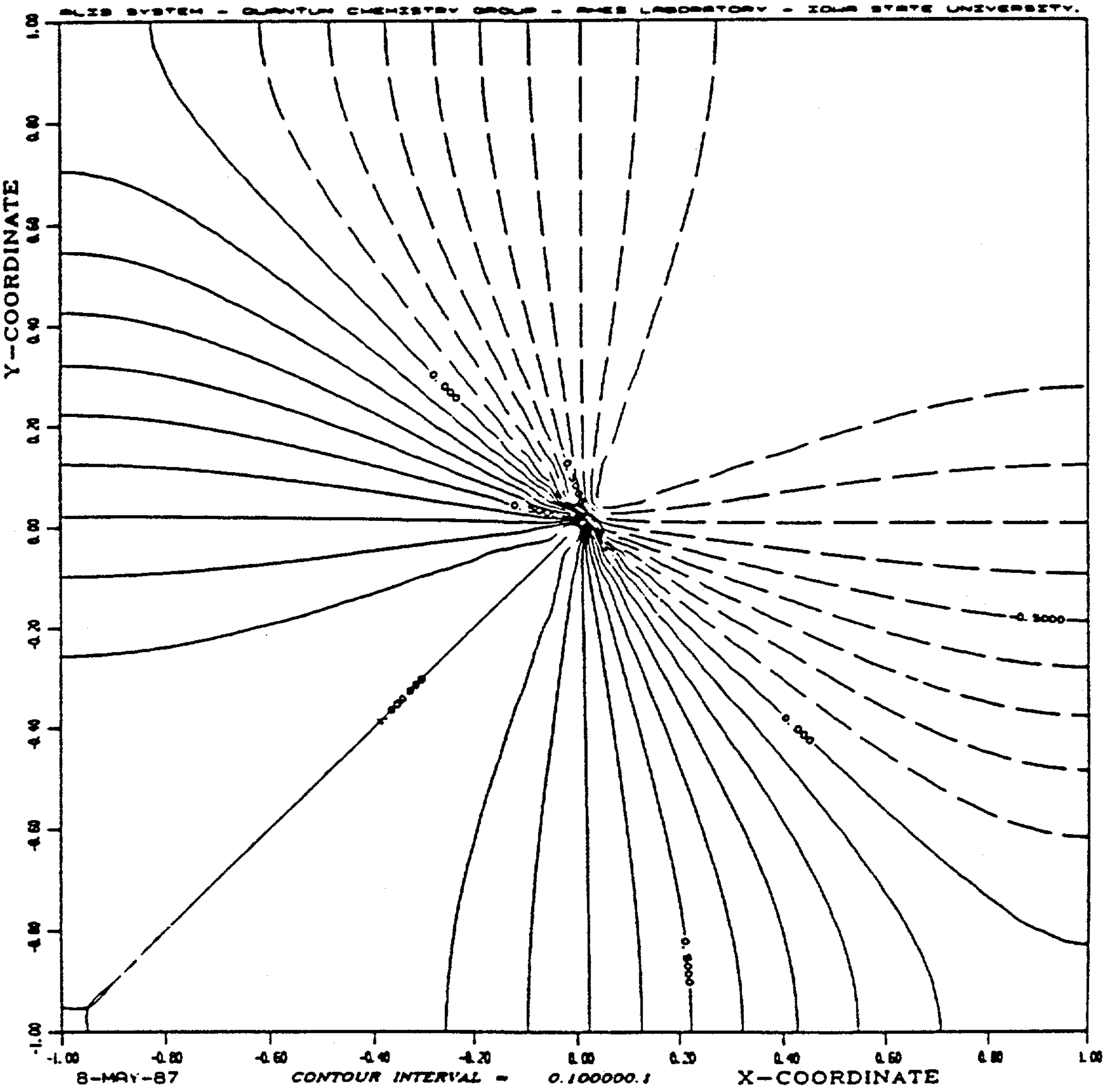

Fig. 2.7. Josephson critical current density J_c at zero field due to a single positive vortex at (0.01, 0.01) in the unit of $W/2$. All images are included in the calculation.

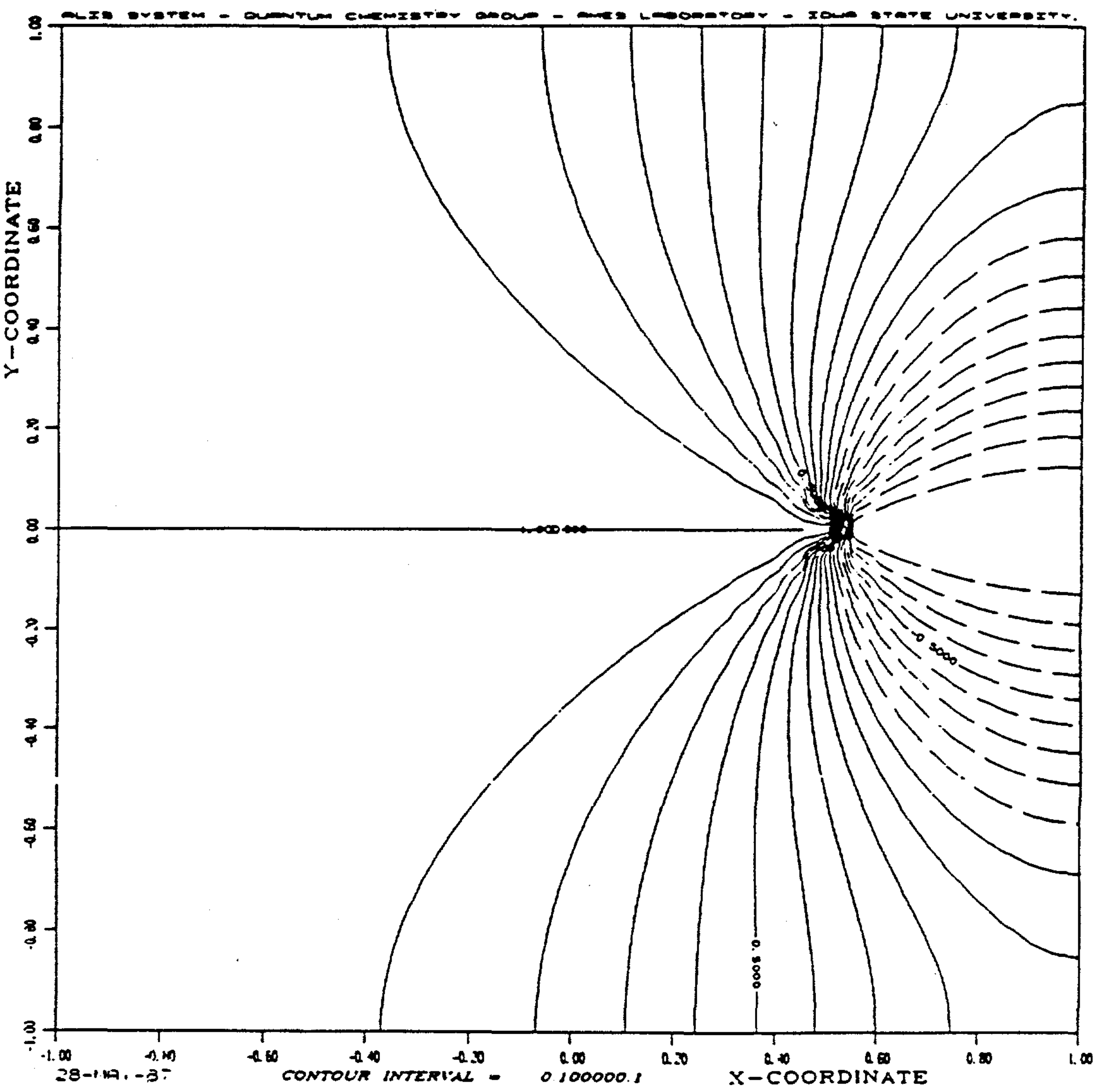

Fig. 2.8. J_c due to a single positive vortex at (0.5, 0.0)

been calculated by O.B. Hyun [Hyun, 1987] especially for a positive-negative dipole case.

2.3.3 Distortion of the Fraunhofer Pattern due to a Vortex

When the junction with the vortices is exposed to the external field $\mathbf{H}$, the total phase induced can be obtained by linear superposition as

$$\varphi(x,y) = \Theta(\mathbf{H}) + \sum\nolimits_{\text{all}} \Theta(\text{vortex}) \tag{2.32}$$

where $\Theta(\mathbf{H})$ is given by the external field $\mathbf{H}$, and $\Theta(\text{vortex})$ is contributed by all the vortices inside the junction area, including their images. After getting the total phase, the critical current I_c can be calculated by equation (2.16). Finally we get the diffraction patterns with the presence of both a vortex and external field. We notice that these diffraction patterns, I_c/I_o vs H_i/H_o where $i = x, y, z$ by scanning the value of external field H_i, become severely distorted. Because this distortion is uniquely dependent on the vortex configuration, except geometrical symmetries, we can use it to locate the vortex inside the junction.

In Fig. 2.9, we see the change of diffraction patterns calculated theoretically according to the various positions of a single positive vortex together with the perfect Fraunhofer pattern which represents no trapped vortex. As the vortex moves from the edge to the center, $I_c(H=0)$ becomes more suppressed and finally the central peak of I_c vs H_y splits into two parts. It is especially interesting to note that the value of I_c at zero field diminishes to zero when the vortex is at the center. For the I_c vs H_z pattern, it is symmetric in H_z without the vortex. With the single

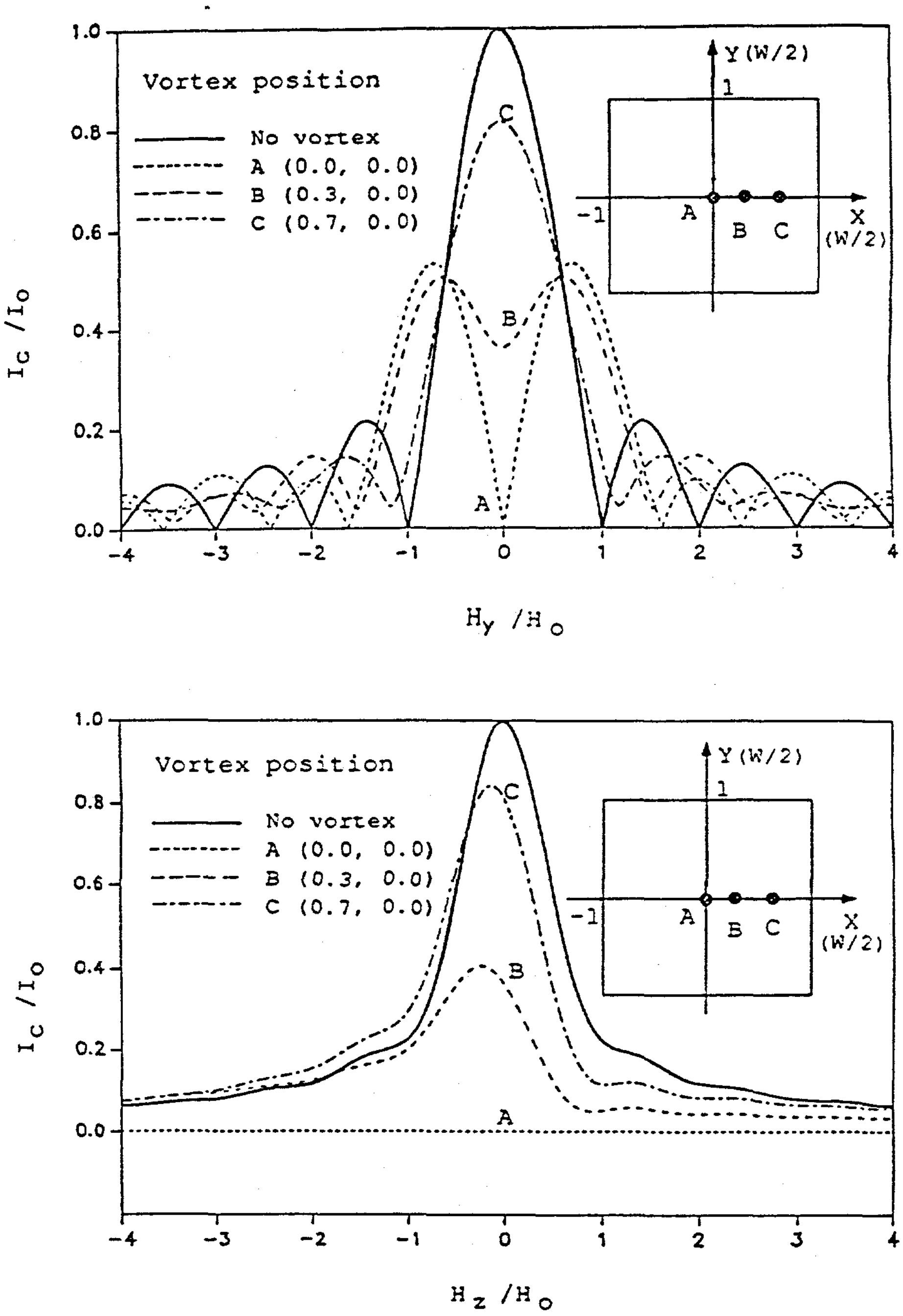

Fig. 2.9. Diffraction patterns, I_c/I_o vs H_y/H_o, and I_c/I_o vs H_z/H_o, for various single vortex positions

vortex, however, the pattern is no longer symmetric. Cancellation of J_c values by symmetry causes I_c to be zero for all H_z's when the vortex locates at the center.

The vortex diffraction pattern is strongly affected by the parallel component of the vortex field inside the junction. When the vortex is near the edge, this component is quite well localized between the vortex and its nearest image, so that influence to the perfect Fraunhofer pattern is weak. As the vortex approaches the center, the image effect becomes weaker, so the vortex field strongly affects all over the junction area. Hence the diffraction pattern is severely distorted. The ratio of the critical current of a junction containing a vortex at zero field I_{co} to the critical current of the same junction without a vortex at zero field, I_o is very useful diagnostic tool to investigate the first sign of the nucleation and motion of a vortex in our experimental procedures. Fig. 2.10 shows that this ratio, I_{co}/I_o, is monotonically decreasing as a function of the single vortex position changing from the edge to the center of the junction.

While we investigate the change of diffraction pattern in this experiment, we focus on the single vortex case, because it has less varieties and more distinguished features than two more vortices involved. In addition, the most noticeable feature in the diffraction pattern of the Josephson junction containing a single vortex happens in a range of a few H_o, typically H_x and H_y in between $\pm 2H_o$. Thus most information needed to determine the vortex location is included in this low field data.

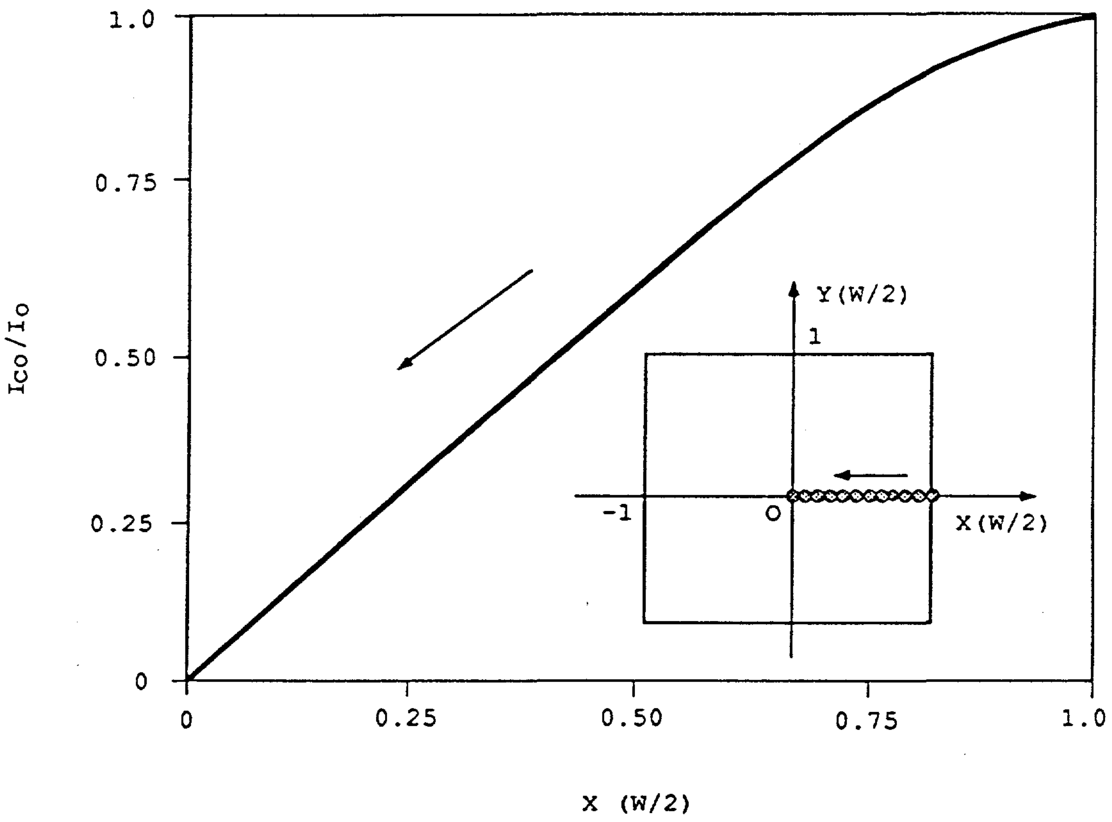

Fig. 2.10. I_{co}/I_o monotonically changes as a function of the single vortex position in the junction. The inset shows a vortex progressing from the edge to the center.

2.3.4 Symmetry of a Vortex Configuration and Symmetry Breaking

In order to correctly map out a vortex configuration, we should consider the geometrical symmetries of the junction because different vortex configurations can possibly generate the same diffraction pattern. It is valuable to notice that the cancellation and addition between vortex field and external field inside the junction barrier cause the asymmetry of the pattern, I_c vs H_y. For example, for a positive vortex at upper half of the junction, $H_y > 0$ is canceled in larger area of the junction, while added in smaller area. Thus the peak value of I_c lies in $H_y > 0$ value. Similarly, the peak value of I_c lies in $H_y < 0$ value if the vortex locates at lower half of the junction. Thus changing the field direction is equivalent to changing the vortex position from $(x,\ y)$ to $(x,\ -y)$. The above discussion is also true for H_x if x and y are exchanged each other. Considering the parallel field H_y only, the symmetries are shown in Fig. 2.11. The diffraction patterns I_c vs H_y of two single vortices at (x_0, y_0) and $(-x_0, y_0)$ are same. In addition, we obtain the same diffraction patterns by reversing the pole of vortex and changing the vortex position from y_0 to $-y_0$. Thus any of the four locations in Fig. 2.11a has the same I_c vs H_y pattern. Some methods to remove the ambiguity in determining the vortex position have been done in our experiment by investigating the response of the vortex to external forces such as those caused by transport current or perpendicular field. By measuring the critical current I_c after applying the transport current I_{py}, we can tell which one of the group, shown in Fig. 2.11b and Fig. 2.11c, is possible. Next in the presence of H_z, the force to the positive vortex is along the field line, while against for a negative vortex. So two vortices with different poles move same direction as shown in Fig. 2.12. By measuring I_c, we can tell the type of vortex pole. This idea has been also performed by Miller, Hyun, and Li in their earlier works. After determining the pole type and position of the nucleated vortex, we don't need to check any more because the nucleation of a vortex is quite reproducible.

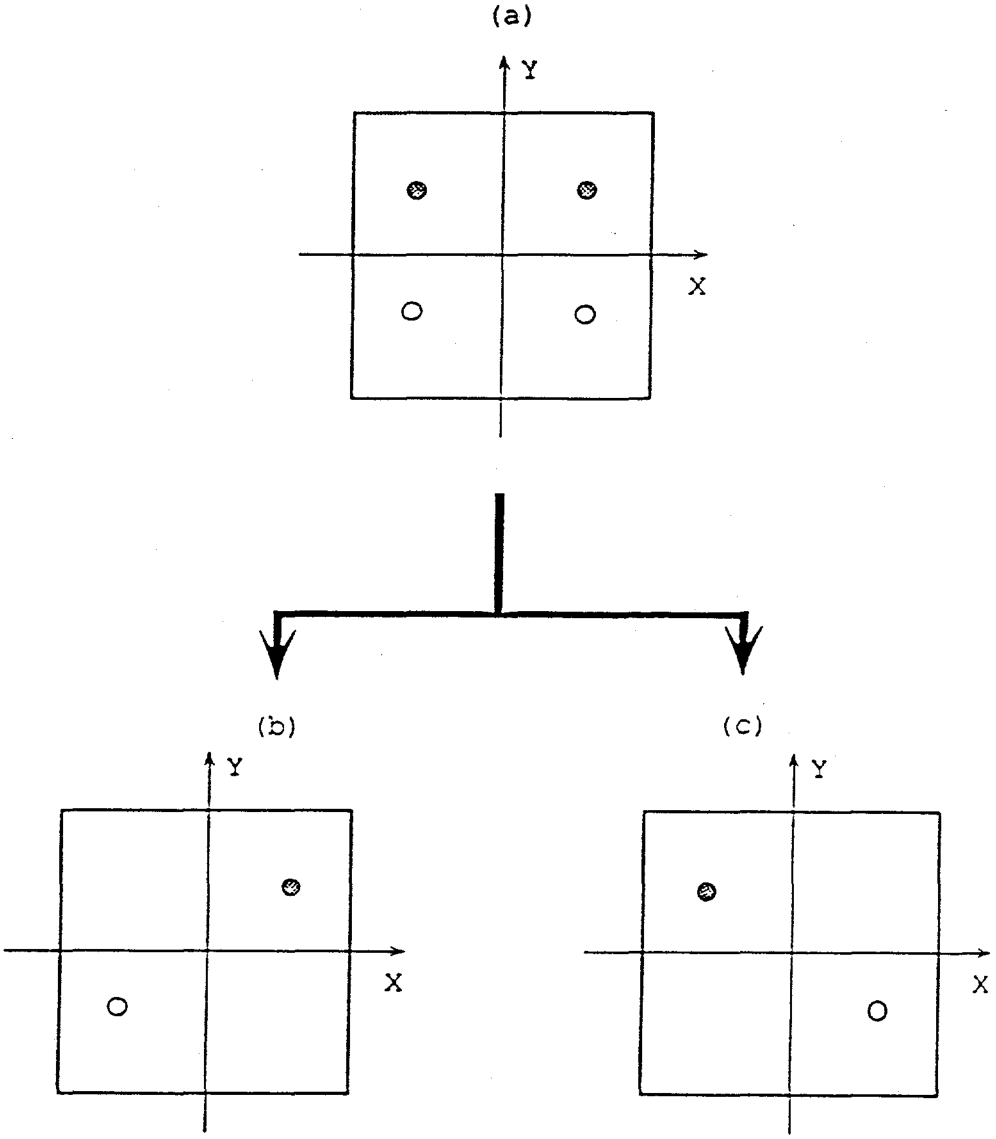

Fig. 2.11. Sketch to show that different vortex locations can produce the same diffraction patterns, where the vortex pole symbolized by open circle is opposite to that of solid circle. Any of the four locations in (a) has the same I_c vs H_y pattern. After applying I_{py}, we can tell which one of the group (b) and (c) is possible.

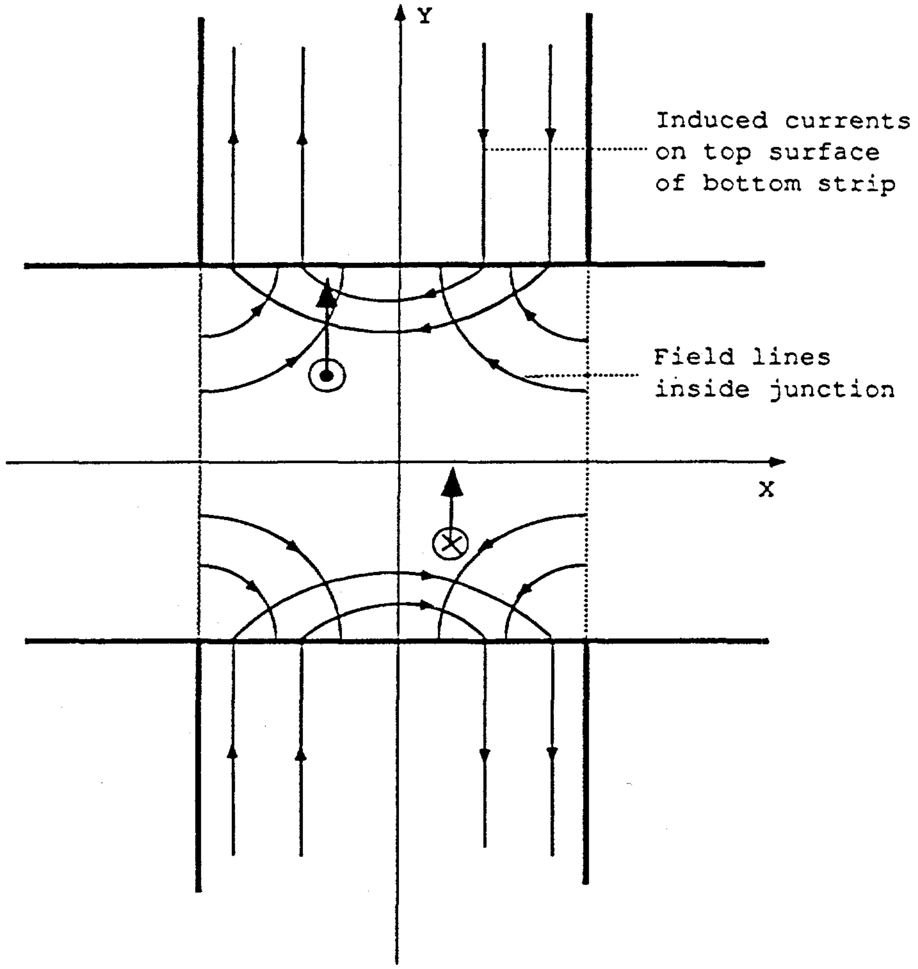

Fig. 2.12. The magnetic field lines in the junction barrier and induced screening currents on the top surface of the bottom Pb film generated by a perpendicular magnetic field H_z.

CHAPTER III. EXPERIMENTAL DETAILS

In this chapter, we present the experimental details of sample fabrication and data acquisition. The basic properties of this type of Josephson junction will be discussed, including the investigation of junction quality.

3.1 Fabrication of S-N-I-S Josephson Junctions

The central experimental problem in constructing a Josephson junction to study the motion of a single Abrikosov vortex is to make the barrier uniform enough to give good Fraunhofer diffraction patterns and still have the desired thickness and impedance. Superconductor-normal metal-superconductor (S-N-S) junctions were used for all of the earlier work [Miller, 1984; Hyun, 1987] in this field. The difficulty with the S-N-S junctions, however, is that the impedance is very low so that voltages are in the pV range and require superconducting quantum interference device (SQUID) detection. A more appropriate combination is a S-N-I-S type junction, in which I layer provides most of the impedance and N layer gives thick barrier needed to decouple the magnetic monopoles on each side of barriers. Two examples are the work of Li and Sanders [Li and Finnemore, 1991; Li et al., 1991; Sanders et al., 1993] with a cross-strip Pb/Al/Al_2O_3/PbBi, (S-N-I-S) junctions which were constructed by thermal evaporation system, and a Nb/Al/Al_2O_3/Nb was prepared by the dc magnetron sputtering system in recent work [Sok and Finnemore, 1994].

3.1.1 Thermal Evaporation for Pb/Al/Al_2O_3/PbBi Junction

The first step in junction fabrication is to prepare a substrate with an array of Au lines. A Si wafer is oxidized to give an insulating layer on the surface, and then the wafer is sequentially coated with a 10 *nm* thick layer of Ti and a 20 *nm* thick layer of Au. The function of the Ti is to provide a better sticking coefficient for the Au. Standard photolithography techniques were used to form an array of parallel Au strips approximately 2 μm wide spaced 60 μm apart. Only one Au line was in contact with the subsequently deposited Pb film, but the array of Au lines was necessary because the placement of the Pb strip relative to a single Au line was not sufficiently precise. The goal was to have one Au line lying near the center of the Pb strip. A gold strip in contact with the Pb film provides suitable pinning sites because normal electrons from the Au cross into the Pb and suppress the order parameter in that region of the Pb [Campbell and Evetts, 1972]. The presence of Pb_3Au precipitates that may form [Lahiri, 1978] near the Au strip also could provide pinning. A cross strip S-N-I-S junction consisting of Pb/Al/Al_2O_3/PbBi was deposited by the thermal evaporation system on the substrate, with the Pb strip nearly parallel to the Au lines. A sketch of the evaporation system used for sample preparation is shown in Fig. 3.1. The entire junction deposition process was carried out in a vacuum system with a base pressure less than 1×10^{-8} *Torr* and without opening the vacuum system.

The substrate with Au lines was attached to a copper block(1″×0.5″×0.5″) with Apiezon-N grease. The copper block act as a heat reservoir during evaporation. The substrate was always lifted by a Teflon string attached to the

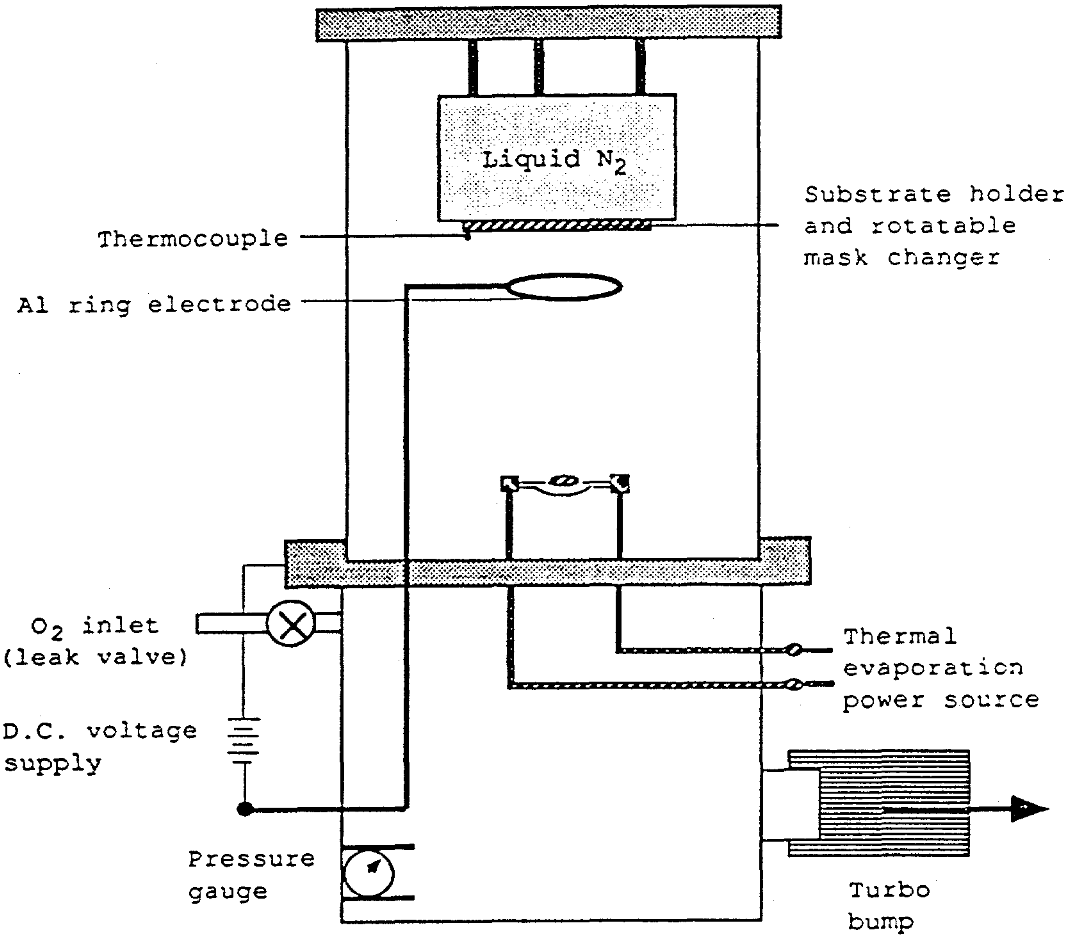

Fig. 3.1. A sketch of the evaporation system for sample preparation.

copper block in order to avoid scratching the pre-deposited film while changing the masks. The bottom strip of superconducting film (Pb layer) was evaporated from an electrically heated molybdenum boat at a rate of about 50 *Å/sec*. A large pad of pure Al about 1*mm* square was evaporated from an electrically heated tungsten coil basket at a rate of 20 *Å/sec*, immediately after the first film was deposited. The oxidation of the deposited Al surface was done in a glow discharge of oxygen at a pressure of 50 *mTorr*, where a negative high voltage Al ring having inner diameter of 11 *cm* was placed 3 *cm* below the substrate holder. Oxygen gas was supplied through a leak valve inlet. The discharge process was carried out by -350~-400 dc voltage. It was found that it was much easier to control the growth of the oxide if the Al had a large area with the junction in the middle. The rotatable mask change was employed to rotate various masks for each film evaporation. For the top superconducting film deposition(Pb 2.5 at.% Bi layer), the mask for the bottom superconducting film had been rotated by 90 degrees so that the bottom and top superconducting films had exactly the same width and were perpendicular to each other to form a cross strip junction. The PbBi layer goes superconducting at a higher temperature than the Pb layer so the PbBi will act as a superconducting ground plane while a vortex is being nucleated in the Pb layer. The more detailed procedures was explained in the previous work [Li, 1991].

3.1.2 DC Magnetron Sputtering for Nb/Al/Al_2O_3/Nb Junction

Sputtering is an atom-by-atom process, instead of depending on heat to vaporize the material. The target is bombarded by ions which physically chip atoms off the target, causing them to be ejected from the target surface and subsequently strike the substrate and adhere. In this manner a high quality film is gradually built up. As vacuum technology became more sophisticated, sputtering was largely replaced by vacuum evaporation using electron beams or resistance heating techniques which offered higher rates of deposition. But the interest in sputtering as a film deposition technique persisted because many materials could not be evaporated by resistance heating method.

Because there are so many interactions among parameters in sputtering system, it is impossible to separate them completely. In this section, first we will give a brief, simple overview of this subject and then discuss the dc magnetron sputtering processes for Nb/Al/Al_2O_3/Nb Josephson junction.

3.1.2.1 Choice of Nb Superconducting Electrode

Nb/Al/Al_2O_3/Nb Josephson junction has been proved to have the high quality junction characteristics far surpassing those of other junctions made of various combinations of superconducting and barrier material [Gurvitch et al., 1983; Morohashi et al., 1985; Morohashi et al., 1987]. The inherent high quality characteristics of Nb/Al/Al_2O_3/Nb junction give a small leakage current in the subgap voltage region, a sharp gap voltage defined in Fig. 3.2, including excellent stability both during long term storage and thermal cycles, and controllability of critical current. Based on these reliable characteristics, Josephson integrated circuit technology using Nb/Al/Al_2O_3/Nb junctions has developed steadily since their first application to Josephson circuits in 1985. At present, it becomes possible to construct a small scale Josephson computing system, previously considered unfeasible due to unreliable lead alloy junctions.

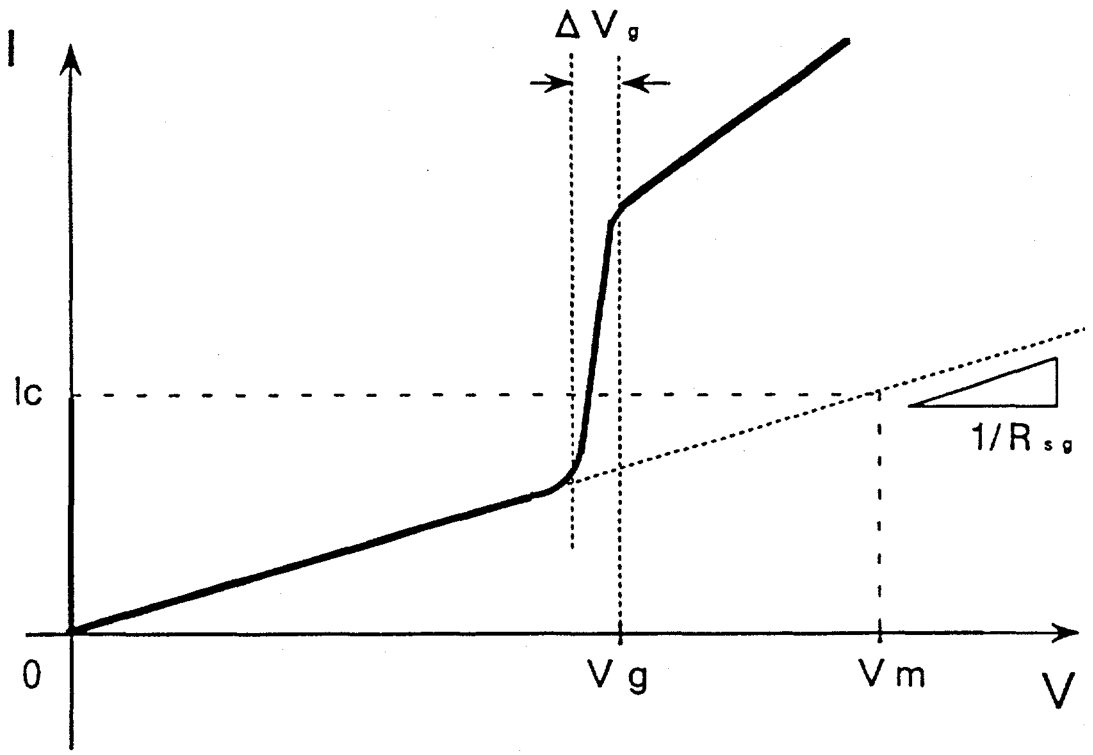

Fig. 3.2. Quality parameters of Josephson junction in *I-V* curve. V_m is defined by I_cR_{sg}. I_c is the Josephson critical current and R_{sg} is the subgap resistance which is normally defined by $2mV/I(2mV)$. V_g is the gap voltage. ΔV_g is the sharpness of the gap voltage. V_m and R_{sg} estimate the completeness of barrier. V_g estimates the superconductivity of S layer and proximity effect between S layer and barrier.

The superiority of $Nb/Al/Al_2O_3/Nb$ junction is mainly due to three properties : first is the stability of refractory Nb with hardness and smooth surface, second is the affinity of Al layer to underlying Nb, and third is the integrity of the thin Al_2O_3 grown on Al layer. The $Nb/Al/Al_2O_3/Nb$ multilayered structures are deposited in a single vacuum run to eliminate possible contamination around the Al_2O_3 barrier. The many successful operations have been proved that $Nb/Al/Al_2O_3/Nb$ junctions with high quality characteristics can be reproduced using a high vacuum sputtering system with double targets of Nb and Al.

3.1.2.2 Principle and Structure of DC Magnetron Sputtering Gun

Shown in Fig. 3.3 are the processes and structure of dc magnetron sputtering gun. This gives highly efficient plasma sputtering sources that depend on crossed electric and magnetic fields to produce high ion densities and high deposition rates with minimal substrate bombardment. Our 2-inch magnetron sputtering guns are commercially manufactured by AJA Int'l, and able to use for either a negative dc source or an alternating rf source. A toroidal shaped , closed path of the magnetic field is presented in order to trap and concentrate the electrons produced in the discharge at the target surface. This high density cloud of electrons promotes ionization of the high purity Ar sputtering gas (99.9995%) in the region close to the target surface. The target is fixed to a water-cooled cathode block that is electrically connected to a negative dc source. Positive Ar ions in the plasma are accelerated toward the target material and impact with energies of 100-800 eV. The effect of this Ar ion bombardment is to remove material, atom by atom, from the

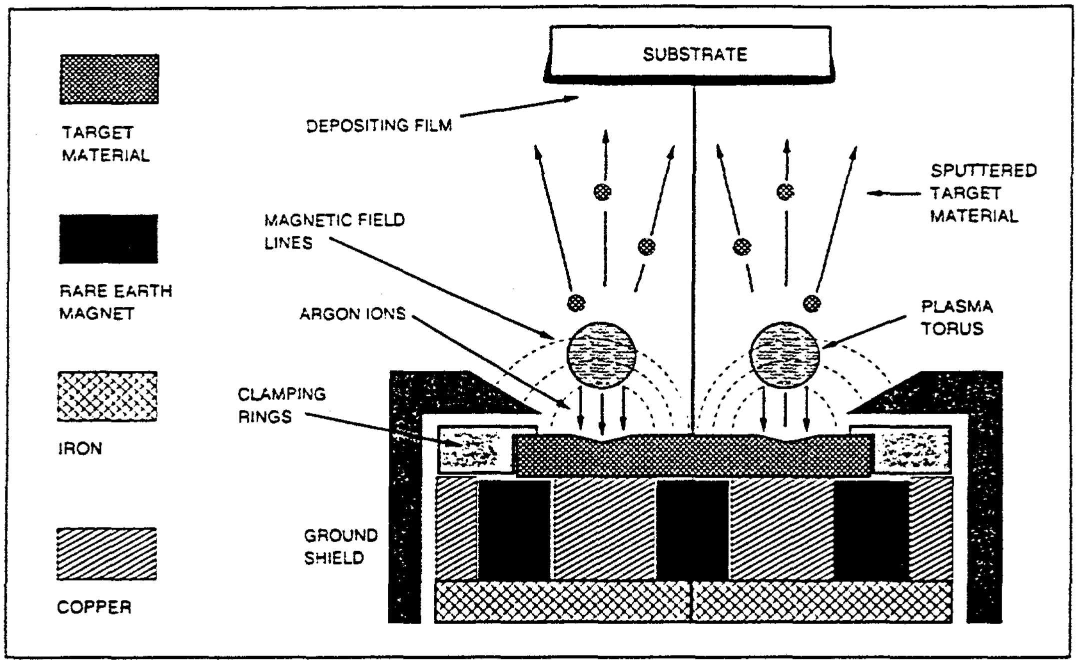

Fig. 3.3. Schematic representation of the gun's structure and sputtering process to produce thin films.

target and deposit it onto the substrate near the target surface. Because the electron leakage is restricted by the magnetic field, the bombardment of the substrate is minimized and the heating of the growing film and substrate is substantially reduced.

3.1.2.3 Hardware of the Sputtering System

As shown in Fig. 3.4, three guns which have Ag, Nb, and Al targets respectively, are built inside the chamber. Also each gun is connected to the dc power supply which reliably delivers the full power of 500 *V*, 3.0 *A* and has a full interlock string to prevent the application of high voltage when it is not desired. In our system vacuum interlock and water interlock for the guns are set up in the power supply. The use of shielding chimney in conjunction with the integral gas ring on the gun head further enhances the creation of a high pressure differential at the target surface which is necessary to sustain the plasma and prevent the cross contamination of targets. The gases (Ar, O_2) are supplied through a mass flow controllers which are connected to the power supply/readout to power and monitor the flow rate. A thermocouple is located near the substrate holder for monitoring the temperature of the substrate. Four legs with 5″ long are mounted between the sample holder and liquid nitrogen tank inside the vacuum chamber so that the short distance between target and substrate could act to increase the deposition rate and improve the thickness uniformity. As long as atoms travel in a straight line from target to substrate, it is possible to use masks to define film patterns. Rounding of the film edges arises from diffusive motion of the sputtered atoms. Once the film is

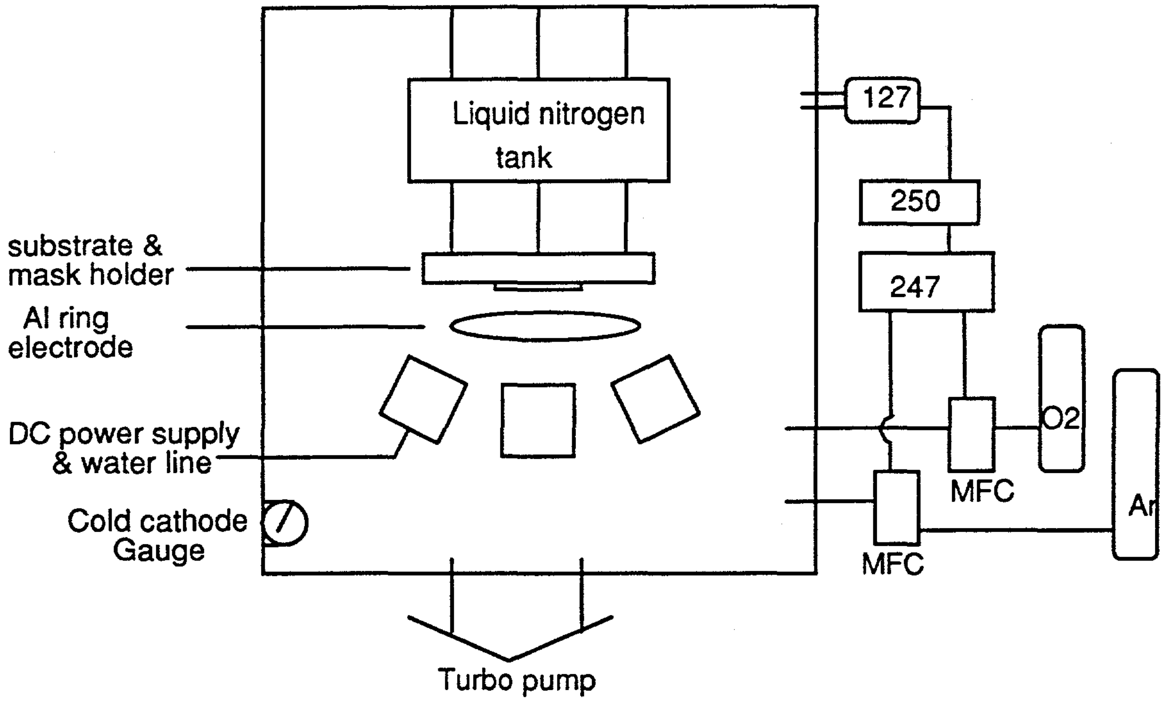

127 : Capacitance gauge
250 : Pressure & Flow controller
247 : Power supply & readout

Fig. 3.4. DC magnetron sputtering system for the fabrication of $Nb/Al/Al_2O_3/Nb$ junction.

deposited, the plasma oxidation process and rotatable mask change follow the same pattern as explained in 3.1.1.

3.1.2.4 Deposition Procedures and Optimal Conditions of Sputtering Parameters

Although the exact parameters for optimal deposition are system-dependent, some review papers [Imamura et al., 1992; Imamura and Hasuo, 1992; Shiota et al., 1992] give a guide for initial run. Listed below is the typical procedure followed in making junction.

<u>DC magnetron sputtering process sheet for Nb/Al/Al_2O_3/Nb junction</u>

1. Load an oxidized Si substrate in the mask holder
    Turn on mechanical pump
    Open roughing valve
    Turn on turbo pump
    Pump down to $< 2 \times 10^{-6}$ *Torr*
2. Bake out the chamber
    Vacuum reaches to $< 5 \times 10^{-8}$ *Torr* base pressure
3. Silver film for the contact of lead lines
    - Ag target : 2″ × 0.125″ circular sheet, 99.99% purity
    - Ar pressure : 2.5 *mTorr*
    - Cathode power : 0.5 *A*, 485 *V*, 248 *W*
    - Presputtering period : 3 *min.*
    - Sputtering period : 3*min* 30*sec*
    - Deposition rate : 35 *Å/sec*

4. Bottom Nb film
    - Nb target : 2″ × 0.125″ circular sheet, 99.9% purity
    - Ar pressure : 4.6 *mTorr*
    - Cathode power : 1.5 *A*, 323 *V*, 482 *W*
    - Use liquid nitrogen trap
    - Presputtering period : 10 *min.*
    - Sputtering period : 4 *min.*
    - Deposition rate : 14.5 *Å/sec*
5. Al film
    - Al target : 2″ × 0.125″ circular sheet, 99.999% purity
    - Ar pressure : 4.6 *mTorr*
    - Cathode power : 0.5 *A*, 409 *V*, 214 *W*
    - Use liquid nitrogen trap
    - Presputtering period : 10 *min.*
    - Sputtering period : 4 *min.* 30 *sec*
    - Deposition rate : 6.5 *Å/sec*
6. Oxidation of Al surface

    With the use of liquid nitrogen trap, pure oxygen gas was fed in through mass flow controller to 18 *mTorr*. The glow discharge was initiated by applying a dc voltage of about -400 *V* to -450 *V* on the aluminum ring for 2 minutes.
7. Top Nb film

    All parameters are same as those of bottom Nb case except 5 *min.* sputtering and 13 *Å/sec* deposition rate.

8. After whole deposition, the chamber was vented with the Ar gas. The junction surface was checked by optical microscope before making electric connections for low temperature measurements.
9. Thin platinum (or copper) wires are used as the contact lead line which is attached to the silver contact film by putting a small piece of indium on the platinum wire and applying pressure. In another method the wires were connected to the silver pad film by the indium soldering.

In the fabrication of Nb films, four sputtering parameters which are usually evaluated in terms of the stress, surface morphology, superconductivity, and crystal structure - Ar pressure, cathode current, cathode voltage, and deposition rate- critically affect the film properties. The Ar pressure and cathode current are independent parameters, but the cathode voltage and deposition rate depend on the two independent parameters. Besides the four sputtering parameters, film properties also depend on other factors such as the base pressure, substrate temperature, and distance between the Nb target and substrate [Huggins and Gurvitch, 1985]. After careful consideration through the published articles, the optimum sputtering parameters in the deposition procedures were determined by experimental try-and-error.

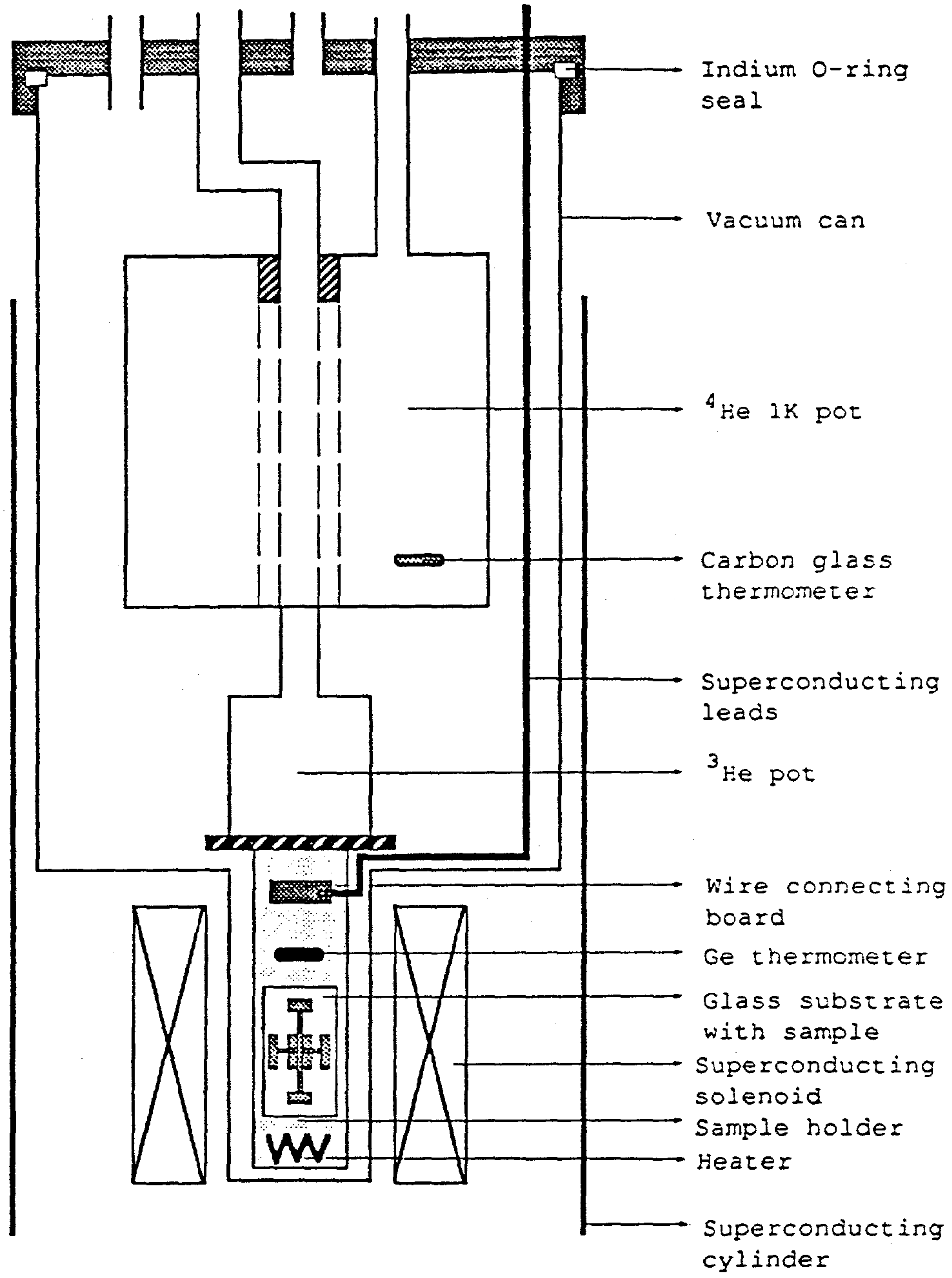

Fig. 3.5. Longitudinal section of cryostat.

3.2 Low Temperature Measurements

3.2.1 Cryostat

Fig. 3.5 shows a He^4 cryostat in which the sample was mounted. It can be operated between 0.4K and 15K. The substrate was attached with a thin layer of Apiezon N-grease to a 3/16" thick copper holder on the back of which is a calibrated germanium thermometer. A heater was also mounted on the copper sample holder for the purpose of temperature control. A temperature controller (Lake Shore Cryotronics, Model DTC 500-SP) was used to keep the sample temperature constant to a precision of a few millikelvin. To ensure a stable operating temperatures, a fairly low pressure ($< 1\times10^{-5}$ *Torr*) was maintained through the diffusion pump in the vacuum can which is sealed by an indium "O" ring. Two orthogonal magnetic fields could be applied to the sample using two pairs of properly oriented Helmholtz coils. The coils were mounted on the vacuum can surrounding the sample and inside the superconducting shield. Even with distortions of magnetic field by the lead cylinder and soldering blocks around the sample, the experimental results showed that parallel and perpendicular fields with good quality were produced by the coils. A superconducting lead cylinder is mounted just inside the helium dewar, which is surrounding the vacuum can and Helmholtz coil. The helium dewar was also surrounded by another μ-metal shield. This combination of shields not only provided the desired and stable magnetic environment surrounding the sample, but also sufficiently screened out electrical and magnetic noise from outside environment. The calibration constants of the magnets are very accurate to ± 3% error.

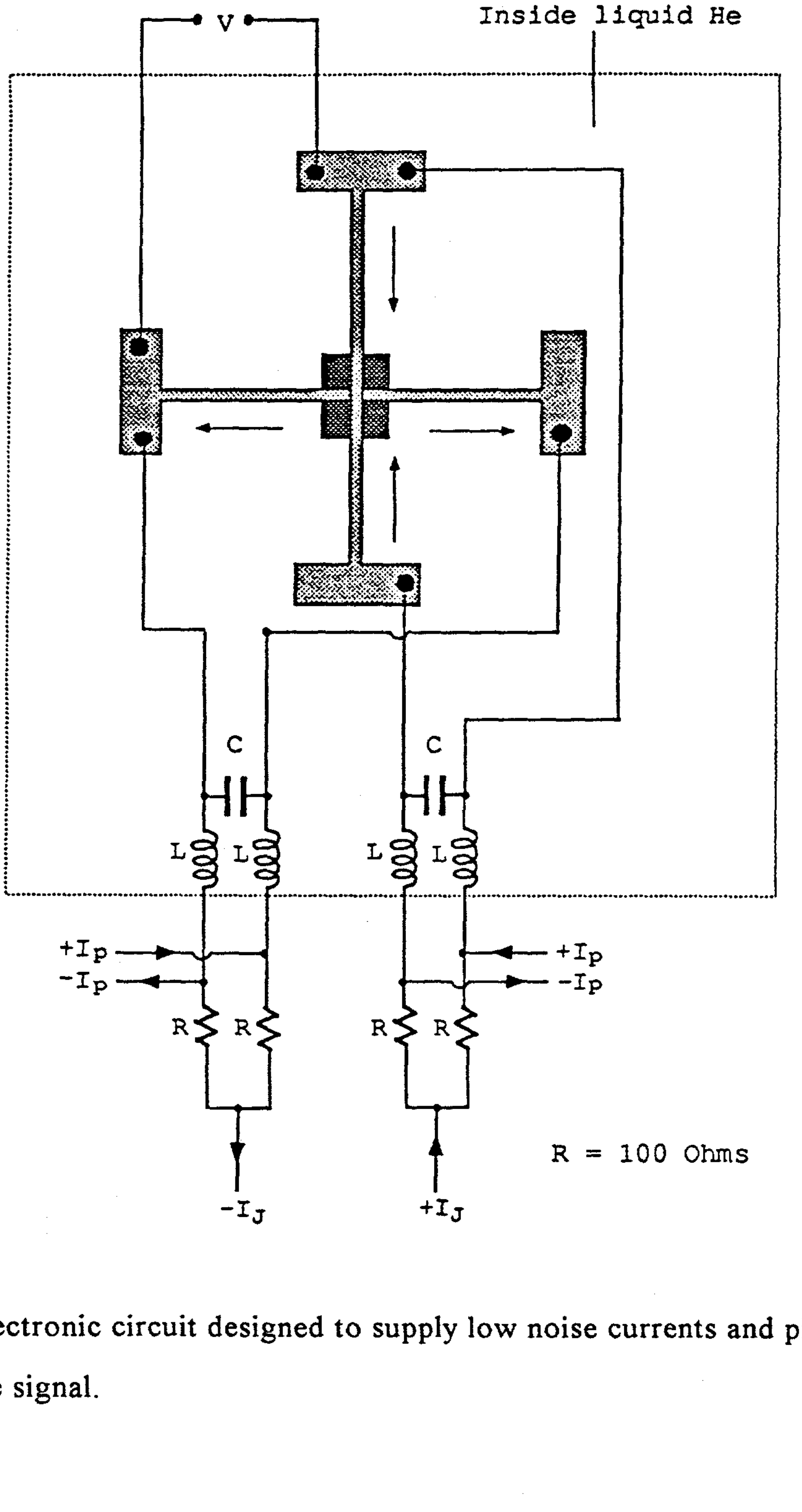

Fig. 3.6. The electronic circuit designed to supply low noise currents and pick up voltage signal.

Electrical connections for current and voltage leads were made using superconducting niobium wires which were extended to outside of the vacuum can. The electronic circuit in Fig. 3.6 are designed to supply the symmetric Josephson current and measure the junction voltage. Two low pass LC filters were used to feed low noise transport current, I_p, through one of the superconducting films. The symmetric supply of Josephson current was obtained by splitting I_J through two identical 100 Ω resistors (R). The total resistance of all connecting wire around the liquid helium temperature is negligibly small compared to R. The resistors have the effect of damping out induced currents arising from changing magnetic fields. Joule heat arising from various heating, cooling, and measuring operation inside the vacuum can was normally less than 0.5×10^{-6} watts so that Apiezon N-grease and GE 7031 varnish were adequate for thermal grounding.

3.2.2 Data Acquisition

In the present experiment, the main variables to be measured were critical currents as a function of fields and temperatures. The critical currents were measured by taking junction *V-I* characteristics at various values of field and temperature. The schematic diagram of whole measurement system is shown in Fig. 3.7. It consists of the temperature measurement, external field measurement, and the sweep of *V-I* curves at various fields. The measurements were performed by a computer, which also stored data. In order to get the critical currents I_c, the raw data of *V-I* curves were fitted by a *V-I* fitting program and the *V-I* fitting processes were monitored in the computer screen. Finally, we obtain the Fraunhofer

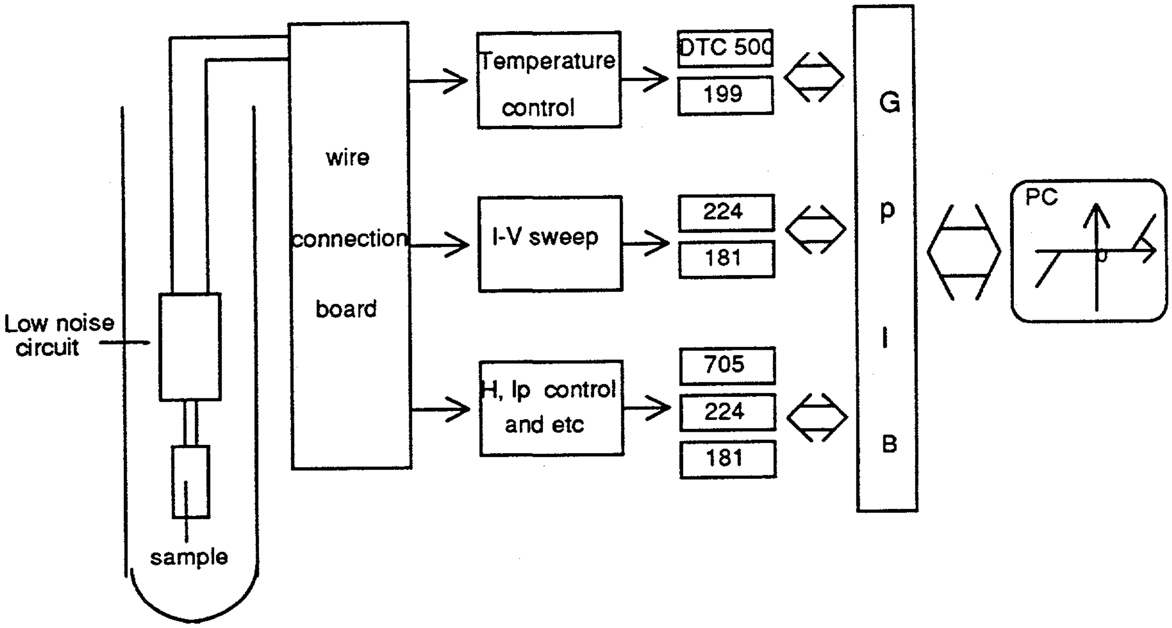

Fig. 3.7. Schematic diagram of measurement system.

diffraction pattern and find the location of a vortex in comparison with the theoretical pattern.

3.2.2.1 Junction *V-I* Characteristic Measurement

A preliminary scan of the dc Josephson tunneling features of the junction was obtained with the sample in a liquid helium bath and using a sweep of dc current to display the *V-I* characteristic on a computer screen. After getting the critical current at zero field I_o, the *V-I* curves of the junction as a function of fields were then recorded by biasing the junction with a programmable current source(Keithley 224) and measuring the corresponding voltage by means of a high-impedance nanovoltmeter(Keithley 181). The voltage out in a S-N-I-S junction is approximately 0.2 mV so that a Keithley 181 could be sufficient to pick up the signal. Another current source(Keithley 224) in conjunction with the scanner(Keithley 705) is used with the computer control of several purposes to provide currents for the measurements of the fields, temperature(± 10 μA), and transport currents.

3.2.2.2 Temperature Measurement

The temperature was measured by means of a calibrated Ge thermometer fed by a constant current of ± 10 μA. The resistance of the thermometer was determined by reading the voltage across the thermometer and a standard resistor(100 Ω) with a digital multimeter(Keithley 199 DMM/Scanner), reversing the current and repeating the measurement. Thermal emf's were averaged out by the reversing current measurement. The temperature was calculated from the thermometer resistance to a precision of ± 3 millikelvin.

3.2.2.3 External Field Measurement

The magnitude of the applied magnetic field was determined from the measured current through the coils. This was done by measuring the voltage across a standard resistor(1 Ω) in series with the circuit. There was another way to apply a parallel field to the junction just by passing transport currents through either layer of the superconducting films. By reading the transport currents I_p, we could calculate the field to less than 2% error as compared to the field generated by coils.

3.2.2.4 Vortex Configuration

With the measured diffraction pattern transferred from a personnel computer, I_c vs $H_x(H_y, H_z)$, the program calculates theoretical critical currents I_c^{th} for each experimental value of field. Then the program sums up the difference between I_c^{exp} and I_c^{th} which is to be minimized. Using that program, we calculated and compiled a "dictionary" which gives the theoretical diffraction patterns(parallel field only) for single vortex positions located on a grid of different points to carry out a detailed fitting. The dictionary is used to find the general region and then the computer does a least square fit. Symmetry may be employed to determine the patterns in the other quadrants. A measured I_c vs $H_x(H_y)$ was fitted with one single vortex having two variables, x and y coordinates as its position which have limited ranges with the guide of "dictionary". If one vortex fitting was not successful, two vortices with four variables were used to do fitting, and so on. But the difficulty usually arose for more than two vortices due to the computation capability and the experimental errors. Thus we focus on the single vortex fitting in our experiment.

3.3 Investigation of Junction Quality

The quality of the junction is normally assessed by measuring the transition temperature T_c of each film, the junction resistance, the shape of *V-I* curves, and the Fraunhofer pattern with no vortex in the junction. In this section we present basic properties of the S-N-I-S Josephson junctions.

3.3.1 Voltage-Current Characteristics

The resistively shunted junction(RSJ) model introduced by McCumber[McCumber, 1968] and Stewart[Stewart, 1968] gives the simplest expressions for the current components through a Josephson junction : (1) for the supercurrent I_s, (2) for the normal current I_n, and (3) for the displacement current I_d, as shown in Fig. 3.8. The *V-I* characteristic of the junction displays the average voltage across the junction as a function of the applied dc current. In order to determine the curve, we need to solve the following equation,

$$I = I_o \sin\varphi + \frac{V}{R_n} + C\frac{dV}{dt} \tag{3.1}$$

Using $\frac{\partial\varphi}{\partial t} = \frac{2e}{\hbar}V$, we obtain

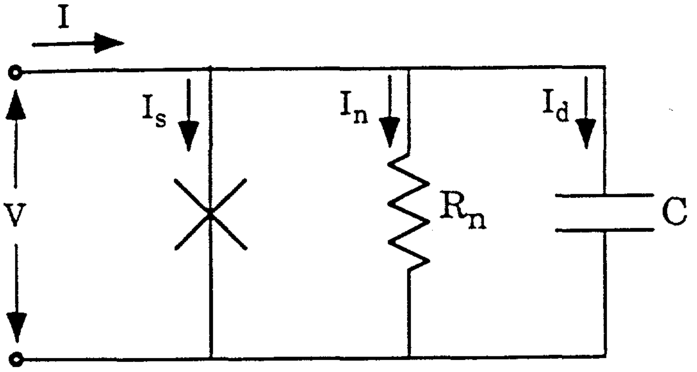

Fig. 3.8. Equivalent circuit of a Josephson junction in the resistively shunted junction (RSJ) model.

$$I = \frac{\hbar C}{2e}\frac{d^2\varphi}{dt^2} + \frac{\hbar}{2e}\frac{1}{R_n}\frac{d\varphi}{dt} + I_c \sin\varphi \tag{3.2}$$

Using the RSJ model, three Josephson junction parameters are essential : (1) the critical current I_c, (2) the normal state resistance R_n, (3) the capacitance C. Defining a new time variable, $\tau = w_c t$, where w_c is a characteristic frequency of the junction given by

$$w_c \equiv \frac{2eI_cR_n}{\hbar} = \frac{2eV_c}{\hbar} \tag{3.3}$$

where $V_c = I_cR_n$ is a characteristic voltage of the junction.

Equation (3.2) becomes

$$\frac{I}{I_c} = \beta_c \frac{d^2\varphi}{d\tau^2} + \frac{d\varphi}{d\tau} + \sin\varphi \tag{3.4}$$

The parameter β_c is a dimensionless capacitance parameter given by

$$\beta_c \equiv w_cR_nC = \frac{2eI_cR_n^2C}{\hbar} = \frac{2\pi I_cR_n^2C}{\Phi_o} \tag{3.5}$$

The junction with $\beta_c << 1$ is usually referred to as those with small capacitance or high damping, and the junction with $\beta_c >> 1$ as those with large capacitance or low damping. The term "damping" refers to the effective inertia of the quasiparticles.

The time-averaged voltage as the solution of the equation (3.4) only for the case $\beta_c = 0$ which implies zero capacitance is

$$\overline{V} = 0 \qquad \text{for } I < I_c$$
$$\overline{V} = I_c R_n \sqrt{\left(\frac{I}{I_c}\right)^2 - 1} \qquad \text{for } I > I_c \tag{3.6}$$

The S-N-S junction essentially behaves like an overdamped Josephson junction and the RSJ model applies well [Hsiang and Finnemore, 1980].

Generally, the small S-N-S junctions are in the small capacitance limit($\beta_c \approx 0$), which corresponds to the reversible *V-I* curve. Ideal S-I-S junctions are usually in the large capacitance limit ($\beta_c \approx \infty$), which usually yields hysteresis in the *V-I* curve. Unlike S-N-S junctions having low resistance and a negligibly small capacitance, the S-N-I-S junction usually has a finite capacitance which may cause hysteresis in the *V-I* curve.

The hysteresis ratio may be characterized by introducing a parameter $\alpha = I_{ret}/I_c$, which is the ratio of the lower switching current(return zerovoltage current) to the critical current. The relation of α vs. β_c may be approximated by [Stewart, 1974]

$$\alpha^2 = 1 - \left(1 - \frac{8}{\pi^2 \beta_c}\right)^2 \tag{3.7}$$

which shows that values of β_c less than 0.5 are usually believed to give reversible *V-I* characteristics.

A rough estimation of the order of magnitude of β_c for the Nb/Al/Al$_2$O$_3$/Nb junction could be made to compare with the experimental results. The junction had a normal state resistance at 10K of 14 $m\Omega$ and a critical current 5 mA at 4.2K.

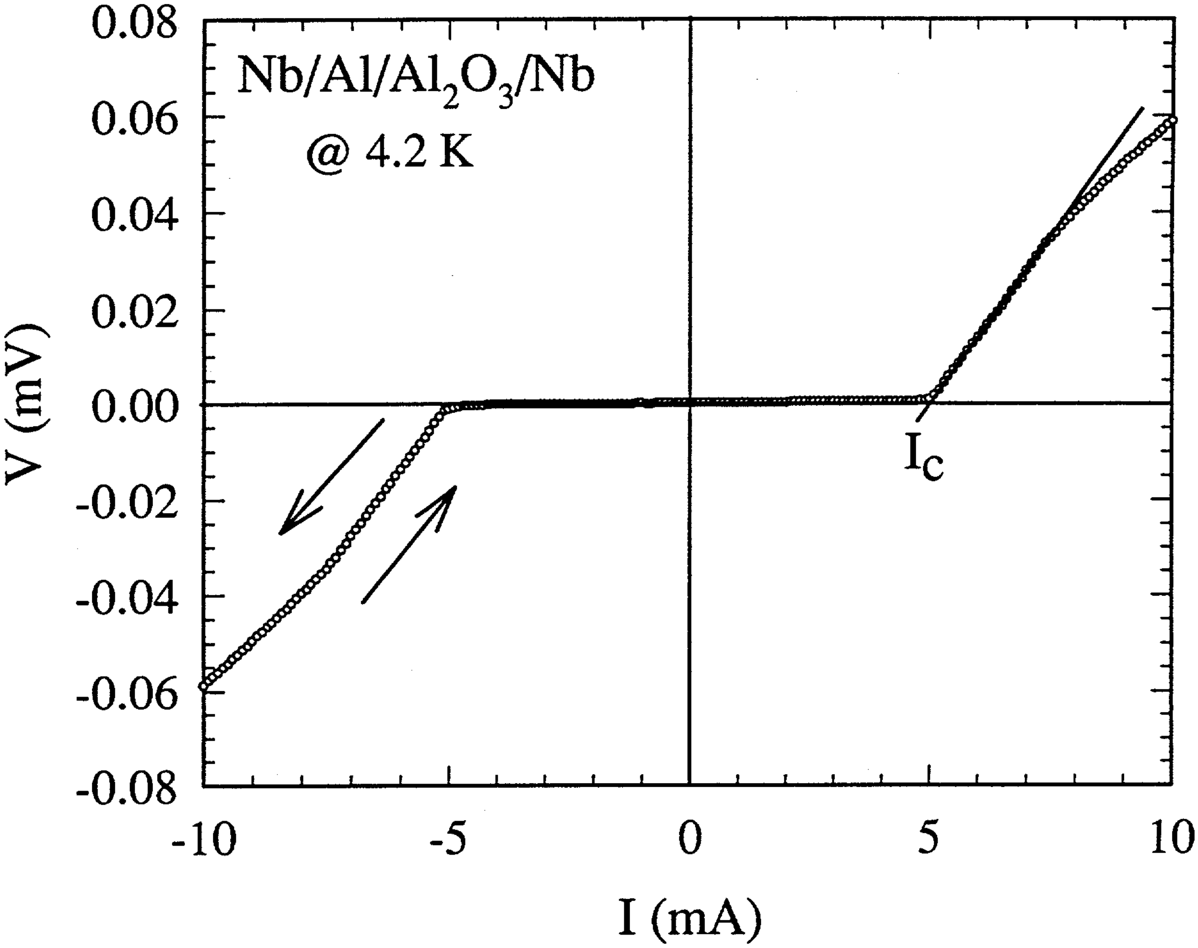

Fig. 3.9. Voltage-current characteristics of Nb junction measured at 4.2K. It shows the reversible *V-I* curve and critical current I_c.

With the value of the capacitance C of about $10^2\ pF$ [Soerensen, 1977], β_c is calculated from equation (3.5) to be of the order of 10^{-1}, which results in reversible *V-I* curves at 4.2K as shown in Fig. 3.9.

The critical current I_c, is defined by the maximum zero voltage current in the *V-I* curve. The transition from zero voltage state to voltage state is rounded. This rounding near $V = 0$ was usually found less severe in the S-N-S Josephson junction, where the very low resistance and capacitance of the junction give much less sensitivity to noise and thermal fluctuation. When the thermal energy k_BT is on the order of the Josephson coupling energy, thermal fluctuations can have the effect of destroying the phase coherence across the junction which causes the early thermally-induced pair breaking as the bias current approaches I_c and the temperature gets closer to T_c. The critical current is taken from extrapolating the steepest slope portion of the curve to the zero voltage line as shown in Fig. 3.9, which is $I_c = 5\ mA$ and $J_c = 200\ A/cm^2$ at 4.2K in Nb/Al/Al_2O_3/Nb junction.

3.3.2 Temperature Dependence of I_c

In this section we present brief discussion on the temperature dependence of critical currents for S-I-S, S-N-S, and S-N-I-S Josephson junctions. The critical current and its temperature dependence have been experimentally investigated by many authors for various Josephson junctions [Yang and Horng, 1988; Nagata and Yang, 1981]. The amplitude of Josephson current could be approximately treated to be proportional to the product of the order parameter immediately on either side of the barrier. The order parameter near the boundary of the normal metal barrier in Josephson junction could be provided by the proximity effect from the N-S interface. Within the superconducting layer, the linear Ginzburg-Landau equation is used to describe the behavior of the order parameter. Within the normal metal, the de Gennes-Werthamer theory [Werthamer, 1963; de Gennes, 1964] is used for the order parameter. The condensation amplitude of finding Cooper pairs in the superconducting state at position x is defined by $F(x)$. In the case of S_1-I-S_2 junctions, there is little depression of $F(x)$ in the superconductor caused by the insulating barrier as shown in Fig. 3.10a. Near T_c, the I_c is proportional to the product of two condensation amplitudes on both sides of insulator, as

$$I_c \propto F^L_{BCS} F^R_{BCS} \tag{3.8}$$

For the temperature close to T_c, F_{BCS} varies as $(1\text{-}T/T_c)^{1/2}$. In the case of tunneling between identical superconductors, I_c is then proportional to $(1\text{-}T/T_c)$ near T_c. For the low temperature ($T << T_c$), I_c is essentially independent of temperature reflecting the similar behavior of the condensation amplitudes in the superconducting films over that range of temperatures.

For S-N-S junction [Hsiang and Finnemore, 1980], the critical current obeys

$$J_c = J_o\left(1-\frac{T}{T_c}\right)^2 \exp\left(-K_n d_n\right) \tag{3.9}$$

to rather good accuracy for dirty normal metal barrier, where the coherence length $\xi_n(T) = K_n^{-1} = \left(\hbar v_F l \big/ 6\pi k_B T\right)^{1/2}$ and thickness d_n of the normal layer. For temperature near T_c, the dominant term in equation (3.9) is $(1\text{-}T/T_c)^2$. Thus I_c

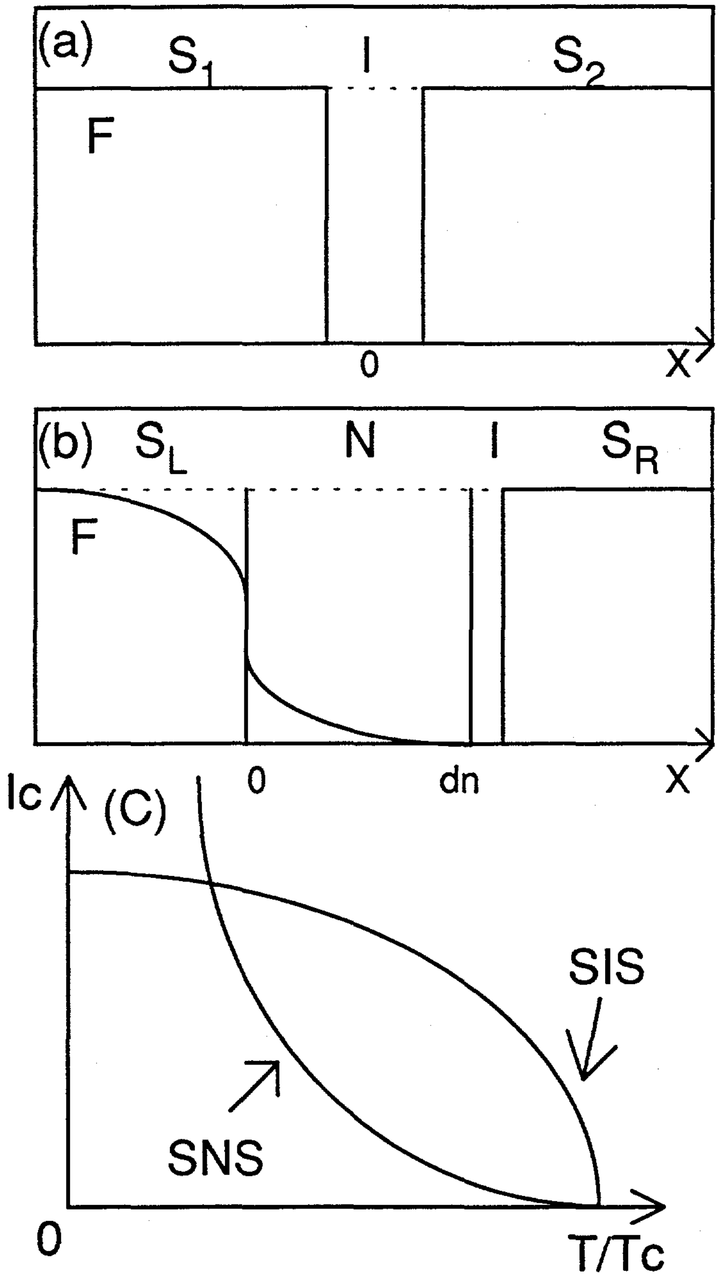

Fig. 3.10. Qualitative sketch of the order parameter behavior for S-I-S and S-N-I-S junction. Qualitative sketch of Ic as a function of temperature for ideal S-I-S, S-N-S junction is shown in (c).

varies as ($1\text{-}T/T_c)^2$. At $T << T_c$, the dominating temperature dependence of J_c is the exponential term,

$$J_c = B\exp(-K_n d_n) \tag{3.10}$$

where B is only weakly dependent on temperature. Thus I_c increases rapidly with decreasing temperature, caused by the exponential dependence on K_n^{-1}, which is proportional to $T^{1/2}$.

For the S-N-I-S junction as shown in Fig. 3.10b, we can treat the problem as that of an ordinary unsymmetric junction with insulating barrier I. In S_R the condensation amplitude can be taken to be $F_{BCS}^{R}(T)$ throughout only with a slight depression near the insulating boundary. $F_n(d_n)$ is that at the N-I boundary due to the proximity effect. With the de Gennes boundary condition [Greenspoon and Smith, 1976] for solving $F_n(d_n)$ and from equation (3.8), we have finally

$$I_c \propto F_{BCS}^{L} F_{BCS}^{R} \left(\frac{D_s}{D_n}\right) \frac{1}{K_n \xi_{GL}^{L}} \left\{\frac{1}{\sinh(K_n d_n)}\right\} \tag{3.11}$$

The BCS stands for the value calculated from BCS theory from the measured T_c. $D = \frac{1}{3} v_F l$ is the diffusion coefficient, v_F is the Fermi velocity and l is the electron mean free path. ξ_{GL} is the Ginzburg-Landau coherence length. The temperature dependencies of F_{BCS}^{L}, F_{BCS}^{R}, and ${\xi_{GL}^{L}}^{-1}$ dominate the temperature dependence of I_c near T_c, which vary with temperature as ($1\text{-}T/T_c$)$^{1/2}$ respectively. In addition, since our superconducting film is very thick so that the transition temperature of the N-S system will be close to the transition temperature of the superconductor. Near T_c

the $T^{1/2}$ dependence of K_n will be small with respect to F_{BCS} and ξ_{GL}. To a good approximation, we have from equation (3.11),

$$I_c(T) \propto \left(1 - \frac{T}{T_c}\right)^{3/2} \qquad \text{near } T_c \tag{3.12}$$

In Fig. 3.11, we have plot the experimental value of I_c, $I_c^{2/3}$ vs T for the Pb/Al/Al_2O_3/PbBi and Nb/Al/Al_2O_3/Nb junction. These give good agreements. At low temperature $T < 0.5T_c$, $F_{BCS}(T)$ and ξ_{GL} vary only very slightly with temperature ($F_{BCS}(0.5T_c) = 0.9569F_{BCS}(0)$). Therefore the temperature dependence of I_c is governed by the condensation amplitude at the N-I boundary, $F_n(d_n)$. Thus we obtain from equation (3.11), noting that $K_n^{-1} \propto T^{1/2}$

$$I_c(T) \propto F_n(d_n) \propto \left\{T^{1/2}[\sinh K_n d_n]\right\}^{-1} \tag{3.13}$$

Furthermore, in case of thick normal layer, $K_n d_n >> 1$, $\sinh K_n d_n \approx \frac{1}{2}\exp(K_n d_n)$, such that $I_c(T) \propto \left[T^{1/2}\exp(K_n d_n)\right]^{-1}$. This behavior of I_c of S-N-I-S junction with the condition of low temperature and thick normal layer is identical with that of S-N-S junction, whose curvature of I_c vs T is concave. For S-I-S junction I_c is normally saturated at low temperature so that the curvature of I_c vs T is convex. The schematic behavior of I_c vs T for ideal S-I-S junction and S-N-S junction is in Fig. 3.10c. Therefore I_c vs T for S-N-I-S junctions should change in curvature from concave to convex, as the thickness of the normal layer decreases. Nb junction has $d_n = 180$ *nm* and $K_n^{-1} = 110$ *nm* at 4.2K. Thus $K_n d_n$ is larger than 1.6 at entire

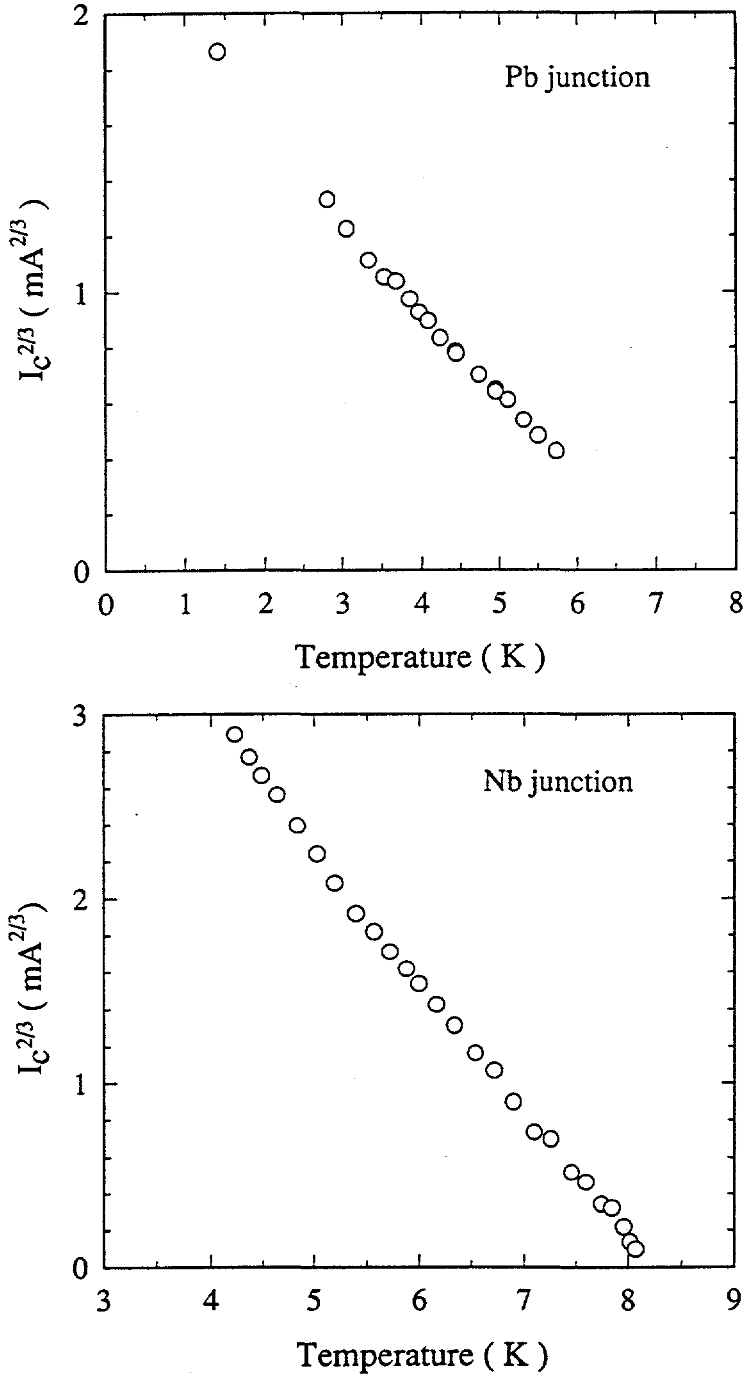

Fig. 3.11. Experimental plots of $I_c^{2/3}$ vs T for each junctions. Both data show good linear behavior.

operating temperatures which means that the junction behaves more like as S-N-S junction.

3.3.3 External Field Dependence of I_c

Fraunhofer oscillations of regular periodicity were produced by the S-N-I-S junction in the presence of an externally applied parallel magnetic field. For convenience of discussion, a coordinate system is used in which the bottom film lies along the y- axis, the top film lies along the x- axis, and the Josephson currents flow through the junction along the z- axis as shown in Fig. 3.12. The external fields generated by two sets of Helmholtz pairs give the parallel magnetic fields along the y- direction, with the perpendicular field along the z- direction. An alternative way to get a Fraunhofer pattern for the junction is to use the field in the junction generated by the transport current in the top or bottom strip [Hyun and Finnemore, 1986]. According to the calculation made by Huebener et al.[Huebener et al., 1986], the transport current passing through the thin film strip of thickness d_s and width W produces parallel magnetic field of

$$H_{\parallel}(\text{surface}) = (0.8\ G \cdot cm / A)\ \frac{I_p}{(d_s + W)} \tag{3.14}$$

This field modulates the Josephson currents and finally a diffraction pattern can be obtained.

As a test of the junction quality, the Fraunhofer pattern was observed at 5K. for Pb junction and Nb junction. The regular periodicity of the Fraunhofer

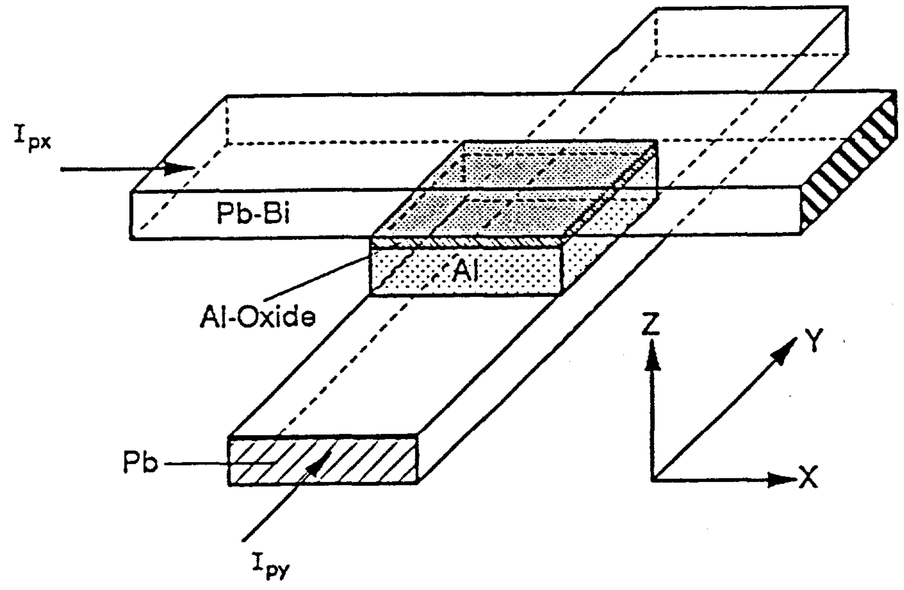

Fig. 3.12. Sketch of the S-N-I-S junction geometry and coordinate system chosen for the convenience of discussion.

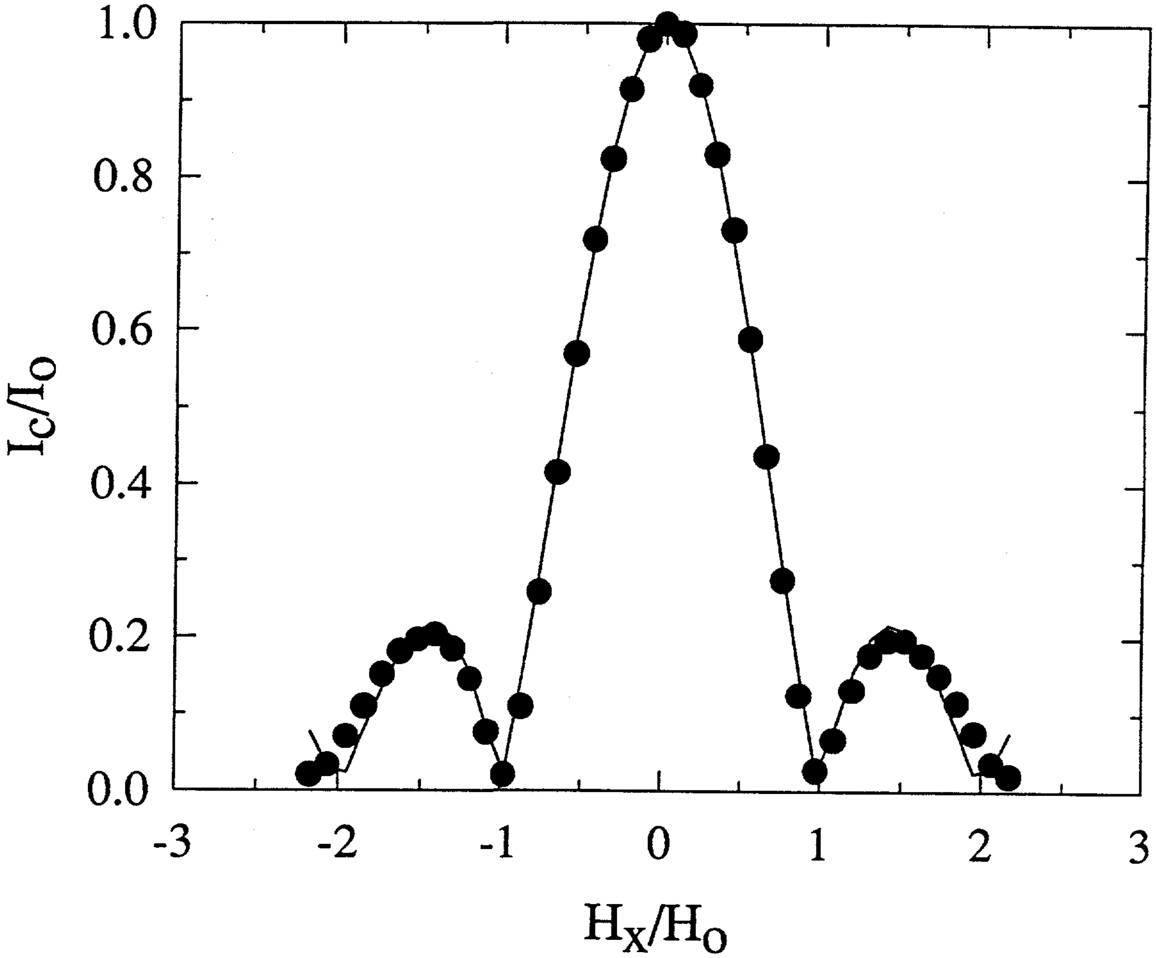

Fig. 3.13. The Fraunhofer pattern of the Pb junction measured by applying transport current I_{py} in the Pb strip, where $I_o = 0.445\ mA$, $H_o = 1.33\ G$. The solid circles are experimental data taken at 5.00K; the lines are theoretical pattern.

oscillations in the parallel applied field confirms a uniform barrier without microshorts. The Fraunhofer pattern of the Pb junction was measured at 5K by applying the transport current I_{py}, in the bottom Pb thin film lying in the y-direction, which is shown in Fig. 3.13. The direction of magnetic fields H_x, generated by I_{py}, is along the x- axis. The line is the theoretical Fraunhofer pattern of $\frac{I_c}{I_o} = \left|\frac{\sin\Theta}{\Theta}\right|$ where $\Theta = \frac{\pi H_x}{H_o}$. With $H_o = \frac{\Phi_o}{d_{eff}\cdot W}$ (3.15)

at which the first minimum of critical current occurs. The Pb junction shows that H_o is 1.33 G. This is the normalizing factor for the x- axis of the diffraction patterns. For a 55 μm wide film, this implies a combined thickness of the Al barrier and penetration depth $d_n + 2\lambda$ ($= d_{eff}$) of 280 nm. With the value of $d_n = 200$ nm, $\lambda_{\mathrm{Pb(Bi)}} = 40$ nm is obtained as same as expected for pure Pb(Bi) at 5K. The Josephson penetration depth λ_J, calculated from equation (2.25) is 79.4 μm, that is, $\lambda_J = 1.44\cdot W$ at 5K. For this value of λ_J, the Josephson current density is uniform across the junction. At $H_x = 0$, the critical current I_o, is 0.445 mA. This is the normalizing factor used along the y- axis of the diffraction patterns.

For the Nb junction, the Fraunhofer pattern was measured at 5K by applying the external fields of the Helmholtz pairs. As shown in Fig. 3.14a, the experimental I_c/I_o vs H_y/H_o curve shows an excellent fit to the ideal Fraunhofer formula of $\frac{I_c}{I_o} = \left|\frac{\sin\Theta}{\Theta}\right|$ where $\Theta = \frac{\pi H_y}{H_o}$ with $H_o = 1.0$ G, the period of oscillations at 5K. The zero field critical current $I_o = 3.3$ mA. The effective thickness d_{eff} is about 400 nm. If the $d_n = 180$ nm, this means that $\lambda_{\mathrm{Nb}} = 110$ nm, a value about twice as large as expected for pure Nb at 5K. The calculated value of λ_J is about half of the junction width. This length provides nearly uniform current density throughout the junction area to about less than 10% of that at zero field. With the perpendicular magnetic field to the junction surface, the diffraction pattern, I_c/I_o vs H_z/H_o at 4.2K, provides another nice fit with the theory of

$$\frac{I_c}{I_o} = \left|\frac{Si(\alpha)}{\alpha}\right| \tag{3.16}$$

where $\alpha = 2\pi H_z/H_o$ and $I_o = 5.0\ mA$, $H_o = 1.0\ G$ at 4.2K. (Fig. 3.14b)

Most of the features of the diffraction pattern for a junction containing vortices are included in the low applied field range from $-2H_o$ to $2H_o$. Therefore it is usually sufficient to do the theoretical fitting in this range.

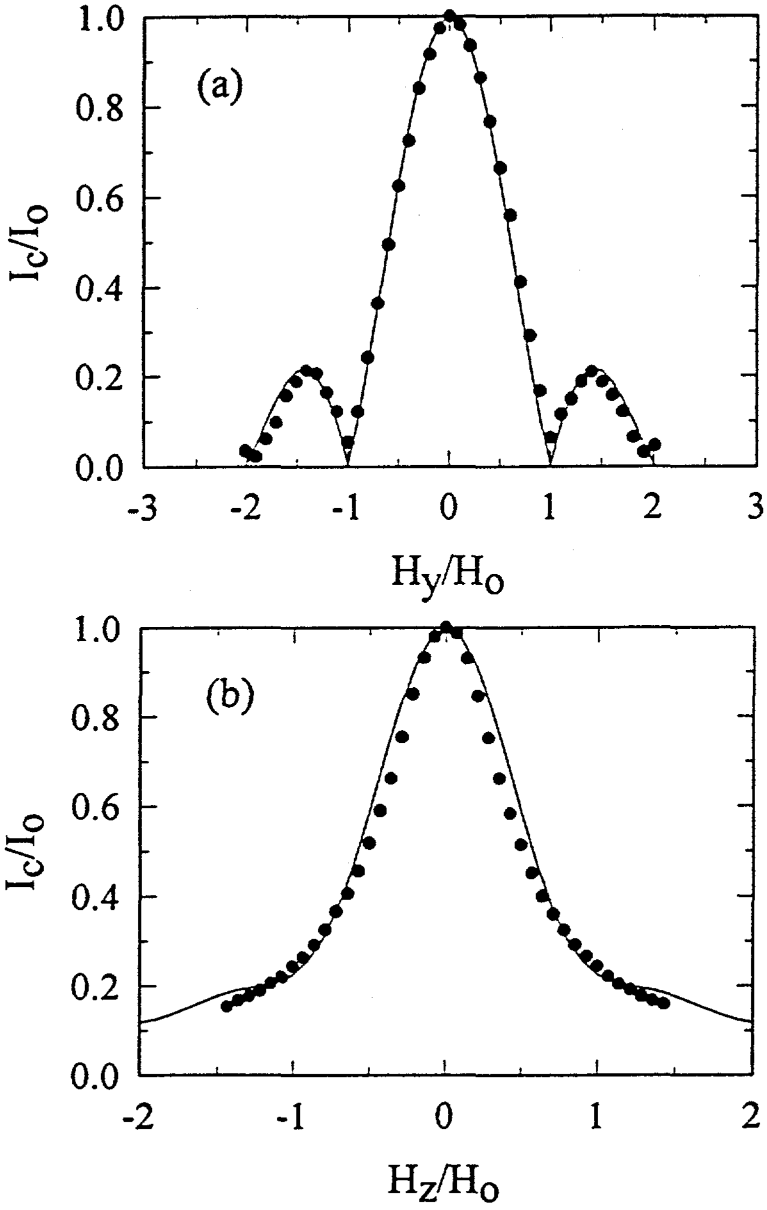

Fig. 3.14. The external field dependence of I_c/I_o for Nb/Al/Al$_2$O$_3$/Nb junction. The above one is I_c/I_o vs H_y/H_o measured at 5.00K, while I_o = 3.3 *mA* and H_o = 1.0 *G*. The below one is I_c/I_o vs H_z/H_o measured at 4.2K, while I_o = 5.0 *mA* and H_o = 1.0 *G*.

CHAPTER IV. EXPERIMENTAL RESULTS AND DISCUSSION

This chapter presents the experimental studies on the pinning and depinning of a single superconducting vortex inside S-N-I-S Josephson junction. Thermal depinning has been mainly studied for a single vortex trapped in a superconducting Nb thin film and Pb thin film respectively in order to determine the value of the superconducting order parameter and the superfluid density when the vortex depins and starts to move around the film.

In the first section we will discuss the techniques used to create a single vortex at the edge of the films by both the transport current and applied perpendicular magnetic field. In the second section we will discuss the experimental results on the single vortex motion by the Lorentz force induced by the transport currents. Actually we have been able to move the vortex to most desirable places in the junction. A brief discussion on the elementary pinning force f_p, will be given. In the third section we will discuss the thermal depinning of a single vortex. Finally in the fourth section the application of controlled vortex motion and future experiments will be proposed.

4.1 Nucleation of a Single Vortex

In nucleating a single vortex, two main methods have been developed successfully in the study of a single vortex motion. One is the field cooling process, and the other one is the nucleation by transport current. Prior to the detailed descriptions of these methods, we present the various interactions of a single vortex inside the junction that need to be considered for the nucleation process.

4.1.1 Interactions of a Single Vortex in S-N-I-S Junctions

The Gibbs free energy of a flux line per unit length is given by [Huebener, 1979], for a semi-infinite superconducting slab,

$$\frac{G}{L}=\frac{\Phi_o}{4\pi}\left[H_a\exp\left(-\frac{x}{\lambda_L}\right)-\frac{1}{2}\frac{\Phi_o}{2\pi\lambda_L^2}K_o\left(\frac{2x}{\lambda_L}\right)-\left(H_a-H_{c1}\right)\right] \tag{4.1}$$

where x is the distance from the edge, H_a is a perpendicular magnetic field, K_o is the zeroth order modified Bessel function, and H_{c1} is the lower critical field. The first term contains the interaction between the vortex line and the external field. The second term describes the attractive interaction between the vortex line with its image lines. The third term represents the energy of the vortex line inside the superconductor far away from the surface.

Three of the most important interactions for a single vortex in S-N-I-S Josephson junctions are the dipole interaction, the vortex-image interaction, and the interaction between the vortex and pinning center, in addition to the Lorentz force between the vortex and any applied transport currents. In this discussion a monopole description is used for mathematical simplicity.

(1) Dipole interaction : In case of a misaligned dipole vortex trapped in Josephson junction, we treat this as the interaction of two magnetic monopole charges as shown in Fig. 4.1. If two inner poles from a dipole are separated by a distance δ, the effective separation of two superconducting layers is d_{eff}, and provided that $\delta >> d_{eff}$, the coupling force can be roughly estimated [Clem, 1975] as

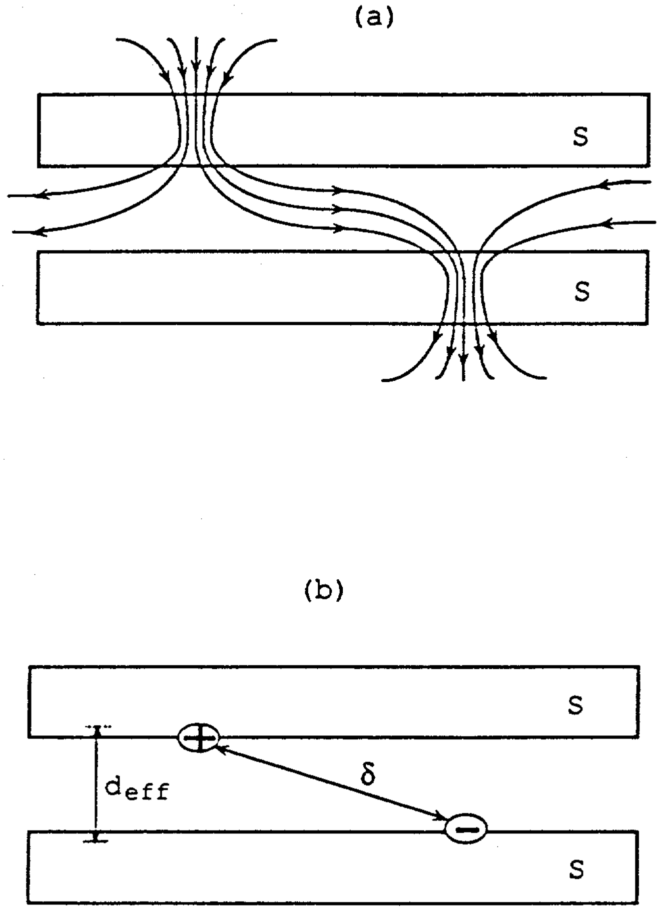

Fig. 4.1. (a) A misaligned dipole vortex, (b) Two magnetic monopole charges separated by a distance δ are theoretically equivalent to a misaligned dipole vortex.

$$F \cong \frac{\Phi_o^2}{\left(8\pi^2 \cdot \delta \cdot d_{eff}\right)} \tag{4.2}$$

The maximum value of F occurs when two inner poles actually line up, i.e. $\delta = d_{eff}$. Then the maximum pinning force is given as

$$F_{\max} \cong \frac{\Phi_o^2}{\left(8\pi^2 \cdot d_{eff}^2\right)} \tag{4.3}$$

This is an order of 10^{-14} N for $d_{eff} = 400$ *nm*. It will be shown later that this coupling force is about one order of magnitude smaller than the measured pinning force in the present experiment. Thus in order to decouple the vortex in the bottom superconducting layer from the top superconducting layer, it is necessary to have a normal metal layer thick enough to reduce the coupling energy between the top and bottom superconducting films. That is several hundred *nm* thick.

(2) Vortex- image interaction : As the vortex moves to the edge, the attractive interaction between the vortex and its images becomes stronger, which is given by

$$\mathbf{F}_{v-i} = \left(\frac{\Phi_o^2}{8\pi^2 \cdot d_{eff}}\right) \cdot \sum \left[p \cdot \frac{(\mathbf{r} - \mathbf{r}_o)}{\left|\mathbf{r} - \mathbf{r}_o\right|^2} \right] \tag{4.4}$$

where $\mathbf{r}_o$ is the vortex position, $\mathbf{r}$ is the position of the images. Here, $p = +1$ for same sense images, $p = -1$ for opposite sense images. The summation is over all images. As the vortex moves to the center of the film, this force decreases as $1/r^2$ which is strongly unfavorable to the motion of a single vortex from the edge to the interior of the junction. $\mathbf{F}_{v\text{-}i}$ is much smaller than the real pinning force if the vortex is not near the edge.

(3) The pinning potential energy associated with individual pinning centers plays the most important role for holding a vortex inside the junction. The pinning centers are local regions of depressed order parameter which vary spatially in material. These can be intrinsic (due to the crystalline structure, an inherent modulation of the G-L order parameter) or extrinsic (crystalline defects or the precipitates). The pinning range is limited to the coherence length for core pinning or the penetration depth for magnetic pinning. $\mathbf{F}_p$ differs from one kind of pinning center to another and is short-ranged to those characteristic lengths. Whether a vortex can be trapped inside the junction depends on the strength of these pinning forces.

4.1.2 Nucleation of a Vortex by the Transport Current

When a thin film superconductor carries a transport current above a certain value, it has been shown that vortex can be nucleated on an edge. It propagates into the film by the Lorentz force due to the transport current itself, and stops at a grain boundary or defect, called as pinning center, where the pinning force exceeds the Lorentz force.

4.1.2.1 Vortex Entry Fields

Vortex nucleation can occur either in intermediate state of type-I superconductor if the thickness is small enough(less than about 500 *nm*) or in mixed state of type-II superconductor. In the presence of a transport current I_p, a strong transverse magnetic field is built up near the film edge, because currents flow predominantly along the edge of the strip. When the local magnetic field at the edge of the film reaches a value of the order of the critical field H_c for type-I material and H_{c1} for type-II material, a normal region(or mixed state region) appears along the edge of the film and vortices are nucleated. The vortex nucleated at the edge may be pulled into the junction by the transport current itself, and trapped at the pinning center. This allows the junction to retain a vortex even after I_p is removed.

Consider a single superconducting strip of thickness d_s and width W. The magnetic field generated by the transport current I_p which flows through this strip can be expressed in terms of I_p [Huebener et al., 1972] as

$$H_{\parallel}(\text{surface}) = \frac{0.8 I_p}{(d_s + W)} \qquad (G \cdot cm / Amp), \tag{4.5}$$

$$H_{\perp}(\text{edge}) = \frac{0.4 I_p}{d_s} \qquad (G \cdot cm / Amp) \tag{4.6}$$

Although the transverse field at the edge reaches the value of H_c, a vortex may not be nucleated immediately due to the free energy barrier near the edge given in equation (4.1) against magnetic flux entry into the superconductor. Including this free energy barrier, the minimum flux entry field at the edge is given by [Clem et al., 1971],

$$H_{en}(T) = H_c(T) \cdot \left[1 + \frac{(2Wa_n)^{1/2}}{4d_s} \right] \tag{4.7}$$

where a_n is the radius of the vortex core. The threshold entry field is larger than H_c, because the condition $Wa_n >> d_s^2$ is normally true for our junctions.

Combining equation (4.6) into (4.7), we obtain the minimum flux entry current, or so-called nucleation current I_n, as

$$I_n = \left[\frac{H_c(T)}{0.4}\right] \cdot \left[d_s + \frac{(2Wa_n)^{1/2}}{4}\right] \quad \left(\frac{Amp}{G \cdot cm}\right) \tag{4.8}$$

The meaning used here for the core size of the vortex a_n is to describe the scale of magnetic flux enclosed in a vortex, not the scale of the normal electrons enclosed in the vortex ξ. So the value of a_n can be assumed to be taken as the penetration depth $\lambda_L(T)$. But a_n should be clearly calculated from $\pi a_n^2 \cdot H_c = \Phi_o$, as suggested by Clem [Clem, unpublished], which gives $a_n = 2^{3/4}(\lambda\xi)^{1/2}$. Furthermore in the perpendicular orientation of thin film as predicted by Tinkham [Tinkham, 1963; Tinkham, 1964], the transition field $H_\perp$ obeys the mixed state relation up to a critical thickness d_c ($\approx 10\ k\AA$ at 4.2K) as

$$H_\perp(T,d_s) = \sqrt{2}\kappa(T,d_s)H_c(T) \tag{4.9}$$

where κ is given by

$$\kappa(T,d_s) = \left[2\sqrt{2}\pi\lambda^2(T,d_s)H_c(T)\right] / \Phi_o \tag{4.10}$$

where $H_c(T)$ is the thermodynamic critical field, $\lambda(T,d_s)$ is the weak field penetration depth which depends on the temperature and possibly on the thickness of the film, and $\kappa(T,d_s)$ is the Ginzburg-Landau parameter which is defined only near T_c, but in the treatment of Tinkham, is used in the above form over the entire temperature range. This result has been explained by the depression of $H_\perp$ far below H_c by the effect of geometry and a positive surface energy. In the calculation of critical field we use the value $H_\perp(0) = 470\ G$ for thin Pb film. Using $\lambda_L(0) = 39\ nm$, $\xi(0) = 83\ nm$ together with their temperature dependence near T_c for Pb and inserting $d_s = 400\ nm$ for S-N-I-S #20, we get the nucleation current I_n near T_c for Pb film as

$$I_n^{Pb}(T) = 142.7 \cdot (1 - t_{Pb}) \cdot \left[1 + 1.58 \cdot (1 - t_{Pb})^{-1/4}\right] \qquad (mA) \qquad (4.11)$$

The transition temperatures for S-N-I-S #20 are 7.35K for PbBi film and 6.96K for Pb film. The T_c for the Pb film was significantly lower than expected for pure Pb (T_c = 7.25K), and it is speculated to result from diffusion of Au lines into the Pb film. The calculated value of I_n^{Pb} at 6.7K from equation (4.11) is 24.5 *mA* with the use of T_c = 6.96K. This value is compatible with the experimental value I_n^{Pb}(6.7 K) = 24 *mA*.

4.1.2.2 Temperature Dependence of I_n

Knowledge of the temperature dependence of I_n is necessary in order to specify the temperature region where depinning current can be measured. The depinning current should be less than the nucleation current I_n in order to avoid the nucleation of another vortex by the depinning current. This specifies the temperature window where the f_p measurement can be made.

To measure the temperature dependence of I_n, first the sample temperature is raised above 9K to eliminate possibly pinned vortices in the junction and subsequently cooled down to the reference temperature (5K) below T_c. The zero field critical current of the junction without any vortices I_o, is measured as a reference point. Then the sample is warmed up to desired temperature and a transport current I_p, is increased to a certain value through one leg of the junction and decreased to zero. Then the sample is cooled down to the reference temperature (5K) and the critical current I_{co} at zero field is measured to see if I_{co} changed from I_o. If such a change does not occur, the above process will be repeated with higher I_p's and the value of I_p is recorded, until the change does occur which indicates that a vortex has been nucleated. The minimum nucleation current I_n is defined as the lowest value of transport current I_p corresponding to the first change of I_{co} from I_o.

It is found that there are well defined and reproducible nucleation currents for given temperature at which a vortex is trapped. After taking the minimum nucleation currents at each temperature, the temperature dependence of I_n for the Pb film is obtained as shown in Fig. 4.2. The solid line is the calculated curve from equation (4.11). There is a reasonable agreement between the curve and experimental values.

4.1.2.3 Nucleation of a Single Vortex in each Pb and Nb Junctions

The nucleation process using a transport current in the thin film has proved to be very reproducible and the Fraunhofer diffraction pattern confirms the location of a single vortex. Any relatively weak spot near the edge of the film in the junction area can be the place where the first single vortex is nucleated and subsequently pushed to the interior. The experiments concerning the single vortex

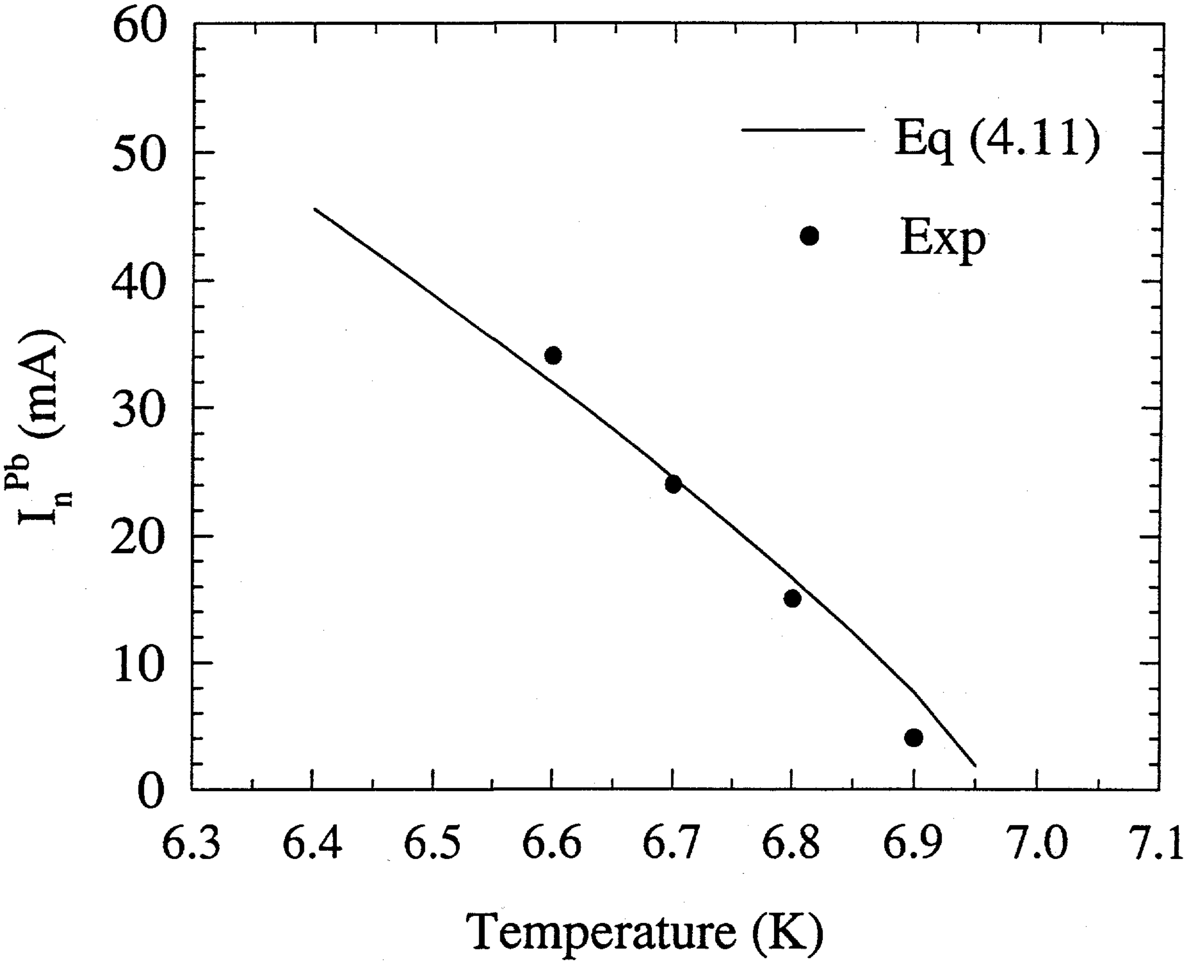

Fig. 4.2. Nucleation current I_n as a function of temperature. The solid line is calculated by using Eq. 4.11.

motion reported here, were performed on sample S-N-I-S #20(Pb/Al/Al_2O_3/PbBi with a gold line) and sample Nb/Al/Al_2O_3/Nb junction. For Pb junction, the vortex was always nucleated in the bottom layer (Pb layer). By contrast, for Nb junction, the vortex was always nucleated in the top Nb layer because it shows the good superconducting transition temperature (9.16K).

The typical procedure to nucleate a vortex in the Pb film is as follows :

(1) The sample is warmed above 9K, and held for a few minutes to eliminate possibly pinned vortices in the junction.

(2) The sample is slowly cooled through T_c down to 5K and I_o is measured as a reference point.

(3) The sample is slowly warmed up to a desired temperature, say 6.80K. The current in the Pb film I_n^{Pb}, is increased to some value and then decreased to zero.

(4) The sample is cooled back to 5K again. The critical current at zero field I_{co} is then measured to see if it has changed from I_o.

(5) If I_{co} has not changed from I_o, steps (3) to (4) will be repeated with a little higher currents I_n^{Pb} until some change of I_{co} is observed. If I_{co} has changed from I_o, a full diffraction pattern I_c/I_o vs H_x/H_o is normally taken to determine the configuration of the vortices. I_{co} changing from I_o indicates vortices have been nucleated.

All of the diffraction patterns are taken at 5K where the critical currents are high and the temperatures are easy to control. Ultimately the accuracy of the diffraction patterns measured at 5K permits the determination of the vortex location by performing the theoretical fitting to those diffraction patterns to 1% of the junction width.

For the Nb junction, several new procedures including the nucleation of a vortex are introduced to see how they would work. First, some exposed regions of the bottom Nb film were degraded somewhat during the glow-discharge preparation of the Al_2O_3 and so the vortex always was nucleated in the top film rather than the bottom film as was done in the Pb junction. Second, to nucleate a vortex, a transport current was applied to the top film and the sample was slowly cooled through T_c with the current applied. This process looks similar to the field cooling process by which Hyun [Hyun, 1987] had trapped a single vortex in one of the superconducting layers of his S-N-S junction. The detailed experimental procedure has been described in his Ph. D dissertation. The difference of the transition temperatures between top and bottom Nb layer makes sure that a vortex will be trapped only in the top layer and will leak out the edge of the junction. Fig. 4.3 shows the diffraction patterns with the theoretical fittings after nucleation of a single vortex in each junctions.

4.2 Motion of a Single Vortex

In the previous section it was found that the nucleation procedure using transport currents is very reproducible and gives well-defined locations of a single vortex in the both junctions. In this section we will give the results of depinning experiments using transport currents in either one of the strips of the junction and using the thermal activation. The Lorentz force acting on a vortex per its unit length is given by

$$\mathbf{F} = \mathbf{J} \times \vec{\Phi}_o / c \tag{4.12}$$

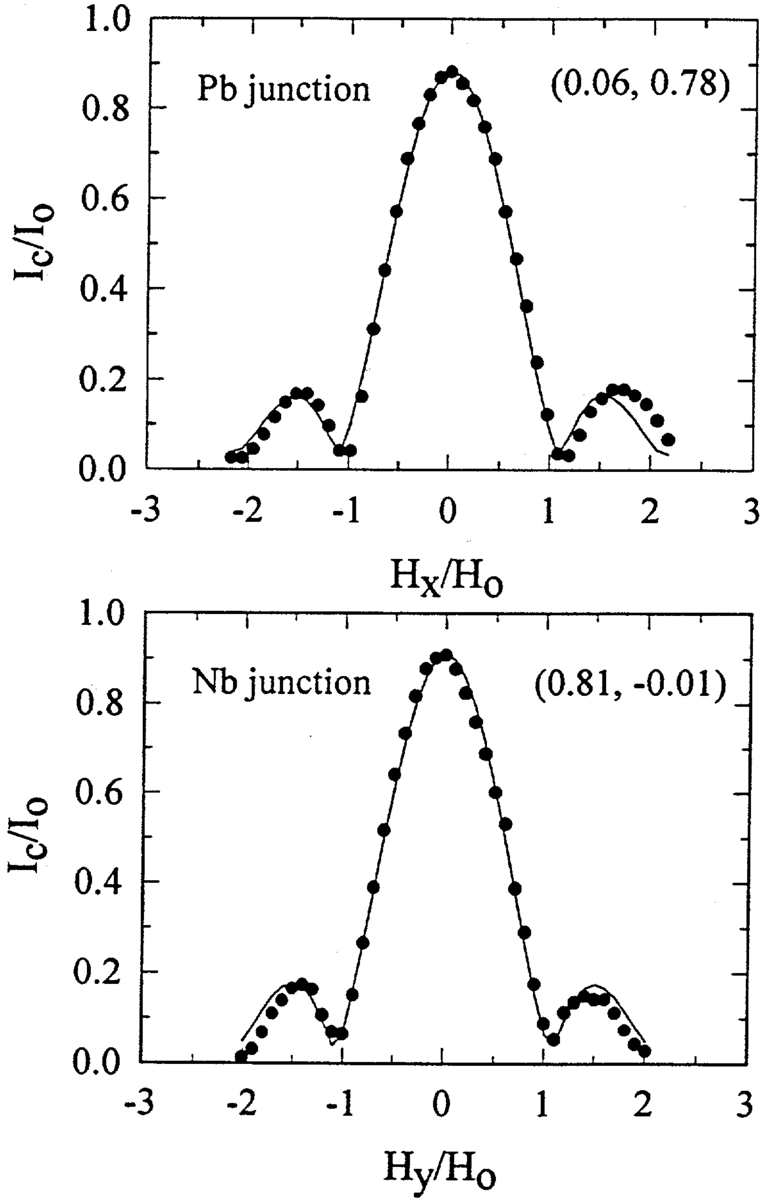

Fig. 4.3. Diffraction patterns with the theoretical fittings after nucleation of a single vortex in each junction.

which is related to the transport current. The elementary pinning force f_p is determined [Hyun et al., 1987; Li et al., 1991] through measuring the minimum amount of depinning current I_d, applied to depin a single vortex from a particular pinning center.

Regarding the thermal activation [Sanders et al., 1993; Sok and Finnemore, 1994], one can remove the Lorentz force of a transport current and start warming the sample to determine the temperature where the vortex thermally depins and begins to move. As the temperature rises, the order parameter and the superfluid density gradually decrease and the thermal activation will cause the vortex to hop across a saddle point into the next pinning potential valley. Because Nb and Pb obey the BCS theory rather well, the value of the order parameter Δ and the superfluid density ρ can be determined from the ratio of the temperature T to the transition temperature T_c, which is given by

$$\Delta = 3.2 k_B T_c \left(1 - \frac{T}{T_c}\right)^{1/2}, \quad \rho = \Delta^2 \tag{4.13}$$

near T_c. The order parameter at $T = 0$, Δ_o, is given by $\Delta_o = 1.76 k_B T_c$.

4.2.1 Pb/Al/Al$_2$O$_3$/PbBi Junction with a Gold Line

A single vortex could be positioned on the Au line's pinning center by cooling the sample in the presence of a field directed perpendicular to the plane of the junction. For this field cooling method, the sample was warmed to about 9K and slowly cooled through T_c in a field of 10 mG, which value corresponds to about

1.5 flux quanta(Φ_o). An analysis of the diffraction pattern given by Fig. 4.4a showed that the location of a vortex is indeed on the Au line in the Pb film at (x = -0.60, y = 0.52), the position marked No.2 on Fig. 4.5. This vortex also penetrates the PbBi film at (x = 0.00, y = 0.98).

An alternate way to position a single vortex on the Au line is to nucleate the vortex at the edge of the junction using a transport current in the Pb film and subsequently to push the vortex over to the Au line. The Pb film is sufficiently thin (< 500 *nm*) that it behaves like a type-II superconductor and vortices enter as separate quanta and not as flux bundles [Tinkham, 1963]. A typical procedure would be to cool the junction in zero field to 6.80K, applying a transport current of I_n^{Pb} = -16 *mA* and turn it off. As shown in Fig. 4.3a, measurement of a complete diffraction pattern shows that the resulting vortex is located at (x = 0.06, y = 0.78) called point No.1 on Fig. 4.5. This means that the vortex nucleated at the left edge of the junction and crossed the Au line on its way to the pinning site 1. A detailed analysis shows that this vortex leaks out the edge of the junction and does not pass through the PbBi layer in contrast to the case of the field-cooled vortex. This nucleation procedure was repeated many times and the location of the vortex was the same to the accuracy of the measurement of 2 μm. It was found that the easiest way to push the vortex over to the Au line was to push in the negative y- direction with a current of 11 *mA* in the PbBi film at 6.80K. As illustrated in Fig. 4.6, the transport current I_{PbBi} in the top PbBi film creates a magnetic field in the barrier region which in turn induces screening currents I_{in}, flowing along the x- direction across the top surface of the Pb film. These currents then produce a Lorentz force on the vortex in the Pb film along the y- direction. The final location of the vortex on the strip had the diffraction pattern of Fig. 4.4a. Analysis shows that the location was (x = -0.60, y = 0.52), which is the same location as the vortex created by field cooling method. It is labeled point No.2 on Fig. 4.5.

Now let's perform the thermal depinning of this vortex. The sample was warmed to some prescribed temperature and cooled to 5K. A V-I curve was taken and if the value of I_{co} was not changed, the process was repeated. If the value I_{co} did change, then a full diffraction pattern was taken to determine the new location. The vortex first depinned at 6.86K and moved through 4 distinct locations before it left the junction. The locations are shown on the sketch of Fig. 4.5, as site numbers 3, 4, 5, and 6. The diffraction patterns for each of these locations are shown in Fig. 4.4. At 6.86K the vortex hopped down and to the left from site No.2 at (x = -0.60, y = 0.52) to site No.3 at (x = -0.70, y = 0.49), a distance of 2.9 μm. The two diffraction patterns of Fig. 4.4a and 4.4b are not very different, but there is no doubt that the vortex moved. The vortex was then stable until the temperature reached 6.88K, at which temperature it jumped 20.8 μm to site No.4 at (x = 0.00, y = 0.78). The diffraction pattern of Fig. 4.4c is quite different from Fig. 4.4b and more nearly symmetric because the vortex is on the y- axis. Site No.4 located 1.7 μm from site No.1, where the vortex came to rest when it was first nucleated by the transport current at 6.80K. At 6.89K the vortex moves down slightly to site No.5 at (x = 0.00, y = 0.76), with the diffraction pattern shown in Fig. 4.4d. At 6.90K the vortex took a large jump (10.3 μm) to position No.6 at (x = -0.16, y = 0.42), a position much closer to the junction center, with the diffraction pattern shown by Fig. 4.4e. The fit of the model to the data is more difficult than for the other locations. For the theoretical fit shown for location (x = -0.16, y = 0.42), the fit is good near the minima at H_x/H_o equals plus and minus 1.4. The asymmetry of the theoretical curve can be removed by moving the location closer to the y- axis at (x =

0.02, $y = 0.48$), but then the two minima of the theoretical curve are closer together than the data. It is possible that there is a second vortex somewhere near the edge of the junction. Finally after increasing the temperature to 6.91K, the vortex is no longer in the area of the junction and the diffraction pattern returns to the undistorted Fraunhofer pattern of Fig. 4.4f.

In another sequence of thermal depinning, the vortex was nucleated at 6.80K by nucleating the vortex at the edge of the junction and pushing it to the Au line at site No.2. The temperature was then raised to 6.86K and the vortex was observed to move to site No.3. Subsequently the temperature was raised to 6.88K and the vortex was observed to move to site No.4. In every aspect the vortex obeyed the same depinning and motion sequence. The motion is not random. Instead, the vortex follows a definite trajectory and moves over the same sequence of saddle points in the pinning potential. This may arise because the depinning sequence is controlled by the changes in the spatial variation of the pinning potential map as the order parameter decreases with increasing temperature.

If we take equation (4.13) as a BCS temperature dependence for the order parameter near T_c, then the normalized order parameter Δ/Δ_o varies from $\Delta/\Delta_o = 0.20$ at 6.86K, where the vortex first depins, to $\Delta/\Delta_o = 0.16$ at 6.91K, where the vortex leaves the junction. Here Δ_o is the value of the order parameter at T = 0K. Because the superfluid density varies as the square of the order parameter, the depinning occurs as the bulk or global superfluid density changes from 4% to 2.5% for this sample. Presumably the changes in the pinning potential surface are driven primarily by local spatial variations in the superfluid density. As the global average superfluid density diminishes with increasing temperature, successive pinning sites become unstable and the vortex moves to one of the remaining stable pinning sites

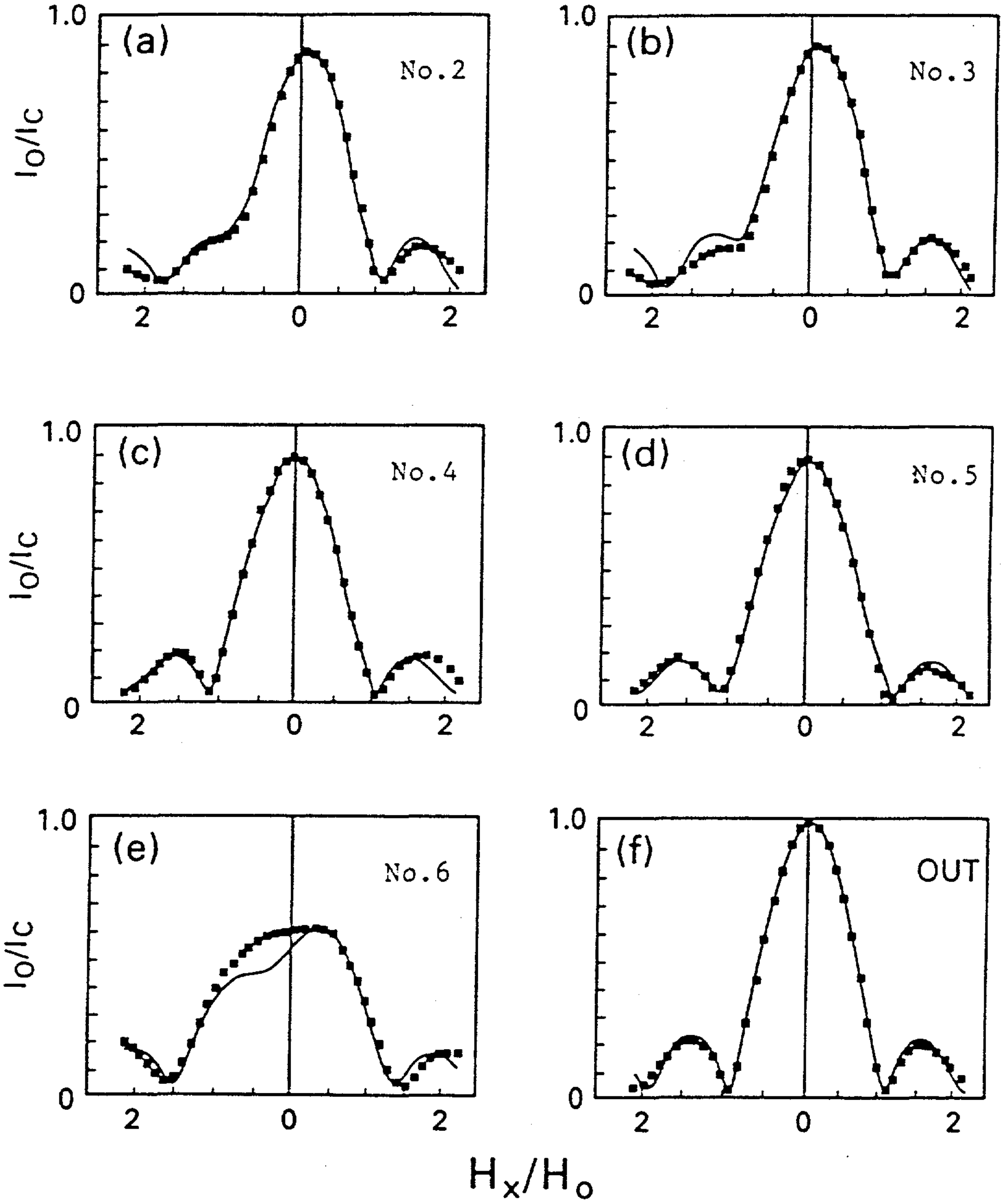

Fig. 4.4. Diffraction patterns for each of the pinning sites in the Pb junction where the vortex stops as successively higher temperatures are reached.

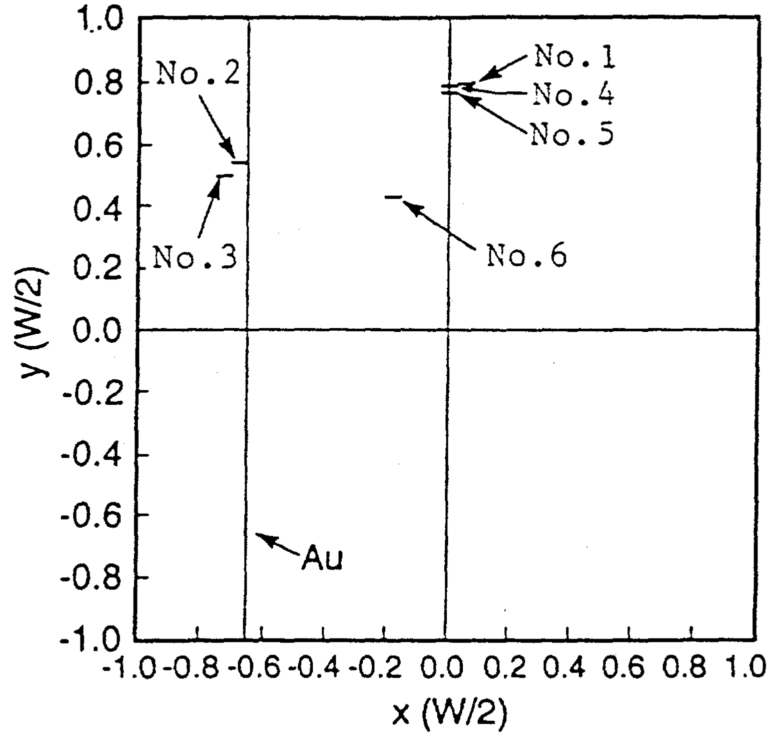

Fig. 4.5. Sketch of the junction area showing the location of the various pinning sites in the Pb junction.

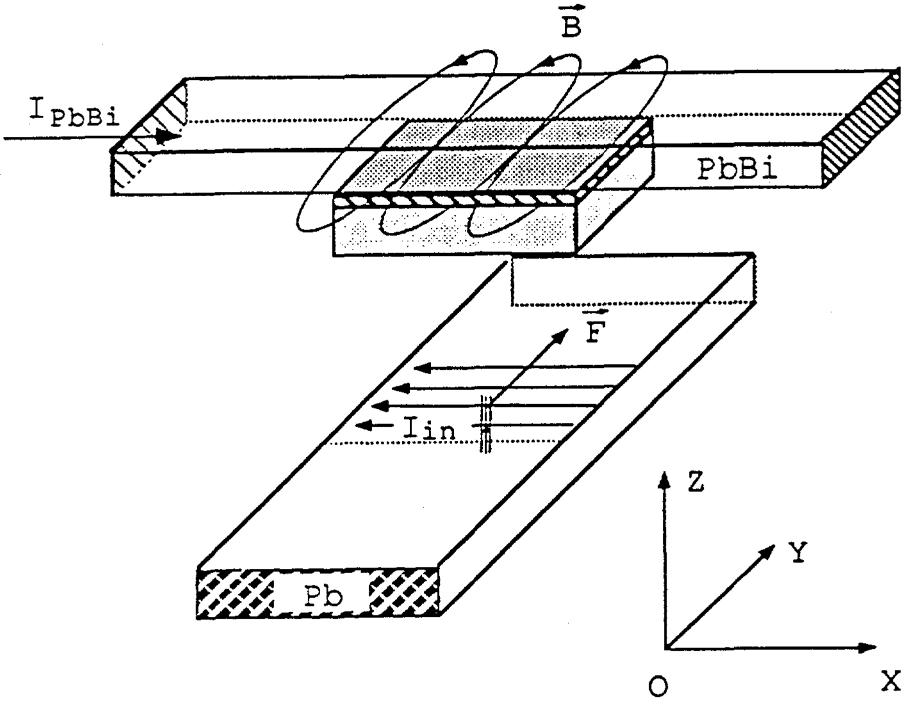

Fig. 4.6. Junction geometry showing the currents induced in the Pb film, I_{in} by transport currents in the PbBi film, I_{PbBi}. Hence the vortex in the Pb film is pushed by a Lorentz force along the *y*- direction.

that has the easiest path or the lowest saddle point for motion. The sequence of the traps is reproducible and the vortex follows the same trajectory.

4.2.2 Nb/Al/Al_2O_3/Nb Junction

To test the uniformity of the top Nb layer, a vortex was reproducibly nucleated by slowly cooling through T_c (9.20K) with an applied current of -2.1 *mA* in the top Nb layer. The diffraction pattern taken at 5K is shown by the open circles in Fig. 4.7b and compared with theory shown by the solid line. The fit shown in Fig. 4.7b reveals that the vortex is at (0.81, -0.01) where distances are measured in units of half the junction width. Hence the vortex is essentially on the *x*- axis as sketched in the inset. It is assumed that small deviations of the fit from the data arise because the barrier thickness and the films are not quite uniform.

To test our ability to move the vortex around reproducibly, a vortex is nucleated and moved to position (0.81, -0.01). Then the sample is warmed to 8.95K and a depinning current of -0.5 *mA* is applied in the lower Nb film and turned off. We checked to see that these currents will never nucleate another vortices through whole experiments. This current in the lower film induced currents in the upper Nb film in the *y*- direction and thus a Lorentz force on the vortex along the *x*-axis. If the sample is then cooled to 5K, the diffraction pattern of Fig. 4.7c is obtained. The fit shows that the vortex is now located at (0.56, 0.02) so that the vortex was moved in the direction of the Lorentz force in the negative direction along the *x*- axis. Repeating the above procedure, the sample was warmed to 8.95K and a current of -1.2 *mA* was applied to the bottom Nb strip and turned off. The diffraction pattern of Fig. 4.7d taken at 5K shows that the vortex again moved

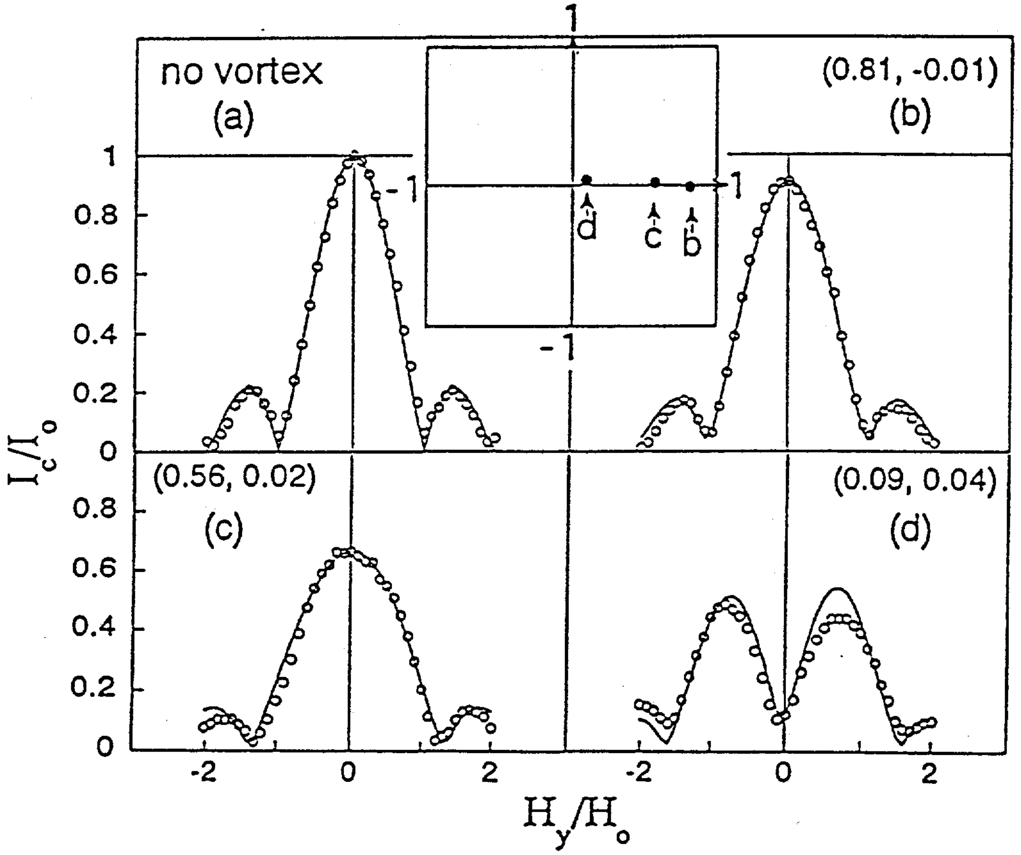

Fig. 4.7. Motion of a vortex along the negative *x*- axis direction using various depinning currents at 8.95K.

further along the *x*- axis in the negative *x*- direction to a new location of (0.09, 0.04).

To check whether the vortex could be pushed along the *x*- axis in the positive *x*- direction with equal ease, a vortex was nucleated by cooling through T_c with a current of -2.1 *mA* in the upper Nb film. This nucleates a vortex and moves it to position (0.06, -0.19) which is rather close to the center of the junction. The diffraction pattern used to determine the location and the fit are shown in Fig. 4.8a. By applying a current of + 14.4 *mA* through the lower Nb strip at 8.85K, the vortex is moved to (0.17, -0.28) as shown by the diffraction pattern of Fig. 4.8b. A further application of 15.0 *mA* pushes the vortex to (0.40, -0.12) as shown in Fig. 4.8c. Finally it can be pushed to (0.80, 0.09) of Fig. 4.8d by the application of 15.5 *mA* through the bottom Nb strip at 8.85K. Hence the vortex can be moved back and forth along the *x*- axis with relative ease. The trajectory is not in a straight line but the motion is predominantly along the direction of the force. This behavior of moving in the same direction as the applied force is to be contrasted with the Pb film reported previously where the vortex often went off in a diagonal direction to the force. This is taken to mean that the Nb film is more uniform.

To study thermal depinning in the sample, a vortex was first prepared at a location fairly close the center of the junction. This was done by cooling through T_c with a current of -2.35 *mA* in the upper Nb layer. After pushing the vortex around with several pulses of current, the vortex was located at (0.08, 0.04) as determined from the diffraction pattern in Fig. 4.9a. This sites is illustrated in the inset as position *a*. Successive warming to ever higher temperature with no external force on the vortex showed that the vortex first thermally depinned at 8.99K. The diffraction pattern taken at 5K, shown in Fig. 4.9b, showed that the vortex moved

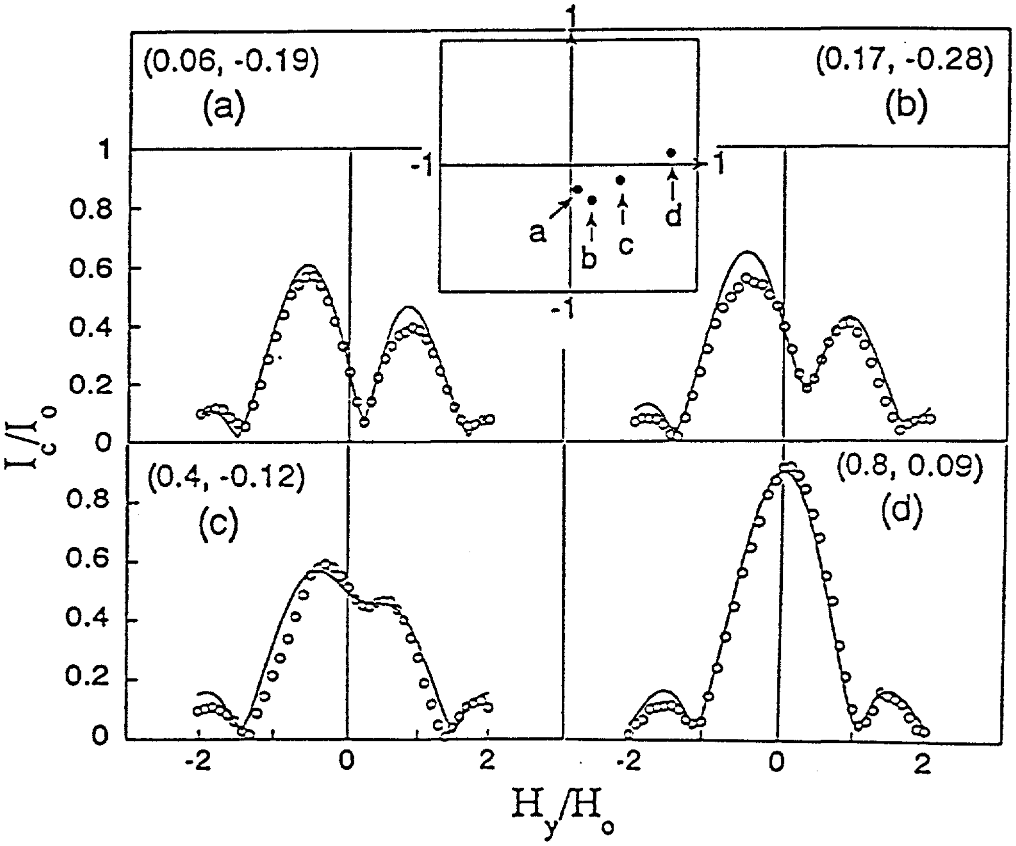

Fig. 4.8. Motion of a vortex along the positive *x*- axis direction using various depinning currents at 8.85K.

mostly along the x- axis to (0.19, 0.04). The locations of the starting position and first stop are shown in the inset as positions *a* and *b*. The value of Δ/Δ_o derived from BCS theory is 0.24 at this temperature and ρ_s/ρ_{so} is 6.0%. The second hop to position *c* took place at 9.02K and the vortex moved mostly along the y- axis to (0.20, 0.14) of Fig. 4.9c. The corresponding values are $\Delta/\Delta_o = 0.22$ and $\rho_s/\rho_{so} =$ 4.8%. The third hop to position *d* took place at 9.03K to location (0.78, -0.30) of Fig. 4.9d. The corresponding values are $\Delta/\Delta_o = 0.21$ and $\rho_s/\rho_{so} = 4.4\%$. Positions *c* and *d* are sketched in the inset. Finally when the sample was warmed to 9.04K, the vortex left the junction and the undistorted Fraunhofer pattern is recovered. The corresponding values of $\Delta/\Delta_o = 0.20$ and $\rho_s/\rho_{so} = 4\%$ were obtained for the final exit of the vortex.

Thermal depinning from a different site followed a similar pattern. A vortex was nucleated and pushed to site *a* at (0.34, 0.31) as determined from the diffraction patterns of Fig. 4.10a. The thermal depinning events took place at 8.94, 8.97, and 9.06K for the successive locations illustrated in Fig. 4.10b-d. The vortex left the junction at 9.07K. To illustrate the reproducibility of the results, a vortex was nucleated and moved to (0.81, -0.01). It was then moved to (0.47, 0.21) with a pulse of current, -4 *mA*, through the bottom Nb strip at 8.90K. On warming, it depinned at 9.02K and hopped back to (0.81, -0.01). This experiment was repeated 3 times.

There is an implication from the above results that there is a temperature interval close to T_c where the sample is superconducting but it excludes all the vortices. To test this, the sample was cooled in 3 *Oe* and cooled through T_c to trap hundreds of vortices. It was warmed to 9.07K in a field of a few *mOe* and then cooled to 5K. An undistorted Fraunhofer pattern was obtained indicating that there

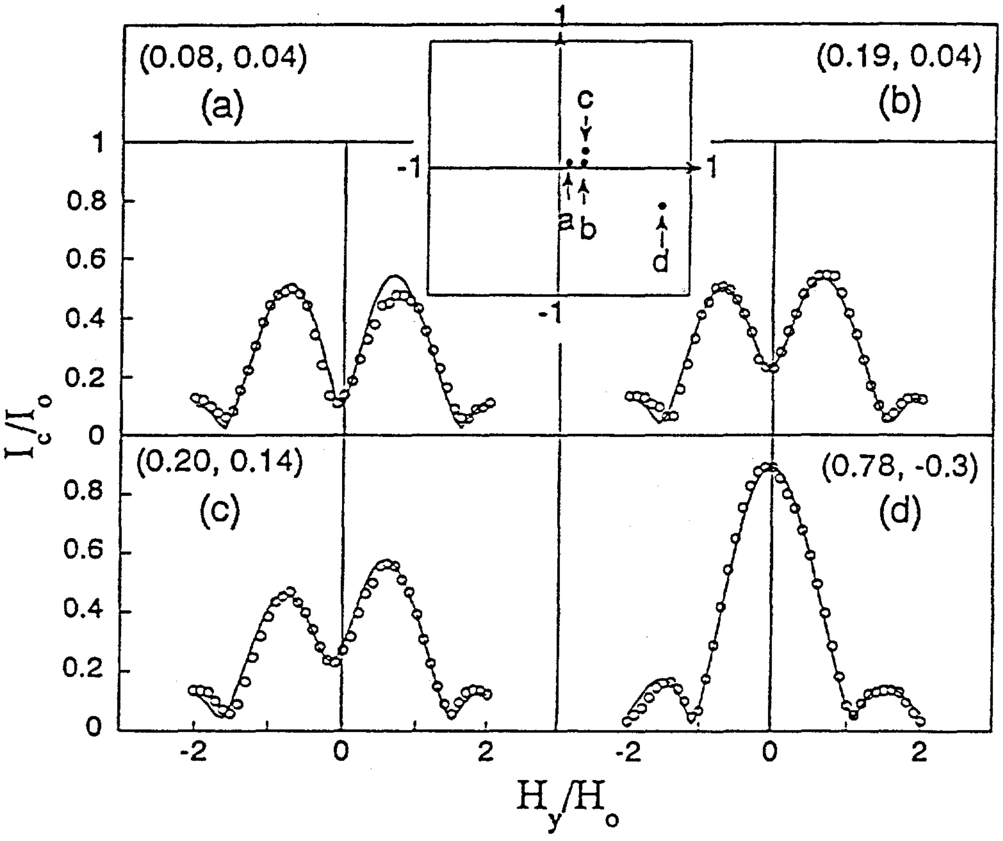

Fig. 4.9. Thermal depinning starting from a location near the center of the junction.

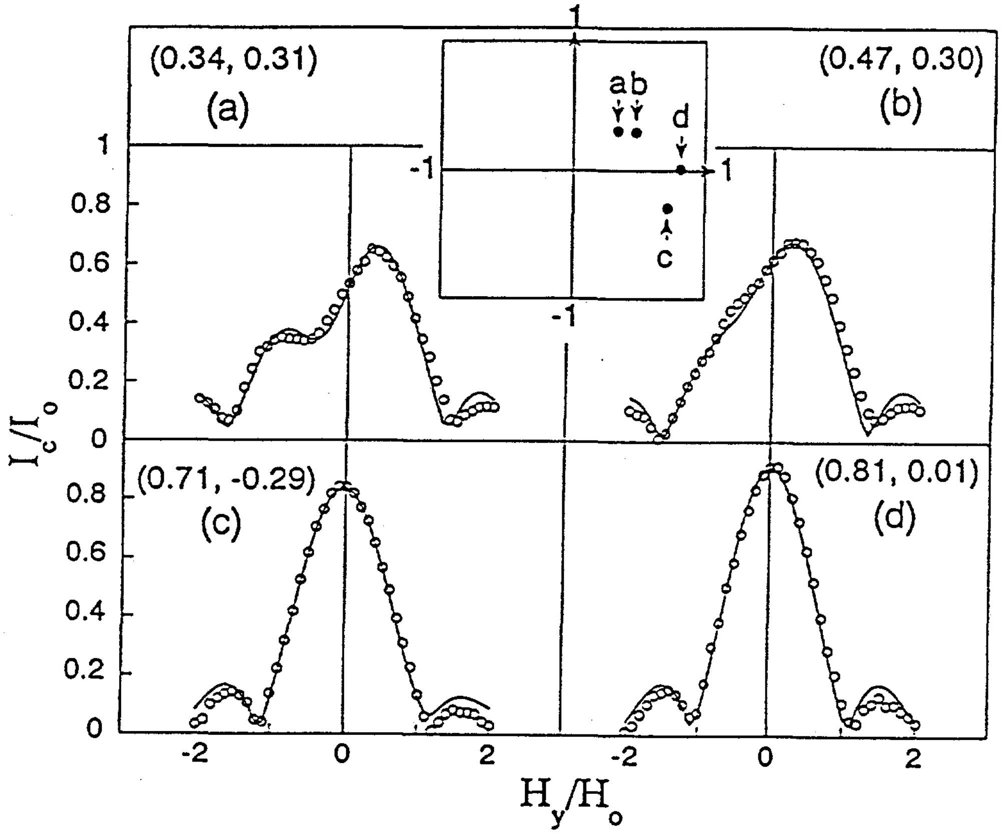

Fig. 4.10. Thermal depinning starting from a site along the junction diagonal.

were no more vortices trapped. Hence the vortices can be swept out by cycling to 9.07K and back.

4.3 Application and Future Work

One of the most difficult problems in the development of the superconducting electronics based on the Josephson junctions is the controlled fabrication of high quality, robust, and stable junction. From this standpoint, the fabrication processes have been thoroughly investigated and improved to obtain comparatively stable lead-alloy Josephson tunnel junction. However it is now hoped that new device technologies are developed to fabricate highly reliable Josephson junctions. Josephson tunnel junctions composed of refractory materials including superconducting Nb or its compounds with high transition temperatures have been promising candidates because of their extremely high reliability for low temperature operation at 4.2K, for long term storage and against repeated thermal cycling between room temperature and 4.2K.

It is essential to achieve the more reproducible fabrication of Nb/Al/Al_2O_3/Nb junction and perform a complete procedure of nucleation and motion of a single vortex. In the present work the pinning centers inside the Nb junction are naturally formed grain boundaries, defects or voids. So the motion between two pinning sites, separated by a large distance, is normally not reversible. In order to confine the vortex at specific regions, weak superconducting regions are needed which can be made artificially. Methods have been proposed by Hyun and Finnemore [Hyun, 1987] to make the pair potential of a desired region lower than the other part of the superconducting film in the junction area. Deposition of a thin and narrow normal metal (Ag, Cu) strip (or dots) which is positioned just underneath the bottom superconducting film may work for the purpose. This extra strip of normal metal provides suitable pinning sites because normal electrons from the Au(Cu) strip suppress the order parameter of the superconducting film.

Regarding the controlled motion of a flux shuttle, there are attractive points searching the pinning mechanism of artificial pinning centers and elementary pinning forces, moreover performing the logic operation [Li, 1991] which will be suited for the development of an Abrikosov vortex memory devices.

Another useful device has been offered by Kroger et al. [Kroger, 1980] who described junctions with the semiconductor barrier. The use of both single crystal and novel amorphous materials has confirmed that relatively thick semiconductor barriers can support large Josephson current densities.

CHAPTER V. CONCLUSIONS

The motion of an Abrikosov vortex in S-N-I-S Josephson junctions has been studied both under the influence of a Lorentz force and under the influence of thermal motion. It was demonstrated that vortices in clean Nb films move roughly in the direction of the applied Lorentz force with relatively little effect from the pinning potential forces in the film. From thermally activated hopping of the vortex, it was possible to determine the minimum superfluid density required to hold a vortex on a variety of pinning sites. It was shown that as the temperature rises, the order parameter and the superfluid density gradually decrease and the surface of the flux pinning potential diminishes accordingly. Whenever the reduced superfluid density is below the depinning threshold of about 4%, the vortices will begin to hop around and freely flow for a variety of sites. Thus it is a measure of the point in the *H-T* plane where defect pinning vanishes for that region of the sample.

Specifically, for the Pb film in Pb/Al/Al_2O_3/PbBi Josephson junction having a gold line, the vortex first depinned when the reduced order parameter $\Delta/\Delta_o = 0.2$, equivalently the superfluid density was about 4% of the $T = 0$ value. As the temperature increased, the vortex went through five different pinning sites before it exited the sample at 6.91K which gives $\Delta/\Delta_o = 0.16$ and $\rho_s/\rho_{so} = 2.5\%$. From another sequence of thermal depinning experiments, we also found that the trajectory of thermal hopping of a vortex could be realized reproducibly, that is, the motion is not random.

In Nb/Al/Al_2O_3/Nb junction, thermal depinning of a single vortex trapped in a top Nb film consistently occurs when the reduced superconducting order parameter Δ/Δ_o, is approximately 0.22 and the superfluid density is approximately 5% of the total density. These values are about 20% larger than those of a Pb sample having a Au line, but the values are really very close. For the Nb sample, pinning is probably dominated by grain boundaries whereas, for the Pb sample with Au decoration, pinning may have been dominated by an array Pb_3Au precipitates. Because roughly the same answer was obtained for these rather different kinds of pinning site, there is a reasonable chance that this is a general value within factors of 2 for a wide range of materials. In addition to this central conclusion, it is clear that this Nb film is very uniform and the vortex moves under a Lorentz force in approximately the direction of the force. With the suitable sequence of pulses, the vortex can be moved to most any location in the junction. Finally there appears to be a small interval near T_c between 9.1 and 9.2K where the film is superconducting and the pinned vortices are expelled.

REFERENCES

P. W. Anderson and J. M. Rowell, Phys. Rev. Lett. **10**, 230 (1963).

J. Bardeen, L. N. Cooper, and J. R. Schrieffer, Phys. Rev. **108**, 1175 (1957).

A. Barone and G. Paterno, *Physics and Applications of the Josephson Effect*, (John Wiley & Sons, New York 1982), chapter 1.

A. M. Campbell and J. E. Evetts, Adv. Phys. **21**, 199 (1972).

J. R. Clem, Phys. Rev. B**12**, 1742 (1975).

J. R. Clem, Private Communication, Department of Physics and Astronomy, Iowa State University (unpublished).

J. R. Clem, R. P. Huebener, and D. E. Gallus, J. Low Temp. Phys. **12**, 449 (1971).

P. G. de Gennes, Rev. Mod. Phys. **36**, 225 (1964).

A. L. Fetter and P. C. Hohenberg, *Superconductivity*, edited by R. D. Parks, (Marcel Dekker, New York 1969), Vol.2, chapter 14.

R. P. Feynman, *The Feynman Lectures on Physics*, (Addison-Wesley, Reading MA. 1965), Vol.3, chapter 21.

L. P. Gor'kov, Sov. Phys. JETP **36**,1364 (1959).

S. Greenspoon and H. J. T. Smith, Can. J. Phys. **49**, 1350 (1976).

M. Gurvitch, W. A. Washington, and H. A. Huggins, Appl. Phys. Lett. **42**, 472 (1983).

A. F. Hebard and R. H. Eick, J. Appl. Phys. **49**, 338 (1978).

T. Y. Hsiang and D. K. Finnemore, Phys. Rev. B**22**, 154 (1980).

R. P. Huebener, *Magnetic Flux Structures in Superconductors* (Springer-Verlag, Berlin-Heidelberg, 1979), chapter 4.

R. P. Huebener, R. T. Kampwirth, and J. R. Clem, J. Low Temp. Phys. **6**, 275 (1972).

H. A. Huggins and M. Gurvitch, J. Appl. Phys. **57**, 2103 (1985).

O. B. Hyun, Ph.D. dissertation, Iowa State University, (1987).

O. B. Hyun, J. R. Clem, and D. K. Finnemore, Phys. Rev. B**40**, 175 (1989).

O. B. Hyun, D. K. Finnemore, L. A. Schwartzkopt, and J. R. Clem, Phys. Rev. Lett. **58**, 599 (1987).

T. Imamura and S. Hasuo, IEEE Trans. Appl. Supercon. Vol.**2**, No.2 (1992).

T. Imamura, T. Shiota, and S. Hasuo, IEEE Trans. Appl. Supercon. Vol.**2**, No.1 (1992).

B. D. Josephson, Phys. Lett. **1**, 251 (1962).

B. D. Josephson, Adv. Phys. **14**, 419 (1965).

B. D. Josephson, *Superconductivity*, edited by R. D. Parks, (Marcel Dekker, New York 1969), Vol.**1**, chapter 9.

M. B. Ketchen, IEEE Trans. Mag. MAG-**27**, 2916 (1991).

S. Kotani, N. Fujimaki, T. Imamura, S. Hasuo, and T. Yamaoka, Japan. J. Appl. Phys. **24**, 421 (1985).

H. Kroger, IEEE Trans. **ED-27**, No.10, 2016 (1980).

S. K. Lahiri, J. Vac. Sci. Technol. **13**, 148 (1978).

Q. Li, Ph.D. dissertation, Iowa State University, (1987).

Q. Li, J. R. Clem, and D. K. Finnemore, Phys. Rev. B**43**, 12843 (1991).

Q. Li and D. K. Finnemore, IEEE Trans. Mag. MAG-**27**, 2913 (1991).

K. K. Likharev and V. K. Semenov, IEEE Trans. Superconductivity **1**, 1 (1991).

D. E. McCumber, J. Appl. Phys. **39**, 3113 (1968).

S. L. Miller, Ph.D. dissertation, Iowa State University, (1984)

S. L. Miller, K. R. Biagi, J. R. Clem, and D. K. Finnemore, Phys. Rev. B**31**, 2684 (1985).

S. Morohashi and S. Hasuo, J. Appl. Phys. **61**, 4835 (1987).

S. Morohashi, F. Shinoki, A. Shoji, M. Aoyagi, and H. Hayakawa, Appl. Phys.

Lett. **46**, 1179 (1985).

S. Nagata and H. C. Yang, Physica **108B**, 997 (1981).

J. M. Rowell, Phys. Rev. Lett. **11**, 200 (1963).

S. C. Sanders, J. Sok, D. K. Finnemore, and Qiang Li, Phys. Rev. B**47**, 8996 (1993).

S. Shapiro, Phys. Rev. Lett. **11**, 80 (1963).

T. Shiota, T. Imamura, and S. Hasuo, IEEE Trans. Appl. Supercon. Vol.**2**, No.4 (1992).

O. H. Soeren, J. Mygind, and N. F. Pedersen, Phys. Rev. Lett. **39**, 1018 (1977).

Junghyun Sok and D. K. Finnemore, Phys. Rev. B**50**, 12770 (1994).

W. C. Stewart, Appl. Phys. Lett. **12**, 277 (1968).

W. C. Stewart, J. Appl. Phys. **45**, 452 (1974).

M. Tinkham, Phys. Rev. **129**, 2413 (1963).

M. Tinkham, Rev. Mod. Phys. **36**, 268 (1964).

J. R. Tucker and M. J. Feldman, Rev. Mod. Phys. **57**, 1055 (1985).

N. R. Werthamer, Phys. Rev. **36**, 2240 (1963).

H. C. Yang and H. E. Horng, J. Low Temp. Phys. **70**, 493 (1988).

ACKNOWLEDGMENTS

The author wishes to express deep gratitude to Professor D. K. Finnemore for his continuous guidance and encouragement throughout the course of this research.

The author also wishes to thank J. E. Ostenson for his valuable help and advice in building and using experimental apparatus. Special thanks go to Ming Xu for his friendship and many useful discussions regarding this research and many area of superconductivity. Thanks are also extended to O. B. Hyun, S. C. Sanders, Qiang Li, and Y. H. Kim for their friendship and aids in various occasions.

The author wishes to thank his parents, lovely wife, Eunjin, and lovely daughter, Heekyung for their love and support while performing this work.

Finally, the author thanks the Lord God for allowing to meet all these wonderful people.

This work was performed at Ames Laboratory under Contract No. W-7405-ENG-82 with the U.S. Department of Energy. The United State government has assigned the DOE Report number IS-T 1735 to this thesis.